

# Integrated Flight Loads Modelling and Analysis for Flexible Transport Aircraft

Von der Fakultät Luft- und Raumfahrttechnik und Geodäsie der Universität  
Stuttgart zur Erlangung der Würde eines Doktor-Ingenieurs (Dr.-Ing.)  
genehmigte Abhandlung

Vorgelegt von

Christian Reschke

aus Frankfurt am Main

Hauptberichter: Prof. K. H. Well, Ph.D.  
Mitberichter: Prof. Dr.-Ing. C. Woernle  
Tag der mündlichen Prüfung: 27. Juli 2006

Institut für Flugmechanik und Flugregelung der Universität Stuttgart

2006



# Vorwort

Die vorliegende Arbeit wurde durch eine Kooperation des Instituts für Robotik und Mechatronik am Deutschen Zentrum für Luft- und Raumfahrt in Oberpfaffenhofen und der Abteilung Loads & Aeroelasticity der Airbus Deutschland GmbH in Hamburg ermöglicht.

Mein Dank gilt Herrn Prof. Dr.-Ing. G. Hirzinger, dem Leiter des Instituts für Robotik und Mechatronik und Herrn Dr. J. Bals, dem Leiter der Abteilung Entwurfsorientierte Regelungstechnik, für die Ermöglichung dieser Arbeit. Herrn U. Kerlin, dem Leiter der Abteilung Loads & Aeroelasticity, danke ich für die Bereitstellung des Arbeitsplatzes im Rahmen der Patenschaft.

Dem Direktor des Instituts für Flugmechanik und Flugregelung der Universität Stuttgart, Herrn Prof. K. H. Well, Ph.D., danke ich für die wissenschaftliche Betreuung und die Übernahme des Hauptberichts. Bei Herrn Prof. Dr.-Ing. C. Woernle vom Institut für Antriebstechnik und Mechatronik der Universität Rostock bedanke ich mich für sein Interesse an dieser Arbeit und die Übernahme des Mitberichts.

Bei allen Kollegen des Instituts für Robotik und Mechatronik und der Abteilung Loads & Aeroelasticity, die zum Gelingen dieser Arbeit beigetragen haben, bedanke ich mich für die gute Zusammenarbeit.

Besondere Erwähnung verdient hier Herr G. Looye, der stets bereit war wertvolle Diskussionen auf dem Gebiet der Modellierung zu führen. Herrn Dr.-Ing. J. Schuler danke ich für seine engagierte Betreuung und fachliche Unterstützung.

Nicht zuletzt gilt mein ganz besonderer Dank meinen Eltern, die mir meine Ausbildung ermöglicht haben.

Oberpfaffenhofen, im Juli 2006

Christian Reschke



# Contents

<b>Abstract</b>	<b>vii</b>
<b>List of Symbols</b>	<b>xi</b>
<b>1 Introduction</b>	<b>1</b>
1.1 Overview of Previous Work . . . . .	3
1.2 Objective and Scope . . . . .	8
1.3 Thesis Overview . . . . .	9
1.4 Contributions . . . . .	10
<b>2 Equations of Motion</b>	<b>11</b>
2.1 Approach for the Equation Development . . . . .	11
2.1.1 Definitions and Kinematics . . . . .	12
2.1.2 Lagrange's Equations for Quasi-Coordinates . . . . .	16
2.2 Energy Terms . . . . .	17
2.2.1 Kinetic Energy . . . . .	17
2.2.2 Potential Energy . . . . .	22
2.3 Virtual Work of Nonconservative Forces . . . . .	23
2.4 Derivation of the Equations of Motion . . . . .	25
2.4.1 Force Equation . . . . .	25
2.4.2 Moment Equation . . . . .	26
2.4.3 Elastic Equation . . . . .	34
2.5 Validation of the Modal Form . . . . .	37
2.6 Inertially Uncoupled Equations of Motion . . . . .	37
2.7 Application to a Beam Model . . . . .	38
2.7.1 Discussion of the Beam Model . . . . .	39
2.8 Summary of the Results . . . . .	42
<b>3 Equations of Structural Loads</b>	<b>44</b>
3.1 Deformation Approach . . . . .	45
3.2 Momentum Approach . . . . .	46
3.2.1 General Formulation . . . . .	46
3.2.2 Inertially Uncoupled Formulation . . . . .	51

3.2.3	Linearized Formulation . . . . .	51
3.3	Integrated Shear Loads . . . . .	52
3.4	Validation of the General Formulation . . . . .	53
3.5	Summary of the Results . . . . .	53
<b>4</b>	<b>Modelling of External Forces</b>	<b>55</b>
4.1	Aerodynamic Forces . . . . .	55
4.1.1	Quasi-Flexible Aerodynamic Forces . . . . .	56
4.1.2	Flexible Aerodynamic Forces . . . . .	57
4.1.3	Integration of the Aerodynamic Models . . . . .	59
4.2	Other External Forces . . . . .	63
4.3	Summary . . . . .	64
<b>5</b>	<b>Simulation</b>	<b>65</b>
5.1	Simulation Model . . . . .	65
5.1.1	Data Preparation . . . . .	65
5.1.2	Simulation Environment . . . . .	67
5.1.3	Post-Processing . . . . .	70
5.2	Trimming . . . . .	70
5.3	Dynamic Maneuver . . . . .	74
5.3.1	Energy Terms . . . . .	75
5.3.2	Flight Mechanical States . . . . .	76
5.3.3	Modal Elastic States . . . . .	77
5.3.4	Structural Loads . . . . .	80
5.3.5	Spin-Off Result . . . . .	82
5.4	Summary . . . . .	84
<b>6</b>	<b>Summary and Conclusions</b>	<b>85</b>
	<b>Kurzfassung</b>	<b>89</b>
<b>A</b>	<b>Mathematical Notes</b>	<b>97</b>
A.1	Vectors and Matrices . . . . .	97
A.2	Floating Reference Frames . . . . .	99
<b>B</b>	<b>Numerical Results for the EOM Validation</b>	<b>102</b>
<b>C</b>	<b>Numerical Data for the Beam Model</b>	<b>104</b>
<b>D</b>	<b>Numerical Results for the EOL Validation</b>	<b>106</b>
	<b>Bibliography</b>	<b>108</b>

# Abstract

This thesis is concerned with the derivation of nonlinear equations of motion for flexible aircraft in flight. These equations are intended for the accurate simulation of the flight dynamics of flexible aircraft in general and for the analysis of resulting dynamic structural loads in particular. The main focus is on the inertial coupling effects between the maneuvering flight and structural dynamics of the airframe.

The field of flight loads computation is concerned with the provision of loads due to maneuvering flight or turbulence. Hereby, the underlying simulation model consists of a model for the flexible aircraft as well as peripheral models, like the Electronic Flight Control System, a pilot model, etc. The analysis is performed for a variety of flight points and load cases. Subsequently a loads envelope is determined. It consists of maximum structural loads over the airframe due to prescribed maneuvers, gust and turbulence at different flight points and loading conditions.

Traditionally, specific models are used for either maneuver loads or gust loads computation. A six degree of freedom (6DOF) nonlinear aircraft model is employed for maneuver simulation. The dynamic response of the aircraft due to turbulence and gust is estimated with linear aeroelastic models, primarily employed in the frequency domain.

Particularly for large flexible transport aircraft, these specific models have important limitations. Commercial transport aircraft are getting larger and the airframes are becoming more slender and flexible due to lightweight design. This causes an increasing interaction of flight mechanics and structural dynamics, including inertial coupling effects. Therefore, it is important to extend 6DOF quasi-flexible maneuver loads models with finite element based full flexible aircraft models. Secondly, it may become necessary to perform dynamic response analysis in the time domain in order to account for nonlinear flight control systems.

For this reasons a consistent mathematical model that integrates methods and data from both disciplines has to be developed. This implies a derivation of equations of motion and the development of equations for the computation of loads. Furthermore the integration of the respective aerodynamic models has to be addressed.

In a first step the equations of motion are derived from first principles. The formulation is developed in such a way that industrial model data and industrial constraints can be considered and efficiently incorporated. The inertial coupling terms are cast in generalized form providing differential equations suited for rapid time domain simulation.

In a second step the generalized equations of motion are augmented with a consistent set of nonlinear equations for the computation of internal structural loads over the airframe. The new formulation accounts for nonlinear flight mechanical motion and inertial coupling effects with structural dynamics.

In a third step external forces, particularly aerodynamic forces that are driving the equations of motion are modelled. The approach is tailored towards the integration of industrial aerodynamic models used in maneuver loads and dynamic response analysis. The presented integration method extends the distributed quasi-flexible aerodynamic model as used for maneuver loads analysis by unsteady dynamic force increments.

The developed set of equations of motion and equations of loads are implemented in a state-of-the-art industrial simulation environment in order to validate the formulation and to perform simulations. A relevant test case is studied to analyze maneuvering flight, dynamic response and structural loads. The influence of inertial coupling effects is emphasized and structural components that are significantly affected are indicated.

The key result of this thesis is the increased precision of simulation and loads computation at the cost of a minimum increase of computing effort. No additional model data other than currently used for industrial maneuver loads and dynamic response analysis is required.



# Zusammenfassung

Das Thema der vorliegenden Arbeit ist die mathematische Modellbildung, Simulation und Lastenrechnung eines frei fliegenden flexiblen Transportflugzeuges. Hierbei wird das Problem der inertialen Kopplung zwischen der nichtlinearen Bewegung des körperfesten Koordinatensystems und der elastischen Deformation berücksichtigt.

Die Lastenrechnung an Flugzeugen umfasst die Berechnung von Strukturlasten, hervorgerufen durch Flugmanöver und Turbulenz. Dabei wird eine Vielzahl von Lastfällen, Arbeitspunkten und Beladungen betrachtet. Aus den jeweils größten auftretenden Lasten wird eine Einhüllende gebildet, welche die dimensionierenden Lasten für Auslegung und Zulassung liefert.

Traditionell werden unterschiedliche Modelle zur Ermittlung von Manöverlasten und Böenlasten eingesetzt. Modelle für die Manöverlasten basieren auf nichtlinearen Bewegungsgleichungen mit sechs Freiheitsgraden (6DOF), angeregt von Luftkräften aus aerodynamischen Datenbanken. Böenlasten werden mit linearen Aeroelastikmodellen ermittelt, deren Luftkräfte auf der Potentialtheorie beruhen.

Durch immer größere, leichtere und flexiblere Strukturen verringert sich der Abstand der Eigenfrequenzen zwischen Flugmechanik und Strukturmechanik. Weiterhin werden immer größere Winglets und Triebwerke verwendet. Dies führt zu einer verstärkten Wechselwirkung von flugmechanischen und strukturmechanischen Bewegungsgrößen, einschließlich einer größeren inertialen Kopplung. Daher ist eine Erweiterung von 6DOF Manöverlastmodellen auf eine voll flexible FE-Modellbasierte Analyse mit inertialer Kopplung erforderlich. Andererseits ist es nötig, Böenrechnungen im Zeitbereich durchzuführen, um nichtlineare Flugsteuerungssysteme betrachten zu können.

Es ist daher erstrebenswert, ein einheitliches mathematisches Modell aus Bewegungs- und Lastgleichung zu entwickeln. Weiterhin müssen dabei die bestehenden Aerodynamikmodelle von Manöver und Böenrechnung kombiniert werden.

Im ersten Schritt werden die Bewegungsgleichungen in Analogie zur Flugmechanik und Aeroelastik hergeleitet. Die Formulierung berücksichtigt industrielle Randbedingungen und ist auf

die Integration von industriellen Modelldaten ausgerichtet. Alle inertialen Kopplungsterme liegen in einer generalisierten Form vor, sodass die Differentialgleichungen zur effizienten Simulation geeignet sind.

Im zweiten Schritt werden die nichtlinearen Gleichungen zur Berechnung der strukturellen Lasten auf Basis der Trajektorien der generalisierten Bewegungsgleichungen hergeleitet. Die neue Formulierung berücksichtigt sowohl nichtlineare flugmechanische Größen als auch inertielle Kopplungseffekte.

Der dritte Schritt umfasst die Modellierung der aerodynamischen Kräfte. Hierzu werden Aerodynamikmodelle, die zur Berechnung von Manöver- und Böenlasten verfügbar sind, kombiniert. Die neue Methode erweitert die verteilten quasi-flexiblen aerodynamischen Kräfte aus dem Modell für die Manöverrechnung, um instationäre dynamische Inkremente aus dem Modell für die Böenrechnung.

Die inertial gekoppelten Bewegungsgleichungen und die Lastengleichung, sowie das erweiterte Aerodynamikmodell werden in die Simulationsumgebung zur Validation und Simulation integriert. Anhand eines zulassungsrelevanten dynamischen Manövers werden Flugmechanik, Strukturmechanik und Lasten analysiert. Dabei wird der Einfluss der inertialen Kopplungsterme herausgearbeitet, und darüber hinaus werden Strukturkomponenten mit besonderer Beeinflussung identifiziert.

Der wesentliche Beitrag dieser Arbeit besteht in der Verbesserung der Simulationsgenauigkeit und der Lastenrechnung bei lediglich minimaler Erhöhung des Rechenaufwandes. Des Weiteren sind für die neue Formulierung keine weiteren Daten als jene der gegenwärtigen industriellen Manöver- und Böenrechnung erforderlich.

# List of Symbols

Latin Symbols		Eqn.
$\mathbf{e}$	unit vector	(2.67)
$\bar{c}$	reference wing chord	(4.5)
$\mathbf{A}_{gE_i}$	coefficient matrices for RFA	(4.5)
$\mathbf{B}_{EE}$	modal damping matrix	(2.113)
$\mathbf{D}$	transformation matrix for angular body rates	(2.7)
$\mathbf{d}$	elastic deformation in l.r.f	(2.9)
$\mathbf{D}_{gE}$	matrix for RFA	(4.5)
$\mathbf{D}_{jk}$	substantial differentiation matrix	(4.3)
$\mathbf{E}_E$	matrix for RFA	(4.5)
$\mathbf{F}_i$	local force vector	(3.3)
$\mathbf{f}_i$	offset vector for external force	(4.14)
$\mathbf{g}$	gravitation vector	(2.42)
$\mathbf{H}$	momentum	(3.3)
$\mathbf{I}$	identity matrix	(2.9)
$\mathbf{J}_E$	local inertia tensor contribution to total inertia tensor	(2.32)
$\mathbf{J}_i$	local inertia tensor w.r.t. the location of the lumped mass	(2.9)
$\mathbf{J}_S$	Steiner contribution to the total inertia tensor	(2.31)
$\mathbf{J}_{g,i}$	local inertia tensor w.r.t. the location of the grid point	(2.36)
$\mathbf{K}$	stiffness matrix	(2.41)
$\mathbf{L}$	vector of structural loads	(3.1)
$\mathbf{M}$	mass matrix	(2.38)
$\mathbf{M}_i$	local moment vector	(3.3)
$\mathbf{Q}$	generalized force	(2.21)
$\mathbf{Q}_{jj}$	aerodynamic influence coefficient matrix	(4.3)

$\mathbf{R}_0$	position vector of the body frame in inertial reference frame	(2.8)
$\mathbf{R}_E$	matrix for RFA	(4.5)
$\mathbf{R}_i$	position vector of a mass element in the inertial reference frame	(2.9)
$\mathbf{r}_i$	position vector of a grid point in the body reference frame	(2.9)
$\mathbf{R}_{g,i}$	position vector of a grid point in the inertial frame	(2.49)
$\mathbf{s}_i$	position vector of a lumped mass element in l.r.f	(2.9)
$\mathbf{S}_{kj}$	integration matrix	(4.3)
$\mathbf{T}$	transformation matrix between coordinate frames	(2.42)
$\mathbf{u}_g$	vector of elastic displacements	(2.17)
$\mathbf{v}$	defined values for trim point	(5.5)
$\mathbf{V}_b$	velocity of the body frame resolved in body axes	(2.4)
$\mathbf{w}$	free values for trim point	(5.6)
$\mathbf{x}_L$	vector of aerodynamic lag states	(4.7)
$E$	energy	(2.24)
$g$	gravitation constant	(2.43)
$i_H$	horizontal tail plane deflection	(5.3)
$k$	reduced frequency	(4.3)
$m$	total mass of the airplane	(2.31)
$m_i$	lumped mass	(2.9)
$Ma$	mach number	(4.3)
$n_z$	vertical load factor	(4.2)
$p$	roll rate	(2.4)
$q$	pitch rate	(2.4)
$q_\infty$	dynamic pressure	(4.2)
$r$	yaw rate	(2.4)
$s$	laplace variable	(4.5)
$u$	x-component of $\mathbf{V}_b$	(2.4)
$V$	velocity	(4.5)
$v$	y-component of $\mathbf{V}_b$	(2.4)
$W$	work	(2.23)
$w$	z-component of $\mathbf{V}_b$	(2.4)

<b>Greek Symbols</b>		<b>Eqn.</b>
$\alpha$	angle of attack	(4.2)
$\beta$	angle of sideslip	(4.2)
$\delta\alpha$	virtual angular displacements of the body frame	(2.48)
$\delta$	virtual variation	(2.21)
$\delta_F$	thrust setting	(5.3)
$\eta_{wing}$	dimensionless spanwise coordinate of the wing	
$\Gamma_j$	set of grid points contributing to the integration station j	(3.20)
$\eta_E$	vector of generalized elastic coordinates	(2.19)
$\mathcal{L}$	Lagrange variable	(2.21)
$\varphi_i$	rotational elastic deformation in l.r.f	(2.9)
$\phi$	roll attitude angle	(2.2)
$\psi$	heading angle	(2.2)
$\theta$	pitch attitude angle	(2.2)
$\Omega_b$	angular velocity of the body frame resolved in body axes	(2.4)
$\Phi$	modal matrix	(2.19)
$\Theta$	vector of euler angles	(2.2)
$\xi$	aileron deflection	(5.3)
$\zeta$	rudder deflection	(5.3)
$\zeta_i$	modal damping parameter	(2.112)

---

### **Abbreviations**

---

FSM	Force Summation Method
MDM	Mode Displacement Method
AIC	Aerodynamic Influence Coefficients
c.g.	center of gravity
CFD	Computational Fluid Dynamics
DLM	Doublet Lattice Method
DOF	Degrees of Freedom
EOL	Equations of Structural Loads

EOM	Equations of Motion
FAR	Federal Aviation Regulations
FE	Finite Element
l.r.f.	local reference frame
RFA	Rational Function Approximation
RM	Residualized Model
sym	denotes a symmetric matrix

---

### Subscripts

---

0	related to the center of gravity
$b$	body fixed reference frame
$c$	integration station for loads
$E$	elastic mode shape
$e$	inertial reference frame
$g$	grid point degrees of freedom
$j$	aerodynamic control point set
$k$	aerodynamic loading point set
$q$	number of elastic mode shapes
$r$	rotational
$t$	translational
kin	kinetic
nco	non conservative
pot	potential
rel	relative

---

### Operator Symbols

---

$\langle (\dots)_{jk} \rangle$	summation: $\sum_{j=1}^3 \sum_{k=1}^3 (\dots)_{jk} \mathbf{e}_j \mathbf{e}_k^T$
$(\dots)^{-1}$	inverse
$(\dots)^T$	transpose
$(\overset{\circ}{\dots})$	$\frac{d}{dt}$ time rate of change with respect to the body frame
$(\dot{\dots})$	$\frac{d}{dt}$ time rate of change with respect to the inertial frame
$\in$	element of

$\notin$	not element of
$\text{sk}(\dots)$	skew symmetric matrix
$\times$	vector cross product

---

**Superscripts**

---

$(\dots)$	w.r.t. a local mass element
def	deformed
FSM	Force Summation Method
MDM	Mode Displacement Method
prop	propulsion
undef	undeformed
aero	aerodynamic
dyn	dynamic increment
oext	other external forces
qf	quasi-flexible





# 1 Introduction

This thesis is concerned with the derivation of a consistent set of nonlinear equations of motion (EOM) and equations for the computation of internal structural loads (EOL) for flexible aircraft in flight. The equations are intended for the accurate simulation of the flight dynamics and structural dynamics of flexible aircraft in general and for the analysis of resulting dynamic structural loads in particular. The main focus is on the inertial coupling effects between the maneuvering flight and structural dynamics of the airframe.

In the design process of aircraft, loads envelopes are determined in order to provide design loads for the sizing of the airframe structure and the certification of aircraft. A loads envelope provides maximum structural loads over the airframe due to prescribed maneuvers, gust and turbulence at different flight points and loading conditions. Hereby different models are used which are tailored towards the specific type of analysis. Maneuver loads analysis is based on time domain simulation with a 6 degree of freedom (6DOF) nonlinear aircraft model that accounts for the structural flexibility via altering the aerodynamic distribution. Hereby it is assumed that the structure is at all times in a static equilibrium. Therefore the maneuver loads model is referred to as a quasi-flexible model. Dynamic response to turbulence and gust is based on linear aeroelastic models (finite element model plus unsteady aerodynamics), primarily employed in the frequency domain.

What both types of models have in common is that trajectories describing the flight path and attitude and, in the case of dynamic response analysis, also airframe deformation are computed using generalized equations of motion. These trajectories are then used to compute loads distributed over the airframe (for this reason one often speaks of “loads recovery”). The structural loads are obtained from the local static or dynamic equilibrium by a summation of aerodynamic and inertia forces.

Maneuver loads and dynamic response models have important limitations. Firstly, commercial transport aircraft are getting larger and the airframes are becoming more slender and flexible due to lightweight design. This leads to a decreased margin between flight mechanical and elastic eigenfrequencies. Therefore maneuver loads based on 6DOF quasi-flexible models may no longer be sufficient and finite element based full flexible aircraft models are

required instead. Secondly, it may become necessary to perform dynamic response analysis in the time domain in order to account for nonlinear flight control systems. Interestingly, limitations of the one type of model are mostly covered by the other type and vice versa. For this reason there is more and more interest in developing models that integrate methods and data from both disciplines, referred to as integrated models. As an additional advantage, this results in a more simple and consistent industrial design process.

The nonlinear equations of motion are the core of an integrated model. For a flexible aircraft in flight they describe the maneuvering flight of the aircraft by a reference frame similar to a flight mechanics body frame and the elastic deformation of the airframe as relative deformation with respect to the reference frame. This leads to a set of differential equations for the flight mechanical motion and the deformation which is coupled via the external aerodynamic forces. The aerodynamic forces namely depend on both the flight mechanical motion of the aircraft and the structural deformation. This coupling via external forces is referred to as external coupling. Another type of coupling that is mostly neglected is the so-called inertial coupling, arising from direct interaction of the motion variables. In the context of this thesis it is defined as follows:

**Inertial coupling:** Direct coupling between the flight mechanical motion of the body reference frame and the elastic deformation relative to this reference frame.

The effect of inertial coupling is currently not considered for simulation and loads analysis of commercial transport aircraft neither in industrial nor in scientific research. However, aircraft tend to be designed with larger winglets and to be equipped with high bypass ratio engines; with this design concept the distance between the component center of gravity and the elastic axis of the wing is increased. As a consequence the inertial coupling is likely to become more prominent. It is therefore necessary to increase the precision of the simulation environments by accounting for inertial coupling and to apply the approach to flexible transport aircraft especially for highly dynamic maneuvers.

For an integrated model, not only the equations of motion but also the aerodynamic model and the equations for the loads computation have to be addressed.

For the same reason that requires integrated equations of motion, the aerodynamic model integrates data for maneuver and dynamic response analysis. Nonlinear databases are developed for flight mechanics and maneuver loads. The application rules incorporate data from CFD computation, wind tunnel test and also flight test data in the later design stage. By this means quasi-steady aerodynamic forces are acquired for a rigid aircraft. Then a correction for quasi-flexible deformation depending on dynamic pressure, load factor and mass

distribution is applied. Aeroelastic models used in dynamic response require unsteady lift information whereas the aerodynamic forces in flow direction are less important. This leads to the wide use of potential theory. In industry the Doublet Lattice Method enhanced by static corrections from aerodynamic databases or dynamic corrections from unsteady CFD analysis is the preferred method for the computation of unsteady aerodynamic forces.

A number of integration methods exist that combine aerodynamic models from maneuver loads and dynamic response while accounting for overlaps existing between both types of aerodynamic models. However, these methods are developed for generalized aerodynamic forces. Therefore these approaches cannot be used in the frame of loads recovery, where distributed forces are required. An extension of existing methods towards distributed forces is an important task for industrial applications.

In maneuver loads and dynamic response analysis the computation of structural loads is classically based on the summation of distributed aerodynamic and inertia force components. These forces are recovered from trajectories obtained by a simulation with generalized equations of motion. The preferred method for the loads recovery in dynamic response is the so-called Force Summation Method. It is derived from an aeroelastic system, therefore nonlinear maneuvering flight and inertial coupling is not accounted for. In order to perform a loads calculation in combination with nonlinear internally coupled equations of motion, equations of loads have to be re-derived from first principles.

In summary, precise loads analysis is a key element in the design process of aircraft. Hereby the influence of inertial coupling is an important aspect that has to be considered. The result of the new formulation presented in this thesis is an increased precision in simulation and loads computation at the cost of minimum increase in computing effort. No more model data than currently used for industrial maneuver loads and dynamic response analysis is required.

## 1.1 Overview of Previous Work

In the following an overview of previous work is given. Literature concerned with *Equations of Motion* for flexible aircraft is focused on first. Hereby work concerned with inertial coupling and model integration that is suitable for an industrial modelling process is of special interest.

Equations of motion for a free flying flexible aircraft are already addressed by Bisplinghoff and Ashley [8]. The EOM consists of a set of three internally decoupled equations. One equation for the rigid body translation, one for rigid body rotation and one for the elastic deformation. The elastic displacements are expressed by mode shapes of a continuous elastic

structure.

Milne [41] derives equations of motion for a continuous elastic body and discusses different choices for the reference frame, namely attached axes, floating axes and principal axes. The equations are linearized around a steady state assuming that the translation and rotation of the reference frame and elastic deformation are small. A beam model is used for modelling the flexible structure. Milne [42] describes in detail the three different types of reference frames and illustrates the effect on the momentum and the inertia tensor of the flexible body.

A relationship for the orientation of a reference frame attached to an airframe to a floating mean-axes frame is developed by Rodden and Love [52]. The relationship is used to accurately incorporate structural influence coefficients obtained for the restrained structure in an analysis based on equations of motion that assume a mean-axes frame.

Cavin and Dusto [13] use Hamilton's principle to derive equations of motion. Finite element approximations are developed for the dynamic formulation with respect to a reference frame satisfying practical mean-axes constraints. Body rates are assumed to be small eliminating all inertial coupling terms. The development of an effective procedure for the inclusion of inertial coupling terms is recommended for future work.

Waszak and Schmidt [66, 67, 68, 69] derive the equations of motion from first principles using Lagrange's equations. All assumptions and simplifications are clearly mentioned. A floating mean-axes reference frame is used to reduce the inertial coupling. Remaining inertial coupling terms are neglected. The elastic displacement is expressed by free vibration mode shapes, automatically fulfilling the so-called practical mean-axes constraints that locate the reference frame. Aerodynamic strip theory is used to obtain closed-form integral expressions for the generalized forces. A numerical example of a large elastic aircraft is presented. Etkin [16] and McLean [36] augment the flight mechanics equations by elastic degrees of freedom. The resulting equations are identical to the formulation given by Waszak and Schmidt [66].

Buttrill, Zeiler and Arbuckle [11] develop a mathematical model for a free flying flexible aircraft and study inertial coupling effects. Equations of motion are derived using Lagrangian mechanics. A lumped mass model is assumed and all inertial coupling terms are retained during the equation development. Rotational degrees of freedom of lumped masses and local inertia tensor are mentioned but the incorporation in the equations is not shown. An F/A-18 model serves as a test case for the influence of inertial coupling. A comparison between the approaches by Waszak [66] and Buttrill [11] is given in Waszak and Buttrill [65].

Zeiler and Buttrill [73] re-derive the equations of motion presented in [11] starting from

Hamilton's principle and extend the formulation towards centrifugal stiffening. Kane, Ryan and Banerjee [26] deal with dynamic stiffening for rotating beams. Banerjee and Dickens [4] present extensions for an arbitrary structure.

Youssef, Nayak and Gousman [72] develop equations of motion based on the principle of momentum for overall body and flexible body dynamics. It contains rotational degrees of freedom for lumped mass/inertia elements and retains a linearized form of the inertial coupling terms. The effects of the flexibility on the dynamic characteristics are studied for a simple cross-like structure rotating with constant angular velocity. Another derivation of equations of motion based on the principle of momentum is given by Hanel [21]. Nodal rotational degrees of freedom and inertial coupling are partially included.

Bilimoria and Schmidt [7] develop a framework for modelling the dynamics of elastic hypersonic flight vehicles considering a spherical rotating earth and accounting for mutual interaction with the rigid body motion. The equations of motion account for a variation of the mass elements with time, therefore the total inertia tensor is also variable. A set of elastic equations is incorporated using mean-axes constraints. These equations are inertially decoupled from the force and moment equations.

Meirovitch [37] derives Lagrange's equations for quasi-coordinates for an arbitrary body reference frame. An extension to a more general form and state equations in terms of quasi-coordinates are presented in [38]. A similar approach is followed by Olsen [43]. Lagrange's equations and quasi-coordinates are used to receive a general formulation for a unified flight mechanics and aeroelastic theory. The general equations are reduced to the special case of a planar airplane.

Tuzcu [63] and Meirovitch and Tuzcu [39, 40] apply a perturbation approach to the equations of motion in order to obtain nonlinear flight mechanics equations and a set of linear extended aeroelastic equations. The equations of motion are derived in hybrid form based on quasi-coordinates and subsequently discretized in space. The aircraft is discretized by shape functions for each component. A practical example is included in their work.

Equations of motion for an arbitrary flexible body are also considered in the field of multibody dynamics. Roots and perspectives of multibody dynamics are reviewed by Schiehlen [54]. A companion paper by Shabana [58] extends the review towards flexible multibody systems. The two papers present a comprehensive overview of formulations and relevant literature. An introduction to the subject of multibody dynamics is given by Robertson and Schwertassek [50] and Shabana [59]. The latter emphasizes flexible body dynamics. A finite element approach for flexible multibody dynamics is followed by G eradin and Cardona [18] including

an overview of substructuring techniques.

The problem of *aerodynamic model integration* is addressed by the following references.

Gupta, Brenner and Voelker [19] present extensions to the finite element structural analysis routines (STARS) for linear aeroelastic and aeroservoelastic analysis. Aerodynamic forces are assembled from steady rigid air loads and flexible unsteady loads obtained from the doublet lattice method. The formulation of equations of motion only deals with translational elastic degrees of freedom.

Winther, Goggin and Dykman [71, 70] present a method to link dynamic aeroelastic equations of motion with nonlinear 6DOF quasi-steady equations used in flight mechanics. The approach is tailored towards the integration of available aeroelastic and flight mechanics models and developed for real time simulation. An extension towards aeroelastic models containing aerodynamic lag states is presented by Looye [33].

Schuler [55] augments an aeroelastic model by forces in analogy to flight mechanics. Teufel and Hanel and Well [62] use the integrated model presented in [55] to analyze the response of a large transport aircraft to multidimensional gust inputs.

König and Schuler [56] present a method for linking an aeroelastic model with states obtained from 6DOF nonlinear equations for flight mechanics. A detailed comparison of the methods given in [33] and [56] is presented by Reschke and Looye [48].

Spieck [61] extends an existing multi-body-system by linking aerodynamic loads to the modal representation of the elastic body. The work is focused on aircraft ground dynamics.

Mauermann [35] develops a residual unsteady aerodynamic model for simulation that extracts incremental aerodynamic loads from a time stepping potential flow method rather than from a transformed frequency domain model as is common practice.

*Simulation Environments* for flexible aircraft are presented by various works. An overview is given in the following.

Arbuckle and Buttrill [3] describe a procedure for building simulation models based on the equations of motion presented in [11]. The aerodynamic model includes a steady nonlinear model providing aerodynamic loads for the rigid model and an unsteady aerodynamic model for the aerodynamic loading on the flexible modes.

Lavretsky [31] develops a methodology for accessing a simulation code through a MATLAB/SIMULINK interface. The integration approach for flight mechanics and aeroelastic model data basically implements the method proposed by Winther [71].

Hofstee, Kier, Cerulli and Looye [24] present the simulation environment VarLoads. The model features a modular data structure suited for special studies and implementation of new sub-models. The aircraft simulation is based on equations of motion developed in [69].

A multi-disciplinary aircraft model is presented by Looye, Hecker, Kier and Reschke [34]. The model uses object-oriented modelling techniques. The presented flight dynamics library provides models for flexible aircraft and is fully compatible with libraries from other disciplines, like electronics, thermodynamics and control systems.

*Loads computation* for structural dynamics is addressed by a variety of references. Work that is important in the frame of flight loads analysis is given in the following. A compendium of various loads analysis theories and practices as applied to the structural design and certification of commercial transport aircraft certified under the Federal Aviation Regulations (FAR) Part 25 is given in Lomax [32]. A comprehensive introduction to the subject of gust loads is provided by Hoblit [23]. Bisplinghoff [8] addresses equations of motion and the equations of loads directly. A variety of other references focus on the two most common loads recovery techniques, the mode displacement method (MDM) and the force summation method (FSM), also referred to as mode acceleration method.

Bisplinghoff and Ashley [8] use the MDM and FSM for the recovery of nodal loads. A convergence study for a test case shows superior convergence behavior (as a function of the number of modes taken into account) of the force summation method. The MDM and the mode acceleration method for multi degree of freedom systems are derived by Craig [14]. An extension for certain viscous damped systems is presented.

Pototzky [45] reviews existing techniques for the calculation of dynamic loads for aeroelastic systems. A new FSM is developed for a linear time-invariant state space system by computing a rational Laplace approximation of the dynamic loads. Again a comparison of MDM and FSM shows faster convergence of the FSM.

A variety of resources is concerned with the improvement of the MDM convergence behavior. Karpel and Presente [28] analyze the dynamic loads due to impulse excitations. The dynamic loads are expressed by MDM and FSM. Fictitious masses are used to generate so-called artificial load mode shapes. It is shown that the extension of the modal basis with these mode shapes can improve the MDM results. The approach can only be applied for local excitations. Rixen [49] and Fransen [17] deal with the MDM and the modal truncation augmentation method. The reduction transformation matrix is augmented with a set of pseudo-eigenvectors accounting for the quasi-flexible contribution of modes that are not contained in the modal basis.

Engelsen and Livne [15] describe a method for loads recovery from reduced order linear-time-invariant state-space models of aeroservoelastic systems. Convergence studies for MDM and FSM are included. Reschke [47] compares the MDM and FSM for a large passenger aircraft. Both references show the superior convergence behavior of the FSM.

## 1.2 Objective and Scope

From the literature survey it can be concluded that inertially coupled equations of motion have been addressed, but available formulations are not tailored towards the integration of industrial finite element models. Furthermore the effectiveness of implementation and simulation is an important point that requires more precise consideration. A loads equation which is consistent with inertially coupled equations of motion is currently not available.

The first main objective of this thesis is therefore to increase the precision of flight loads computation by deriving a consistent set of inertially coupled equations of motion and equations of loads from first principles. The formulation has to be tailored towards the integration of industrial model data and cast in a form suitable for efficient simulation.

The second main objective is to analyze the inertial coupling effects on structural loads for large flexible transport aircraft, based on the derived model equations. The effects have to be quantified and structural components that are highly influenced need to be identified.

The solution for the EOM/EOL development starts with the derivation of the EOM. The review of literature shows that Lagrange's equations in terms of quasi-coordinates are ideally suited for the derivation of generalized equations of motion. The reason for this is, that an energy method such as Lagrange's equations does not require the formulation of the dynamic equilibrium explicitly. Therefore, generalized coordinates that completely describe the location and orientation of each point of the system can be used which leads to a more convenient formulation. The use of Lagrange's equations in terms of quasi-coordinates instead of Lagrange's equations in generalized form accounts for the direct incorporation of variables in analogy to flight mechanics and dynamic response. The aircraft is described as a collection of lumped masses and respective inertia tensors for compatibility with flight loads data used in industry. It can be seen from the literature that a mean-axes coordinate frame is a suitable choice for the description of the overall airplane motion. The use of a mean-axes frame reduces the inertial coupling to a minimum. The constraints for this frame are fulfilled by the introduction of a set of elastic mode shapes obtained from free-free modal analysis of the structure.



The review of previous work shows that equations of loads should be developed on the basis of the force summation idea for accuracy and good convergence behavior in terms of elastic mode shapes. Since the trajectories of the states of the EOM are known from simulation, the principle of momentum is a direct way of dealing with the equilibrium of nodal forces. The total translational and rotational momentum contains the contributions of the body frame motion and the structural deformation. A new force summation method is obtained that extends existing formulations by accounting for nonlinear rigid body motion and inertial coupling. The equation is reordered in conventional terms and additional coupling terms. The consistency with the EOM is validated using a comparison of generalized elastic forces. New insight in the force summation method is revealed by stepwise simplification of the general formulation to a form suited for inertially uncoupled nonlinear EOM and subsequently to the conventional form for linear aeroelastic systems.

From the literature survey it can be concluded that the so-called Residualised Model Approach (RM-Approach) is ideally suited for the integration of the available aerodynamic models in combination with the derived equations of motion. The approach is to be extended towards the application to distributed instead of generalized aerodynamic models within the scope of this work.

The EOM/EOL and external forces are implemented in the VarLoads<sup>1</sup> simulation environment for validation and analysis. A highly dynamic maneuver serves as a test case for the analysis of inertial coupling effects for a large transport aircraft. The influence on motion variables and structural loads is shown. Mode shapes and structural components that are highly subjected to inertial coupling are identified.

## 1.3 Thesis Overview

The equations of motion (EOM) are derived from first principles in *Chapter 2*. The derivation is based on Lagrange's equations and a mean-axes frame is chosen as a moving reference frame. The emphasis of the derivation is to arrive at a fully generalized formulation that is suitable for rapid time domain simulation. The new generalized form is validated by comparison with the physical formulation. Rotational nodal degrees of freedom, offsets of masses from grid points and full inertial coupling terms are accounted for. All underlying assumptions are clearly mentioned. A simple example illustrates the effect of inertial coupling.

In *Chapter 3* the loads equation (EOL) is derived. The derivation is based on the principle of momentum. The new formulation is a force summation method consistent with the nonlinear

---

<sup>1</sup>Variable Loads Environment [24]

equations of motion with inertial coupling terms. The consistency with the equations of motion is shown.

*Chapter 4* describes the modelling of the external forces. An extension of the Residualized Model approach for the combination of quasi-flexible nonlinear aerodynamic forces from database with dynamic increments from potential theory is presented.

An example, pointing out the influence of the inertial coupling terms on the simulation and loads recovery, is presented in *Chapter 5*. At the beginning of the chapter the simulation environment and the implementation of EOM and EOL is described. Nodal and integrated loads are then analyzed. Inertial coupling effects are quantified and critical structural components are worked out. A guideline for estimating inertial coupling effects in the loads analysis based on conventional uncoupled formulations is presented.

*Chapter 6* summarizes the present work and contains conclusions. Recommendations for future work and further improvements are given.

## 1.4 Contributions

The new contributions of this thesis to flight loads analysis can be summarized as follows:

- Derivation of a consistent set of equations of motion (EOM)/loads equation (EOL) including full inertial coupling. The precision of flight loads computation is increased while available model data can be directly incorporated.
- The equations of motion are cast in an efficient form for implementation. The fully generalized form of all coupling terms is ideally suited for rapid time domain simulation and the calculation of load loops.
- A new loads equation is derived extending the force summation method towards nonlinear rigid body motion and inertial coupling.
- The Residualized Model approach is extended towards distributed quasi-flexible aerodynamic loads. The approach can now be used in combination with force summation loads recovery.
- The effects of inertial coupling for transport aircraft in dynamic maneuver is worked out. The inaccuracy in loads resulting from uncoupled formulation is identified.
- As a spin-off result, an approach for estimating inaccuracies of loads from uncoupled simulation, is presented. This is of important practical relevance since uncoupled formulations are frequently used in industry.

## 2 Equations of Motion

This Chapter describes the derivation of the equations of motion for an elastic aircraft in flight using Lagrange's equations for quasi-coordinates. The inertial coupling between the overall motion of the elastic body and its elastic deformation is included in the formulation. The emphasis of the derivation is to arrive at a fully generalized formulation that is suitable for rapid time domain simulation. A simple beam model example is presented to illustrate inertial coupling effects.

### 2.1 Approach for the Equation Development

Several mechanical principles may be used to derive the equations of motion for a flexible aircraft in flight.

The principle of Newton Euler or conservation of momentum [22] is generally applicable. For equations of motion in analogy to flight mechanics and aeroelasticity it is not the most computationally efficient method since all internal forces including reactive forces have to be considered and individually formulated. The principle of Newton Euler also requires complex kinematic relations.

The Principle of Virtual Work [22] states that the total work of all forces vanishes. It does not require the formulation of reactive forces. The derivation of the equations of motion can be simplified when so-called generalized coordinates are used. Generalized coordinates are independent coordinates which represent possible displacements of a physical system. In finite element methods the displacements are commonly expressed by a superposition of shape functions described by a spatial function, the modes shape and time dependent coefficients, the generalized coordinates. Introducing generalized coordinates in the Principle of Virtual Work leads to the Lagrange's equations [22].

The Lagrange's equations can be cast in a more convenient form by introducing quasi-coordinates. A quasi-coordinate is a linear combination of generalized velocities that can not be integrated to obtain physically meaningful coordinates. The meaning of quasi-coordinates

can be illustrated when one considers the motion of a body fixed reference frame. It is obviously useful to describe its location in terms of a position vector and Euler angles. These coordinates then serve as generalized coordinates. The respective time derivatives of the position and the Euler angles would then be the generalized velocities. However, for the description of the velocity of the reference frame the use of translational and angular rates expressed in body axes is a more convenient choice i.e., a linear combination of generalized velocities is preferred over the use of the generalized velocities itself. This choice is accounted for in the Lagrange's equations in terms of quasi-coordinates.

### 2.1.1 Definitions and Kinematics

The formulation will be tailored towards the integration of available linear finite element models, used in loads analysis and aeroelasticity. Some assumptions then need to be made for the equation development:

**Assumption 1.** *The aircraft is described as a collection of lumped mass elements, with an associated mass  $m_i$  and inertia tensor  $\mathbf{J}_i$ .*<sup>1</sup>

**Assumption 2.** *Linear elastic theory applies.*

**Assumption 3.** *Local translational and rotational elastic deformations with respect to the reference shape are small.*<sup>2</sup>

**Assumption 4.** *Orthogonal mode shapes resulting from a free-free modal analysis are available. The deformation of the airplane may be written as a linear combination of the mode shapes, i.e. the modal approach will be used.*

Next the coordinate frames used in the present formulation will be defined. The use of quasi-coordinates implies the definition of a body fixed coordinate frame moving relative to the inertial frame. The following coordinate frames will thus be used:

- An inertial reference frame  $(x_e, y_e, z_e)$ , attached to the earth surface (origin  $O^e$ ).
- A body fixed reference frame  $(x_b, y_b, z_b)$ , located at the center of gravity (origin  $O^b$ ).
- Local reference frames (l.r.f) located at the position of each grid point (the endpoint of the vector  $\mathbf{r}_i$ , origin  $O^i$ ). The axes are assumed to be parallel to the body reference frame.

See also Figure 2.1 for the location of the coordinate frames.

---

<sup>1</sup>This is the typical case in finite element models used in loads and aeroelastics. Local mass and inertia is for example defined in MSC.Nastran CONM2 cards.

<sup>2</sup>Cumulative deformations may still be considerable e.g. wing tip deflection.

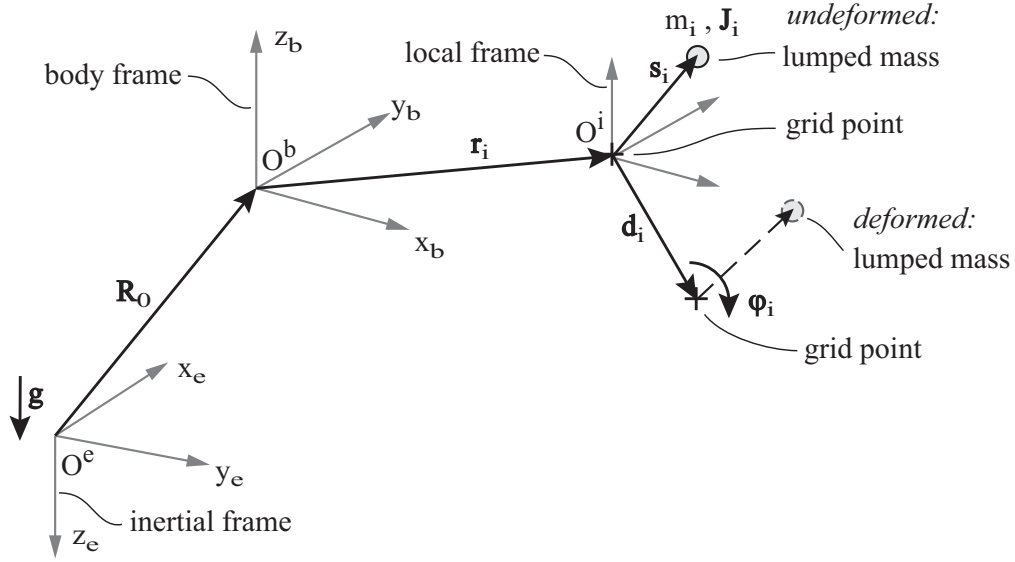


**Figure 2.1:** Coordinate frames for the elastic aircraft and location of a grid point

### Kinematics of the Body Frame

The position of the body fixed frame is defined by the position vector  $\mathbf{R}_{0e}$  resolved in inertial coordinates. It may be written as follows

$$\mathbf{R}_{0e} = \begin{bmatrix} x_{0e} & y_{0e} & z_{0e} \end{bmatrix}^T . \quad (2.1)$$

The orientation of the body fixed frame is defined using the vector of three independent Euler angles  $\Theta$

$$\Theta = \begin{bmatrix} \phi & \theta & \psi \end{bmatrix}^T . \quad (2.2)$$

The corresponding velocity vectors of the body frame resolved in the body frame are defined as follows

$$\mathbf{V}_b = \begin{bmatrix} u & v & w \end{bmatrix}^T , \quad (2.3)$$

$$\mathbf{\Omega}_b = \begin{bmatrix} p & q & r \end{bmatrix}^T . \quad (2.4)$$

The kinematic differential equations can then be written as follows [38]

$$\dot{\Theta} = \mathbf{D}^{-1} \mathbf{\Omega}_b , \quad (2.5a)$$

$$\dot{\mathbf{R}}_{0e} = \mathbf{T}_{be}^{-1} \mathbf{V}_b , \quad (2.5b)$$

note that these expressions can be regarded as the linear combinations relating the so-called quasi-velocities  $\mathbf{\Omega}_b, \mathbf{V}_b$  with true generalized velocities  $\dot{\Theta}, \dot{\mathbf{R}}_{0e}$ .

The transformation matrix from the inertial frame into body axes in (2.5) is expressed by a

series of Euler angle rotations [16]

$$\mathbf{T}_{be} = \begin{bmatrix} 1 & 0 & 0 \\ 0 & \cos \phi & \sin \phi \\ 0 & -\sin \phi & \cos \phi \end{bmatrix} \begin{bmatrix} \cos \theta & 0 & -\sin \theta \\ 0 & 1 & 0 \\ \sin \theta & 0 & \cos \theta \end{bmatrix} \begin{bmatrix} \cos \psi & \sin \psi & 0 \\ -\sin \psi & \cos \psi & 0 \\ 0 & 0 & 1 \end{bmatrix}. \quad (2.6)$$

The transformation matrix between the time derivative of the Euler angles  $\dot{\Theta}$  and the angular velocity vector  $\boldsymbol{\Omega}_b$  is given by

$$\mathbf{D} = \begin{bmatrix} 1 & 0 & -\sin \theta \\ 0 & \cos \phi & \cos \theta \sin \phi \\ 0 & -\sin \phi & \cos \theta \cos \phi \end{bmatrix}. \quad (2.7)$$

The position of the body fixed frame  $\mathbf{R}_{0e}$  resolved in inertial coordinates may also be written as a vector resolved in the body frame

$$\mathbf{R}_{0e} = \mathbf{T}_{be}^{-1} \mathbf{R}_0 \quad (2.8)$$

where  $\mathbf{R}_0$  denotes the position vector resolved in the body frame.

### Kinematics of Mass Elements

The aircraft is assumed to consist of a collection of lumped mass elements (Assumption 1, on page 12). The location of the local lumped mass element  $m_i, \mathbf{J}_i$  in its deformed condition resolved in the body fixed coordinate frame may be written as follows (Figure 2.1)

$$\mathbf{R}_i = \mathbf{R}_0 + \mathbf{r}_i + \mathbf{d}_i + \mathbf{T}(\boldsymbol{\varphi}_i) \mathbf{s}_i \quad (2.9)$$

with the position vectors:

- $\mathbf{R}_0$  position vector of the origin of the body fixed frame in the inertial frame resolved in the body fixed frame
- $\mathbf{r}_i$  position vector of a grid point in the body reference frame
- $\mathbf{d}_i$  elastic deformation in l.r.f.
- $\mathbf{s}_i$  position vector of a lumped mass element in l.r.f
- $\boldsymbol{\varphi}_i$  rotational elastic deformation in l.r.f

and the transformation matrix  $\mathbf{T}(\boldsymbol{\varphi}_i)$ . This matrix describes the rotation of the offset vector  $\mathbf{s}_i$  from the undeformed into its deformed position. The transformation can be written as a series by introducing a Taylor series for trigonometric functions. In accordance with

Assumption 3 (page 12) the linearized version of the transformation matrix will be used [58]:

$$\begin{aligned}\mathbf{T}(\boldsymbol{\varphi}_i) &= \mathbf{I} + \frac{1}{1!} \text{sk}(\boldsymbol{\varphi}_i)^1 + \frac{1}{2!} \text{sk}(\boldsymbol{\varphi}_i)^2 + \frac{1}{3!} \text{sk}(\boldsymbol{\varphi}_i)^3 + \dots \\ &\approx \mathbf{I} + \text{sk}(\boldsymbol{\varphi}_i) \quad , \quad \text{linearized} \quad .\end{aligned}\quad (2.10)$$

The position of the mass element may then be written as follows

$$\mathbf{R}_i = \mathbf{R}_0 + \mathbf{r}_i + \mathbf{d}_i + (\mathbf{I} + \text{sk}(\boldsymbol{\varphi}_i))\mathbf{s}_i \quad (2.11a)$$

$$= \mathbf{R}_0 + \bar{\mathbf{r}}_i + \bar{\mathbf{d}}_i \quad (2.11b)$$

with the vectors

$$\bar{\mathbf{r}}_i = \mathbf{r}_i + \mathbf{s}_i \quad , \quad (2.12)$$

$$\bar{\mathbf{d}}_i = \mathbf{d}_i + \boldsymbol{\varphi}_i \times \mathbf{s}_i \quad (2.13)$$

shortening the formulation. Figure 2.2 shows the location  $\mathbf{R}_i$  of a lumped mass element  $m_i, \mathbf{J}_i$  in its deformed condition.

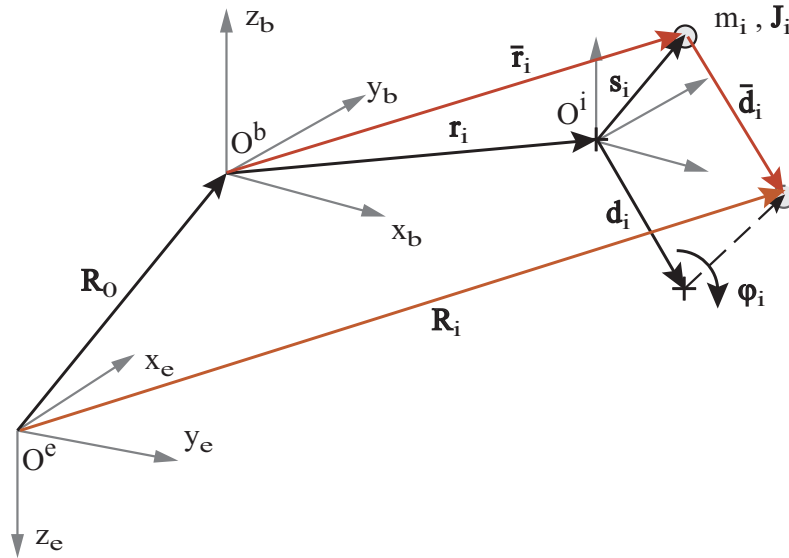


**Figure 2.2:** Location of a mass element in reference and deformed condition

The translational inertial velocity of the local mass element  $m_i$  is then given by the time derivative of the position vector (2.11a) as follows

$$\dot{\mathbf{R}}_i = \mathbf{V}_b + \underbrace{(\dot{\mathbf{d}}_i + \dot{\boldsymbol{\varphi}}_i \times \mathbf{s}_i)}_{\dot{\bar{\mathbf{d}}}_i} + \boldsymbol{\Omega}_b \times (\underbrace{\mathbf{r}_i + \mathbf{s}_i}_{\bar{\mathbf{r}}_i} + \underbrace{(\mathbf{d}_i + \boldsymbol{\varphi}_i \times \mathbf{s}_i)}_{\bar{\mathbf{d}}_i}) \quad (2.14)$$

$$= \mathbf{V}_b + \dot{\bar{\mathbf{d}}}_i + \boldsymbol{\Omega}_b \times (\bar{\mathbf{r}}_i + \bar{\mathbf{d}}_i) \quad (2.15)$$

where the inertial velocity  $\mathbf{V}_b$  of the body frame (resolved in body axes) can also be written as  $\mathbf{V}_b = \dot{\mathbf{R}}_0 + \boldsymbol{\Omega}_b \times \mathbf{R}_0$  since the vector  $\mathbf{R}_0$  is resolved in the body fixed frame.

The rotational inertial velocity of the lumped mass element is the superposition of the rotational velocity of the body frame  $\mathbf{\Omega}_b$  and the rotational velocity due to elastic deformation  $\mathring{\boldsymbol{\varphi}}_i$ , hence

$$\mathbf{\Omega}_i = \mathbf{\Omega}_b + \mathring{\boldsymbol{\varphi}}_i \quad . \quad (2.16)$$

For convenience all local translational  $\mathbf{d}_i$  and rotational  $\boldsymbol{\varphi}_i$  deformations are collected in a vector of elastic displacements

$$\mathbf{u}_g = \begin{bmatrix} \vdots \\ \mathbf{u}_{g,i} \\ \vdots \end{bmatrix} \quad \text{with} \quad \mathbf{u}_{g,i} = \begin{bmatrix} \mathbf{d}_i \\ \boldsymbol{\varphi}_i \end{bmatrix} \quad . \quad (2.17)$$

Next the local translational  $\mathbf{d}_i$  and rotational  $\boldsymbol{\varphi}_i$  deformations are expressed as a linear combination of a number of  $q$  free-free vibration mode shapes (Assumption 4, on page 12)

$$\mathbf{\Phi}_{gE} = \begin{bmatrix} \vdots \\ \mathbf{\Phi}_{g_i E} \\ \vdots \end{bmatrix} \quad . \quad (2.18)$$

The deformation can then be written as follows

$$\mathbf{u}_{g,i} = \begin{bmatrix} \mathbf{d}_i \\ \boldsymbol{\varphi}_i \end{bmatrix} = \begin{bmatrix} \mathbf{\Phi}_{g_i E_t} \\ \mathbf{\Phi}_{g_i E_r} \end{bmatrix} \boldsymbol{\eta}_E = \mathbf{\Phi}_{g_i E} \boldsymbol{\eta}_E \quad (2.19)$$

where the vector  $\boldsymbol{\eta}_E$  denotes the  $(q \times 1)$ -vector of generalized elastic coordinates

$$\boldsymbol{\eta}_E = \begin{bmatrix} \eta_{E_1} & \dots & \eta_{E_q} \end{bmatrix}^T \quad . \quad (2.20)$$

### 2.1.2 Lagrange's Equations of the Second Kind for Quasi-Coordinates

Lagrange's equations of the second kind for quasi-coordinates are used to derive the equations of motion. The Lagrange's equations can be written as follows [38]:

$$\frac{d'}{dt} \left( \frac{\partial \mathcal{L}}{\partial \mathbf{V}_b} \right) + \mathbf{\Omega}_b \times \left( \frac{\partial \mathcal{L}}{\partial \mathbf{V}_b} \right) - \mathbf{T}_{be} \frac{\partial \mathcal{L}}{\partial \mathbf{R}_{0e}} = \mathbf{T}_{be} \mathbf{Q}_t \quad , \quad (2.21a)$$

$$\frac{d'}{dt} \left( \frac{\partial \mathcal{L}}{\partial \mathbf{\Omega}_b} \right) + \mathbf{V}_b \times \left( \frac{\partial \mathcal{L}}{\partial \mathbf{V}_b} \right) + \mathbf{\Omega}_b \times \left( \frac{\partial \mathcal{L}}{\partial \mathbf{\Omega}_b} \right) - (\mathbf{D}^T)^{-1} \frac{\partial \mathcal{L}}{\partial \boldsymbol{\Theta}} = (\mathbf{D}^T)^{-1} \mathbf{Q}_r \quad , \quad (2.21b)$$

$$\frac{d'}{dt} \left( \frac{\partial \mathcal{L}}{\partial \mathring{\boldsymbol{\eta}}_E} \right) - \frac{\partial \mathcal{L}}{\partial \boldsymbol{\eta}_E} = \mathbf{Q}_E \quad (2.21c)$$



where the Lagrange variable  $\mathcal{L}$  is defined as the difference of kinetic and potential energy

$$\mathcal{L} = E_{\text{kin}} - E_{\text{pot}} \quad . \quad (2.22)$$

On the right hand side of the Lagrange's equations the terms  $\mathbf{Q}_t, \mathbf{Q}_r, \mathbf{Q}_E$  represent the generalized nonconservative forces resulting from the virtual work  $\delta W_{\text{nco}}$  due to nonconservative forces

$$\delta W_{\text{nco}} = \delta \mathbf{R}_{0e}^T \mathbf{Q}_t + \delta \boldsymbol{\Theta}^T \mathbf{Q}_r + \delta \boldsymbol{\eta}_E^T \mathbf{Q}_E \quad . \quad (2.23)$$

## 2.2 Energy Terms

In this section the kinetic and potential energy of the aircraft will be formulated for subsequent use in the Lagrange's equations.

### 2.2.1 Kinetic Energy

Each mass element is defined by a lumped mass  $m_i$  and a corresponding inertia tensor  $\mathbf{J}_i$ . Therefore the kinetic energy can be written as a contribution from the mass elements  $E_{\text{kin},t}$  and a contribution of the local inertia tensors  $E_{\text{kin},r}$

$$E_{\text{kin}} = \underbrace{\frac{1}{2} \sum_i \dot{\mathbf{R}}_i^T \dot{\mathbf{R}}_i m_i}_{E_{\text{kin},t}} + \underbrace{\frac{1}{2} \sum_i \boldsymbol{\Omega}_i^T \mathbf{J}_i \boldsymbol{\Omega}_i}_{E_{\text{kin},r}} \quad . \quad (2.24)$$

Translational and rotational energy contributions will now be analyzed in detail.

#### Translational Contribution to Kinetic Energy

The translational contribution  $E_{\text{kin},t}$  results from the lumped mass and is considered first

$$E_{\text{kin},t} = \frac{1}{2} \sum_i \dot{\mathbf{R}}_i^T \dot{\mathbf{R}}_i m_i \quad . \quad (2.25)$$

Expansion with the velocity expression  $\dot{\mathbf{R}}_i$  from (2.14) yields

$$\begin{aligned}
E_{\text{kin},t} &= \frac{1}{2} \mathbf{V}_b^T \mathbf{V}_b m + \frac{1}{2} \sum_i \dot{\bar{\mathbf{d}}}_i^T \dot{\bar{\mathbf{d}}}_i m_i \\
&\quad + \frac{1}{2} \underbrace{\mathbf{\Omega}_b^T \sum_i [(\bar{\mathbf{r}}_i + \bar{\mathbf{d}}_i)^T (\bar{\mathbf{r}}_i + \bar{\mathbf{d}}_i) \mathbf{I} - (\bar{\mathbf{r}}_i + \bar{\mathbf{d}}_i)(\bar{\mathbf{r}}_i + \bar{\mathbf{d}}_i)^T]}_{\mathbf{J}_S} m_i \mathbf{\Omega}_b \\
&\quad + \mathbf{V}_b^T \sum_i \dot{\bar{\mathbf{d}}}_i m_i + \mathbf{V}_b^T (\mathbf{\Omega}_b \times \sum_i (\bar{\mathbf{r}}_i + \bar{\mathbf{d}}_i) m_i) \\
&\quad + \sum_i (\mathbf{\Omega}_b \times (\bar{\mathbf{r}}_i + \bar{\mathbf{d}}_i))^T \dot{\bar{\mathbf{d}}}_i m_i \tag{2.26}
\end{aligned}$$

where  $\mathbf{J}_S$  represents the contribution of all mass elements to the total inertia tensor of the aircraft.

The complexity of the last three terms in (2.26),  $\mathbf{V}_b^T \sum_i \dot{\bar{\mathbf{d}}}_i m_i$ ,  $\mathbf{V}_b^T (\mathbf{\Omega}_b \times \sum_i (\bar{\mathbf{r}}_i + \bar{\mathbf{d}}_i) m_i)$ ,  $\sum_i (\mathbf{\Omega}_b \times (\bar{\mathbf{r}}_i + \bar{\mathbf{d}}_i))^T \dot{\bar{\mathbf{d}}}_i m_i$  depends on the choice of the body reference frame.

At this point of the derivation the body fixed reference frame is further specified. So-called practical mean-axes constraints are chosen [66, 42, 58] for the definition of the reference frame. These constraints minimize the translational and angular momentum relative to the reference frame (see Appendix A.2 for more information on the practical mean-axes constraints). The choice of mean-axes is favorable since it reduces the complexity of the energy expression and it enlarges the range of applicability of the small displacement assumption. Deformations are smallest, when measured with respect to a mean-axes-frame [57].

The practical mean-axes constraints are given by (Appendix A.2):

$$\begin{aligned}
\sum_i (\mathbf{d}_i + \boldsymbol{\varphi}_i \times \mathbf{s}_i) m_i &= \mathbf{0} \quad , \\
\sum_i [m_i \mathbf{r}_i \times (\mathbf{d}_i + \boldsymbol{\varphi}_i \times \mathbf{s}_i) + m_i \mathbf{s}_i \times \mathbf{d}_i + (\mathbf{J}_i + \text{sk}(\mathbf{s}_i)^T \text{sk}(\mathbf{s}_i) m_i) \boldsymbol{\varphi}_i] &= \mathbf{0} \quad .
\end{aligned}$$

The last term of (2.26) can be expanded as follows

$$\sum_i (\mathbf{\Omega}_b \times (\bar{\mathbf{r}}_i + \bar{\mathbf{d}}_i))^T \dot{\bar{\mathbf{d}}}_i m_i = \mathbf{\Omega}_b^T \sum_i (\bar{\mathbf{r}}_i \times \dot{\bar{\mathbf{d}}}_i) m_i + \mathbf{\Omega}_b^T \sum_i (\bar{\mathbf{d}}_i \times \dot{\bar{\mathbf{d}}}_i) m_i \quad . \tag{2.27}$$

Introduction of the practical mean-axes constraints in the last three terms of (2.26) and using

the expansion (2.27) yields

$$\mathbf{V}_b^T \sum_i \overset{\circ}{\mathbf{d}}_i m_i \implies 0 \quad , \quad (2.28)$$

$$\mathbf{V}_b^T (\boldsymbol{\Omega}_b \times \sum_i (\bar{\mathbf{r}}_i + \bar{\mathbf{d}}_i) m_i) \implies 0 \quad , \quad (2.29)$$

$$\sum_i (\boldsymbol{\Omega}_b \times (\bar{\mathbf{r}}_i + \bar{\mathbf{d}}_i))^T \overset{\circ}{\mathbf{d}}_i m_i \implies \boldsymbol{\Omega}_b^T \sum_i (\bar{\mathbf{d}}_i \times \overset{\circ}{\mathbf{d}}_i) m_i \quad . \quad (2.30)$$

The kinetic energy then becomes:

$$E_{\text{kin},t} = \frac{1}{2} \mathbf{V}_b^T \mathbf{V}_b m + \frac{1}{2} \sum_i \overset{\circ}{\mathbf{d}}_i^T \overset{\circ}{\mathbf{d}}_i m_i + \frac{1}{2} \boldsymbol{\Omega}_b^T \mathbf{J}_S \boldsymbol{\Omega}_b + \boldsymbol{\Omega}_b^T \sum_i (\bar{\mathbf{d}}_i \times \overset{\circ}{\mathbf{d}}_i) m_i \quad (2.31)$$

where the last two terms represent the cross coupling between the rigid body motion and the elastic deformation.

### Rotational Contribution to Kinetic Energy

The rotational contribution to the kinetic energy  $E_{\text{kin},r}$  results from local inertia tensors and rotational velocities of each inertia tensor. Expansion of the second term of (2.24) with (2.16) yields

$$\begin{aligned} E_{\text{kin},r} &= \frac{1}{2} \sum_i \boldsymbol{\Omega}_i^T \mathbf{J}_i \boldsymbol{\Omega}_i \\ &= \frac{1}{2} \sum_i (\boldsymbol{\Omega}_b + \overset{\circ}{\boldsymbol{\varphi}}_i)^T \mathbf{J}_i (\boldsymbol{\Omega}_b + \overset{\circ}{\boldsymbol{\varphi}}_i) \\ &= \frac{1}{2} \boldsymbol{\Omega}_b^T \underbrace{\sum_i \mathbf{J}_i}_{\mathbf{J}_E} \boldsymbol{\Omega}_b + \frac{1}{2} \sum_i \left\{ \overset{\circ}{\boldsymbol{\varphi}}_i^T \mathbf{J}_i \overset{\circ}{\boldsymbol{\varphi}}_i + \overset{\circ}{\boldsymbol{\varphi}}_i^T \mathbf{J}_i \boldsymbol{\Omega}_b + \boldsymbol{\Omega}_b^T \mathbf{J}_i \overset{\circ}{\boldsymbol{\varphi}}_i \right\} \end{aligned} \quad (2.32)$$

where the last two terms represent the cross coupling between rigid body motion and elastic deformation.  $\mathbf{J}_E$  is the contribution of all local inertia tensors to total inertia tensor of the aircraft.

### Total Kinetic Energy

The combination of the translational (2.31) and the rotational contribution (2.32) gives the total kinetic energy.

It is useful to introduce the total inertia tensor of the **deformed** aircraft, which is given by

$$\begin{aligned}
\mathbf{J} &= \mathbf{J}_E + \mathbf{J}_S \\
&= \sum_i \mathbf{J}_i + \sum_i \{(\bar{\mathbf{r}}_i + \bar{\mathbf{d}}_i)^T (\bar{\mathbf{r}}_i + \bar{\mathbf{d}}_i) \mathbf{I} - (\bar{\mathbf{r}}_i + \bar{\mathbf{d}}_i)(\bar{\mathbf{r}}_i + \bar{\mathbf{d}}_i)^T\} m_i \\
&= \sum_i \mathbf{J}_i - \sum_i \text{sk}(\bar{\mathbf{r}}_i + \bar{\mathbf{d}}_i) \text{sk}(\bar{\mathbf{r}}_i + \bar{\mathbf{d}}_i) m_i \quad .
\end{aligned} \tag{2.33}$$

With (2.31), (2.32) in (2.24) and (2.33) the total kinetic energy can be written in the following form

$$\begin{aligned}
E_{\text{kin}} &= \frac{1}{2} \mathbf{V}_b^T \mathbf{V}_b m + \frac{1}{2} \sum_i \overset{\circ}{\mathbf{d}}_i^T \overset{\circ}{\mathbf{d}}_i m_i + \frac{1}{2} \boldsymbol{\Omega}_b^T \mathbf{J} \boldsymbol{\Omega}_b \\
&\quad + \boldsymbol{\Omega}_b^T \sum_i (\bar{\mathbf{d}}_i \times \overset{\circ}{\mathbf{d}}_i) m_i + \frac{1}{2} \sum_i \overset{\circ}{\boldsymbol{\varphi}}_i^T \mathbf{J}_i \overset{\circ}{\boldsymbol{\varphi}}_i + \boldsymbol{\Omega}_b^T \sum_i \mathbf{J}_i \overset{\circ}{\boldsymbol{\varphi}}_i \quad .
\end{aligned} \tag{2.34}$$

The second term  $\frac{1}{2} \sum_i \overset{\circ}{\mathbf{d}}_i^T \overset{\circ}{\mathbf{d}}_i m_i$  of (2.34) can be expanded using the expression for the elastic velocity of the mass element  $\overset{\circ}{\mathbf{d}}_i = \overset{\circ}{\mathbf{d}}_i + \overset{\circ}{\boldsymbol{\varphi}}_i \times \mathbf{s}_i$ , defined in (2.14)

$$\begin{aligned}
\frac{1}{2} \sum_i \overset{\circ}{\mathbf{d}}_i^T \overset{\circ}{\mathbf{d}}_i m_i &= \frac{1}{2} \sum_i \{(\overset{\circ}{\mathbf{d}}_i + \overset{\circ}{\boldsymbol{\varphi}}_i \times \mathbf{s}_i)^T (\overset{\circ}{\mathbf{d}}_i + \overset{\circ}{\boldsymbol{\varphi}}_i \times \mathbf{s}_i) m_i\} \\
&= \frac{1}{2} \sum_i \{\overset{\circ}{\mathbf{d}}_i^T \overset{\circ}{\mathbf{d}}_i + 2 \overset{\circ}{\mathbf{d}}_i^T (\overset{\circ}{\boldsymbol{\varphi}}_i \times \mathbf{s}_i) + (\overset{\circ}{\boldsymbol{\varphi}}_i \times \mathbf{s}_i)^T (\overset{\circ}{\boldsymbol{\varphi}}_i \times \mathbf{s}_i)\} m_i \\
&= \frac{1}{2} \sum_i \{\overset{\circ}{\mathbf{d}}_i^T \overset{\circ}{\mathbf{d}}_i + 2 \overset{\circ}{\mathbf{d}}_i^T (\overset{\circ}{\boldsymbol{\varphi}}_i \times \mathbf{s}_i) + \overset{\circ}{\boldsymbol{\varphi}}_i^T \text{sk}(\mathbf{s}_i)^T \text{sk}(\mathbf{s}_i) \overset{\circ}{\boldsymbol{\varphi}}_i\} m_i \quad .
\end{aligned} \tag{2.35}$$

The second term  $\frac{1}{2} \sum_i \overset{\circ}{\mathbf{d}}_i^T \overset{\circ}{\mathbf{d}}_i m_i$  and the fifth term  $\frac{1}{2} \sum_i \overset{\circ}{\boldsymbol{\varphi}}_i^T \mathbf{J}_i \overset{\circ}{\boldsymbol{\varphi}}_i$  of (2.34) with the expression for the local inertia tensor w.r.t to the grid point  $i$

$$\mathbf{J}_{g,i} = \mathbf{J}_i + \text{sk}(\mathbf{s}_i)^T \text{sk}(\mathbf{s}_i) m_i \tag{2.36}$$

can be written as follows

$$\begin{aligned}
& \frac{1}{2} \sum_i \overset{\circ}{\mathbf{d}}_i^T \overset{\circ}{\mathbf{d}}_i m_i + \frac{1}{2} \sum_i \overset{\circ}{\boldsymbol{\varphi}}_i^T \mathbf{J}_i \overset{\circ}{\boldsymbol{\varphi}}_i \\
&= \frac{1}{2} \sum_i \overset{\circ}{\mathbf{d}}_i^T \overset{\circ}{\mathbf{d}}_i m_i + \frac{1}{2} \sum_i 2 \overset{\circ}{\mathbf{d}}_i^T (\overset{\circ}{\boldsymbol{\varphi}}_i \times \mathbf{s}_i) m_i \\
&\quad + \frac{1}{2} \sum_i \overset{\circ}{\boldsymbol{\varphi}}_i^T \mathbf{J}_i \overset{\circ}{\boldsymbol{\varphi}}_i + \frac{1}{2} \sum_i \overset{\circ}{\boldsymbol{\varphi}}_i^T \text{sk}(\mathbf{s}_i)^T \text{sk}(\mathbf{s}_i) \overset{\circ}{\boldsymbol{\varphi}}_i m_i \\
&= \frac{1}{2} \sum_i \overset{\circ}{\mathbf{d}}_i^T m_i \mathbf{I} \overset{\circ}{\mathbf{d}}_i + \frac{1}{2} \sum_i 2 \overset{\circ}{\boldsymbol{\varphi}}_i^T (\mathbf{s}_i \times \overset{\circ}{\mathbf{d}}_i) m_i + \frac{1}{2} \sum_i \overset{\circ}{\boldsymbol{\varphi}}_i^T \mathbf{J}_{g,i} \overset{\circ}{\boldsymbol{\varphi}}_i \\
&= \frac{1}{2} \sum_i \overset{\circ}{\mathbf{d}}_i^T m_i \mathbf{I} \overset{\circ}{\mathbf{d}}_i + \frac{1}{2} \sum_i \overset{\circ}{\boldsymbol{\varphi}}_i^T \mathbf{J}_{g,i} \overset{\circ}{\boldsymbol{\varphi}}_i + \frac{1}{2} \sum_i \{ \overset{\circ}{\boldsymbol{\varphi}}_i^T \text{sk}(\mathbf{s}_i) m_i \overset{\circ}{\mathbf{d}}_i - \overset{\circ}{\mathbf{d}}_i^T \text{sk}(\mathbf{s}_i) m_i \overset{\circ}{\boldsymbol{\varphi}}_i \} \\
&= \frac{1}{2} \sum_i \begin{bmatrix} \overset{\circ}{\mathbf{d}}_i \\ \overset{\circ}{\boldsymbol{\varphi}}_i \end{bmatrix}^T \begin{bmatrix} m_i \mathbf{I} & m_i \text{sk}(\mathbf{s}_i)^T \\ m_i \text{sk}(\mathbf{s}_i) & \mathbf{J}_{g,i} \end{bmatrix} \begin{bmatrix} \overset{\circ}{\mathbf{d}}_i \\ \overset{\circ}{\boldsymbol{\varphi}}_i \end{bmatrix} . \tag{2.37}
\end{aligned}$$

The deformation is now written as a linear combination of the mode shapes  $\boldsymbol{\Phi}_{gE}$  (2.19). Hence (2.37) can be simplified to

$$\begin{aligned}
& \frac{1}{2} \overset{\circ}{\boldsymbol{\eta}}_E^T \sum_i \begin{bmatrix} \boldsymbol{\Phi}_{g_i E_t} \\ \boldsymbol{\Phi}_{g_i E_r} \end{bmatrix}^T \underbrace{\begin{bmatrix} m_i \mathbf{I} & m_i \text{sk}(\mathbf{s}_i)^T \\ m_i \text{sk}(\mathbf{s}_i) & \mathbf{J}_{g,i} \end{bmatrix}}_{\mathbf{M}_{gg_i}} \begin{bmatrix} \boldsymbol{\Phi}_{g_i E_t} \\ \boldsymbol{\Phi}_{g_i E_r} \end{bmatrix} \overset{\circ}{\boldsymbol{\eta}}_E \\
&= \frac{1}{2} \overset{\circ}{\boldsymbol{\eta}}_E^T \sum_i \boldsymbol{\Phi}_{g_i E}^T \mathbf{M}_{gg_i} \boldsymbol{\Phi}_{g_i E} \overset{\circ}{\boldsymbol{\eta}}_E \\
&= \frac{1}{2} \overset{\circ}{\boldsymbol{\eta}}_E^T \boldsymbol{\Phi}_{gE}^T \mathbf{M}_{gg} \boldsymbol{\Phi}_{gE} \overset{\circ}{\boldsymbol{\eta}}_E \\
&= \frac{1}{2} \overset{\circ}{\boldsymbol{\eta}}_E^T \mathbf{M}_{EE} \overset{\circ}{\boldsymbol{\eta}}_E \tag{2.38}
\end{aligned}$$

where  $\mathbf{M}_{gg}$  is the so-called physical mass matrix

$$\mathbf{M}_{gg} = \begin{bmatrix} \ddots & & & \\ & \mathbf{M}_{gg_i} & & \\ & & \ddots & \\ & & & \ddots \end{bmatrix} . \tag{2.39}$$

and  $\mathbf{M}_{EE}$  is the generalized mass matrix. Note that the mass matrix  $\mathbf{M}_{gg}$  incorporates all lumped masses and directly results from the FE-program.

Introducing the above developments into the formulation for the total kinetic energy (2.34) yields the final form

$$\begin{aligned}
E_{\text{kin}} &= \frac{1}{2} \mathbf{V}_b^T \mathbf{V}_b m + \frac{1}{2} \boldsymbol{\Omega}_b^T \mathbf{J} \boldsymbol{\Omega}_b + \frac{1}{2} \overset{\circ}{\boldsymbol{\eta}}_E^T \mathbf{M}_{EE} \overset{\circ}{\boldsymbol{\eta}}_E \\
&\quad + \boldsymbol{\Omega}_b^T \sum_i (\bar{\mathbf{d}}_i \times \overset{\circ}{\mathbf{d}}_i) m_i + \boldsymbol{\Omega}_b^T \sum_i \mathbf{J}_i \overset{\circ}{\boldsymbol{\varphi}}_i \quad . \tag{2.40}
\end{aligned}$$

## 2.2.2 Potential Energy

The potential energy consists of gravitational potential energy and elastic potential energy, that is potential energy stored as a result of the deformation.

For the formulation of the elastic potential energy the physical stiffness matrix of the elastic body is required [5, 44]. This stiffness matrix is obtained from the linear elastic structural finite element model and represents the total structural stiffness of the free-free flexible body. It can be written as follows:

$$\mathbf{K}_{gg} = \sum_m \mathbf{K}^{(m)} \quad (2.41)$$

where  $\mathbf{K}^{(m)}$  denotes the element stiffness matrices. The rows and columns of the stiffness matrix  $\mathbf{K}_{gg}$  correspond to the displacement vector  $\mathbf{u}_g$  (2.17).

The potential energy is then given by [8, 44]:

$$E_{\text{pot}} = - \underbrace{\sum_i (\mathbf{T}_{eb} \mathbf{R}_i)^T \mathbf{g}_e m_i}_{\text{gravitational pot. energy}} + \underbrace{\frac{1}{2} \mathbf{u}_g^T \mathbf{K}_{gg} \mathbf{u}_g}_{\text{elastic pot. energy}} \quad (2.42)$$

where  $\mathbf{g}_e$  is the constant gravitation vector resolved in the inertial frame.

$$\mathbf{g}_e = \begin{bmatrix} 0 & 0 & g \end{bmatrix}^T . \quad (2.43)$$

**Assumption 5.** *Gravity is constant over the airframe.*

The physical displacements  $\mathbf{u}_g$  are now expressed using the modal approach (2.19). The stiffness matrix can then be written in generalized form

$$\mathbf{K}_{EE} = \Phi_{gE}^T \mathbf{K}_{gg} \Phi_{gE} . \quad (2.44)$$

Hence the potential energy becomes:

$$E_{\text{pot}} = - \sum_i (\mathbf{T}_{eb} \mathbf{R}_i)^T \mathbf{g}_e m_i + \frac{1}{2} \boldsymbol{\eta}_E^T \mathbf{K}_{EE} \boldsymbol{\eta}_E . \quad (2.45)$$

Since linear elastic theory is assumed (Assumption 2) the stiffness matrix  $\mathbf{K}_{gg}$  does not depend on the structural deformation. Geometric nonlinearities are not considered in the context of this work.

With the vector  $\mathbf{R}_i$  (2.11a) (defining the location of the mass element) and recalling that the body frame is located in the momentary center of gravity (mean-axes frame, Appendix

A.2), hence  $\sum_i(\bar{\mathbf{r}}_i + \bar{\mathbf{d}}_i)m_i = \mathbf{0}$ , the potential energy (2.42) may be expanded to

$$\begin{aligned}
E_{\text{pot}} &= - \sum_i (\mathbf{R}_0 + \bar{\mathbf{r}}_i + \bar{\mathbf{d}}_i)^T \mathbf{T}_{eb}^T \mathbf{g}_e m_i + \frac{1}{2} \boldsymbol{\eta}_E^T \mathbf{K}_{EE} \boldsymbol{\eta}_E \\
&= - m \mathbf{R}_0^T \mathbf{T}_{be} \mathbf{g}_e + \frac{1}{2} \boldsymbol{\eta}_E^T \mathbf{K}_{EE} \boldsymbol{\eta}_E \\
&= - m \mathbf{R}_{0e}^T \mathbf{g}_e + \frac{1}{2} \boldsymbol{\eta}_E^T \mathbf{K}_{EE} \boldsymbol{\eta}_E \quad .
\end{aligned} \tag{2.46}$$

## 2.3 Virtual Work of Nonconservative Forces

The Lagrange's equations (2.21) require the formulation of the external forces. Conservative external forces are already accounted for in the formulation of the potential energy. The remaining nonconservative external forces and moments are the aerodynamic, thrust forces and other external forces. These will be written as load vector  $\mathbf{P}_g$  collecting the local forces and moments acting on each grid point:

$$\mathbf{P}_g = \begin{bmatrix} \vdots \\ \mathbf{P}_{g,i} \\ \vdots \end{bmatrix} = \begin{bmatrix} \vdots \\ \mathbf{F}_i \\ \mathbf{M}_i \\ \vdots \end{bmatrix} \quad . \tag{2.47}$$

The virtual work of the nonconservative forces  $\mathbf{F}_i$  and moments  $\mathbf{M}_i$  applied at the grid points  $i$  is then given by [37, 58]:

$$\delta W_{\text{nco}} = \sum_i \underbrace{(\delta \mathbf{R}_i)^T}_{\text{virt. displacement}} \mathbf{F}_i + \underbrace{(\delta \boldsymbol{\alpha} + \delta \boldsymbol{\varphi}_i)^T}_{\text{virt. rotation}} \mathbf{M}_i \tag{2.48}$$

where  $\delta \boldsymbol{\alpha}$  is the vector of virtual angular displacements of the body frame. Figure 2.3 shows the local forces and moments and the virtual displacements.

The virtual displacement of the grid point  $i$  may be written as follows [38, 58]:

$$\delta \mathbf{R}_{g,i} = \delta \mathbf{R}_0 + \text{sk}(\delta \boldsymbol{\alpha}) \mathbf{r}_i + \delta \mathbf{d}_i \quad . \tag{2.49}$$

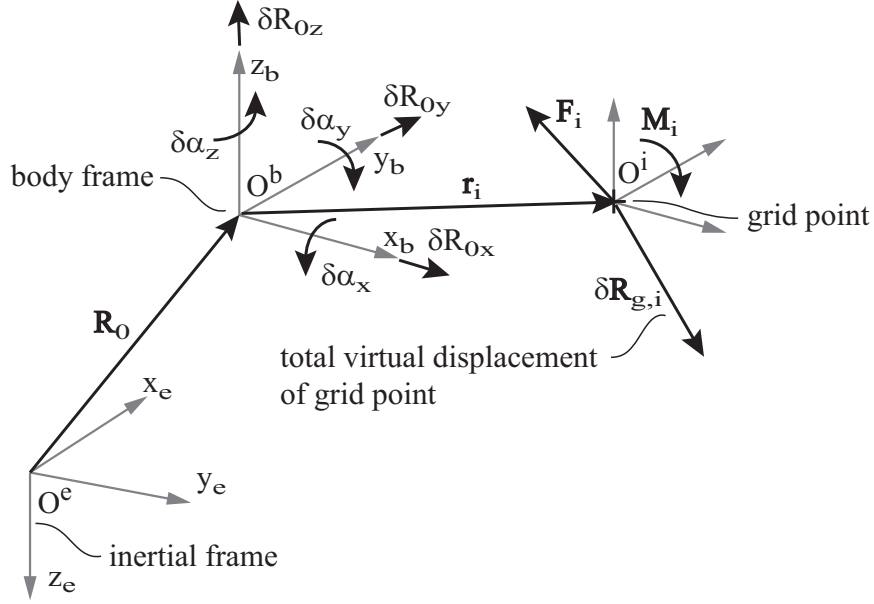


**Figure 2.3:** Virtual Displacements

Inserting (2.49) in (2.48) and applying the modal approach (2.19) yields

$$\begin{aligned}
 \delta W_{\text{nco}} &= \sum_i (\delta \mathbf{R}_0 + \text{sk}(\delta \boldsymbol{\alpha}) \mathbf{r}_i + \delta \mathbf{d}_i)^T \mathbf{F}_i + (\delta \boldsymbol{\alpha} + \delta \boldsymbol{\varphi}_i)^T \mathbf{M}_i \\
 &= \sum_i \delta \mathbf{R}_0^T \mathbf{F}_i + \delta \mathbf{d}_i^T \mathbf{F}_i + \delta \boldsymbol{\alpha}^T \text{sk}(\mathbf{r}_i) \mathbf{F}_i + \delta \boldsymbol{\alpha}^T \mathbf{M}_i + \delta \boldsymbol{\varphi}_i^T \mathbf{M}_i \\
 &= \begin{bmatrix} \delta \mathbf{R}_0^T & \delta \boldsymbol{\alpha}^T \end{bmatrix} \sum_i \underbrace{\begin{bmatrix} \mathbf{I} & \mathbf{0} \\ \text{sk}(\mathbf{r}_i) & \mathbf{I} \end{bmatrix}}_{\boldsymbol{\Phi}_{g_i R}^T} \begin{bmatrix} \mathbf{F}_i \\ \mathbf{M}_i \end{bmatrix} + \delta \boldsymbol{\eta}_E^T \sum_i \boldsymbol{\Phi}_{g_i E}^T \begin{bmatrix} \mathbf{F}_i \\ \mathbf{M}_i \end{bmatrix} . \quad (2.50)
 \end{aligned}$$

With the matrix of rigid body modes

$$\boldsymbol{\Phi}_{gR} = \begin{bmatrix} \vdots \\ \boldsymbol{\Phi}_{g_i R} \\ \vdots \end{bmatrix} = \begin{bmatrix} \vdots \\ (\boldsymbol{\Phi}_{g_i R}^T)_t \\ (\boldsymbol{\Phi}_{g_i R}^T)_r \\ \vdots \end{bmatrix} = \begin{bmatrix} \vdots & \vdots \\ \mathbf{I} & -\text{sk}(\mathbf{r}_i) \\ \mathbf{0} & \mathbf{I} \\ \vdots & \vdots \end{bmatrix} \quad (2.51)$$

representing form functions for unit translations and rotations along the aircraft body axes w.r.t the center of gravity the virtual work can be written as follows

$$\begin{aligned}
 \delta W_{\text{nco}} &= \begin{bmatrix} \delta \mathbf{R}_0^T & \delta \boldsymbol{\alpha}^T \end{bmatrix} \boldsymbol{\Phi}_{gR}^T \mathbf{P}_g + \delta \boldsymbol{\eta}_E^T \boldsymbol{\Phi}_{gE}^T \mathbf{P}_g \\
 &= \begin{bmatrix} \delta \mathbf{R}_{0e}^T \mathbf{T}_{eb} & \delta \boldsymbol{\Theta}^T \mathbf{D}^T \end{bmatrix} \boldsymbol{\Phi}_{gR}^T \mathbf{P}_g + \delta \boldsymbol{\eta}_E^T \boldsymbol{\Phi}_{gE}^T \mathbf{P}_g . \quad (2.52)
 \end{aligned}$$

Expansion of the above equation yields the final form of the virtual work

$$\delta W_{\text{nco}} = \delta \mathbf{R}_{0e}^T \underbrace{\mathbf{T}_{eb} (\boldsymbol{\Phi}_{g_i R}^T)_t \mathbf{P}_g}_{\mathbf{Q}_t} + \delta \boldsymbol{\Theta}^T \underbrace{\mathbf{D}^T (\boldsymbol{\Phi}_{g_i R}^T)_r \mathbf{P}_g}_{\mathbf{Q}_r} + \delta \boldsymbol{\eta}_E^T \underbrace{\boldsymbol{\Phi}_{gE}^T \mathbf{P}_g}_{\mathbf{Q}_E} . \quad (2.53)$$



The generalized nonconservative forces of (2.23) are now put in concrete terms.

## 2.4 Derivation of the Equations of Motion

In this section the equations of motion will be derived by applying Lagrange's equations (2.21). The required energy and virtual work terms are given in:

	Equation	Section
Kinetic Energy	(2.40)	2.2
Potential Energy	(2.46)	2.2
Virtual Work	(2.53)	2.3

The Lagrange's equations (2.21) consist of three vector equations, namely the force equation (2.21a), the moment equation (2.21b) and the elastic equation (2.21c). These will be successively derived in the following sections.

### 2.4.1 Force Equation

First the force equation (2.21a) is considered. Differentiation of the Lagrange Variable (2.22) yields:<sup>3</sup>

$$\frac{\partial \mathcal{L}}{\partial \mathbf{V}_b} = \mathbf{V}_b m \quad , \quad (2.54a)$$

$$\frac{d'}{dt} \left\{ \frac{\partial \mathcal{L}}{\partial \mathbf{V}_b} \right\} = \overset{\circ}{\mathbf{V}}_b m \quad , \quad (2.54b)$$

$$\mathbf{T}_{be} \frac{\partial \mathcal{L}}{\partial \mathbf{R}_{0e}} = m \mathbf{T}_{be} \mathbf{g}_e \quad . \quad (2.54c)$$

The generalized force  $\mathbf{Q}_t$  in (2.21a) is obtained from (2.53) as

$$\mathbf{Q}_t = \mathbf{T}_{eb} (\Phi_{g_i R})_t \mathbf{P}_g \quad . \quad (2.55)$$

Hence, the equations of motion for the translational degrees of freedom becomes

$$m \left[ \overset{\circ}{\mathbf{V}}_b + \boldsymbol{\Omega}_b \times \mathbf{V}_b - \mathbf{T}_{be} \mathbf{g}_e \right] = (\Phi_{g_R}^T)_t \mathbf{P}_g \quad (2.56)$$

where the right hand side of the equation  $(\Phi_{g_R}^T)_t \mathbf{P}_g$  represents the sum of all nonconservative external forces.

---

<sup>3</sup>See A.1 for some notes on vector differentiation

## 2.4.2 Moment Equation

Next the moment equation (2.21b) is developed. The derivatives of the Lagrange Variable are as follows:

$$\frac{\partial \mathcal{L}}{\partial \Omega_b} = \mathbf{J} \Omega_b + \underbrace{\sum_i \left( \bar{\mathbf{d}}_i \times \overset{\circ}{\mathbf{d}}_i \right) m_i + \sum_i \mathbf{J}_i \overset{\circ}{\varphi}_i}_{=\mathbf{h}} \quad , \quad (2.57a)$$

$$\frac{d'}{dt} \left\{ \frac{\partial \mathcal{L}}{\partial \Omega_b} \right\} = \mathbf{J} \overset{\circ}{\Omega}_b + \overset{\circ}{\mathbf{J}} \Omega_b + \underbrace{\sum_i \left( \bar{\mathbf{d}}_i \times \overset{\circ\circ}{\mathbf{d}}_i \right) m_i + \sum_i \mathbf{J}_i \overset{\circ\circ}{\varphi}_i}_{=\overset{\circ}{\mathbf{h}}} \quad , \quad (2.57b)$$

$$\frac{\partial \mathcal{L}}{\partial \Theta} = \mathbf{0} \quad . \quad (2.57c)$$

The generalized force  $\mathbf{Q}_r$  in (2.21b) is obtained from (2.53) as

$$\mathbf{Q}_r = \mathbf{D}^T (\Phi_{gR}^T)_r \mathbf{P}_g \quad . \quad (2.58)$$

Note that  $(\Phi_{gR}^T)_r \mathbf{P}_g$  is the resulting moment of the nonconservative external forces with respect to the center of gravity.

The equation of motion for the rotational degrees of freedom then is

$$\mathbf{J} \overset{\circ}{\Omega}_b + \Omega_b \times \mathbf{J} \Omega_b + \overset{\circ}{\mathbf{J}} \Omega_b + \overset{\circ}{\mathbf{h}} + \Omega_b \times \mathbf{h} = (\Phi_{gR}^T)_r \mathbf{P}_g \quad (2.59)$$

with

$$\mathbf{h} = \sum_i \left( \bar{\mathbf{d}}_i \times \overset{\circ}{\mathbf{d}}_i \right) m_i + \sum_i \mathbf{J}_i \overset{\circ}{\varphi}_i \quad , \quad (2.60a)$$

$$\overset{\circ}{\mathbf{h}} = \sum_i \left( \bar{\mathbf{d}}_i \times \overset{\circ\circ}{\mathbf{d}}_i \right) m_i + \sum_i \mathbf{J}_i \overset{\circ\circ}{\varphi}_i \quad (2.60b)$$

and the inertia tensor  $\mathbf{J}$  defined in (2.33).

The previous moment equation includes the inertial coupling terms  $\mathbf{h}$ ,  $\overset{\circ}{\mathbf{h}}$  and  $\mathbf{J}$ ,  $\overset{\circ}{\mathbf{J}}$  and may already be used for simulation. Note that one can obtain the formulation given by Buttrill [11] from the present moment equation (2.59), when mass offsets and elastic rotational degrees of freedoms are neglected.

The above moment equation has one drawback for simulation. The sums over all grid points in the terms  $\mathbf{h}$ ,  $\overset{\circ}{\mathbf{h}}$  and  $\mathbf{J}$ ,  $\overset{\circ}{\mathbf{J}}$  have to be recalculated at every time step. This can slow down the simulation rate significantly. Therefore it is desirable to eliminate the summation over the grid points in (2.59) by including the modal approach (in accordance with Assumption 4) in the inertial coupling terms. A generalized formulation of the inertial coupling terms is also

required for the derivation of the elastic equation, since the Lagrange's equations includes derivatives by the generalized elastic coordinates.

### Generalization of the Inertia Tensor

The inertia tensor for the deformed aircraft (2.33) used in the moment equation (2.59) will now be analyzed. For subsequent development of the elastic equation and for computational efficiency it is desirable to arrive at a form where only mode shapes have to be multiplied with a set of constant matrices and the summation over grid points is eliminated. Therefore the inertia tensor (2.33) is expanded to

$$\begin{aligned}
\mathbf{J} &= \sum_i \mathbf{J}_i - \sum_i \text{sk}(\bar{\mathbf{r}}_i + \bar{\mathbf{d}}_i)^2 m_i \\
&= \sum_i \mathbf{J}_i - \sum_i \text{sk}(\mathbf{s}_i + \mathbf{r}_i + \bar{\mathbf{d}}_i)^2 m_i \\
&= \sum_i \mathbf{J}_i - \sum_i \{ \text{sk}(\mathbf{s}_i)^2 + \text{sk}(\mathbf{r}_i + \bar{\mathbf{d}}_i)^2 + \text{sk}(\mathbf{s}_i)\text{sk}(\mathbf{r}_i + \bar{\mathbf{d}}_i) + \text{sk}(\mathbf{r}_i + \bar{\mathbf{d}}_i)\text{sk}(\mathbf{s}_i) \} m_i .
\end{aligned}$$

Since the local inertia tensor with respect to the grid point  $\mathbf{J}_{g,i}$  (2.36) is directly available in the system mass matrix (2.38), the following form will be used

$$\mathbf{J} = \sum_i \mathbf{J}_{g,i} - (\text{sk}(\mathbf{r}_i + \bar{\mathbf{d}}_i)^2 + \text{sk}(\mathbf{s}_i)\text{sk}(\mathbf{r}_i + \bar{\mathbf{d}}_i) + \text{sk}(\mathbf{r}_i + \bar{\mathbf{d}}_i)\text{sk}(\mathbf{s}_i)) m_i . \quad (2.61)$$

Full expansion yields

$$\begin{aligned}
\mathbf{J} &= \sum_i \mathbf{J}_{g,i} - \left( \underbrace{\sum_i \text{sk}(\mathbf{r}_i)^2 m_i}_{\mathbf{A1}} + \underbrace{\sum_i \text{sk}(\mathbf{d}_i)^2 m_i}_{\mathbf{A2}} + \underbrace{\sum_i \text{sk}(\text{sk}(\boldsymbol{\varphi}_i)\mathbf{s}_i)^2 m_i}_{\mathbf{A3}} \right. \\
&\quad + \underbrace{\sum_i \text{sk}(\mathbf{d}_i) \text{sk}(\text{sk}(\boldsymbol{\varphi}_i)\mathbf{s}_i) m_i}_{\mathbf{A4}} + \underbrace{\sum_i \text{sk}(\text{sk}(\boldsymbol{\varphi}_i)\mathbf{s}_i) \text{sk}(\mathbf{d}_i) m_i}_{\mathbf{A5}} \\
&\quad + \underbrace{\sum_i \text{sk}(\mathbf{r}_i) \text{sk}(\mathbf{d}_i) m_i}_{\mathbf{A6}} + \underbrace{\sum_i \text{sk}(\mathbf{r}_i) \text{sk}(\text{sk}(\boldsymbol{\varphi}_i)\mathbf{s}_i) m_i}_{\mathbf{A7}} \\
&\quad \left. + \underbrace{\sum_i \text{sk}(\mathbf{d}_i) \text{sk}(\mathbf{r}_i) m_i}_{\mathbf{A8}} + \underbrace{\sum_i \text{sk}(\text{sk}(\boldsymbol{\varphi}_i)\mathbf{s}_i) \text{sk}(\mathbf{r}_i) m_i}_{\mathbf{A9}} \right) . \quad (2.62)
\end{aligned}$$

The terms **A1** to **A9** of (2.62) are now expanded and the modal approach (2.19) is introduced.

- **A1** The **A1** term represents the Steiner-contribution from the grid point locations to

the total inertia tensor. It has the following elements

$$\mathbf{A1} = \sum_i \text{sk}(\mathbf{r}_i)^2 m_i = \begin{bmatrix} \sum_i (-\mathbf{r}_{iz}^2 - \mathbf{r}_{iy}^2) & \sum_i \mathbf{r}_{iy} \mathbf{r}_{ix} & \sum_i \mathbf{r}_{iz} \mathbf{r}_{ix} \\ & \sum_i (-\mathbf{r}_{iz}^2 - \mathbf{r}_{ix}^2) & \sum_i \mathbf{r}_{iz} \mathbf{r}_{iy} \\ \text{sym} & & \sum_i (-\mathbf{r}_{iy}^2 - \mathbf{r}_{ix}^2) \end{bmatrix} m_i \quad (2.63)$$

where all elements are time invariant and require no further development.

- **A2** Expansion of the symmetric matrix **A2** from (2.62) and introduction of the modal approach (2.19) yields the following form

$$\mathbf{A2} = \sum_i \text{sk}(\mathbf{d}_i)^2 m_i = \begin{bmatrix} \boldsymbol{\eta}_E^T \widetilde{\mathbf{A2}}_{11} \boldsymbol{\eta}_E & \boldsymbol{\eta}_E^T \widetilde{\mathbf{A2}}_{12} \boldsymbol{\eta}_E & \boldsymbol{\eta}_E^T \widetilde{\mathbf{A2}}_{13} \boldsymbol{\eta}_E \\ & \boldsymbol{\eta}_E^T \widetilde{\mathbf{A2}}_{22} \boldsymbol{\eta}_E & \boldsymbol{\eta}_E^T \widetilde{\mathbf{A2}}_{23} \boldsymbol{\eta}_E \\ \text{sym} & & \boldsymbol{\eta}_E^T \widetilde{\mathbf{A2}}_{33} \boldsymbol{\eta}_E \end{bmatrix} \quad (2.64)$$

where the  $(q \times q)$  time invariant sub-matrices  $\widetilde{\mathbf{A2}}_{jk}$  in (2.68) are as follows

$$\begin{aligned} \widetilde{\mathbf{A2}}_{11} &= \sum_i \left( -\boldsymbol{\Phi}_{g_{iz} E_t}^T \boldsymbol{\Phi}_{g_{iz} E_t} - \boldsymbol{\Phi}_{g_{iy} E_t}^T \boldsymbol{\Phi}_{g_{iy} E_t} \right) m_i \quad , \\ \widetilde{\mathbf{A2}}_{12} &= \sum_i \boldsymbol{\Phi}_{g_{iy} E_t}^T \boldsymbol{\Phi}_{g_{ix} E_t} m_i \quad , \\ \widetilde{\mathbf{A2}}_{13} &= \sum_i \boldsymbol{\Phi}_{g_{iz} E_t}^T \boldsymbol{\Phi}_{g_{ix} E_t} m_i \quad , \\ \widetilde{\mathbf{A2}}_{22} &= \sum_i \left( -\boldsymbol{\Phi}_{g_{iz} E_t}^T \boldsymbol{\Phi}_{g_{iz} E_t} - \boldsymbol{\Phi}_{g_{ix} E_t}^T \boldsymbol{\Phi}_{g_{ix} E_t} \right) m_i \quad , \\ \widetilde{\mathbf{A2}}_{23} &= \sum_i \boldsymbol{\Phi}_{g_{iz} E_t}^T \boldsymbol{\Phi}_{g_{iy} E_t} m_i \quad , \\ \widetilde{\mathbf{A2}}_{33} &= \sum_i \left( -\boldsymbol{\Phi}_{g_{iy} E_t}^T \boldsymbol{\Phi}_{g_{iy} E_t} - \boldsymbol{\Phi}_{g_{ix} E_t}^T \boldsymbol{\Phi}_{g_{ix} E_t} \right) m_i \end{aligned}$$

and  $\widetilde{\mathbf{A2}}_{jk} = \widetilde{\mathbf{A2}}_{kj}^T$ . The term (2.64) can be written in compact form

$$\mathbf{A2} = \sum_{j=1}^3 \sum_{k=1}^3 \boldsymbol{\eta}_E^T \widetilde{\mathbf{A2}}_{jk} \boldsymbol{\eta}_E \mathbf{e}_j \mathbf{e}_k^T \quad (2.66)$$

where  $\mathbf{e}$  denotes a unit vector

$$\mathbf{e}_1 = \begin{bmatrix} 1 \\ 0 \\ 0 \end{bmatrix} \quad , \quad \mathbf{e}_2 = \begin{bmatrix} 0 \\ 1 \\ 0 \end{bmatrix} \quad , \quad \mathbf{e}_3 = \begin{bmatrix} 0 \\ 0 \\ 1 \end{bmatrix} \quad . \quad (2.67)$$

For convenience and a more compact notation the following form will be used

$$\mathbf{A2} = \left\langle \boldsymbol{\eta}_E^T \widetilde{\mathbf{A2}}_{jk} \boldsymbol{\eta}_E \right\rangle \quad (2.68)$$

where the notation  $\langle \dots \rangle$  is introduced to shorten the summation over the matrix ele-

ments:

$$\langle (\dots)_{jk} \rangle = \sum_{j=1}^3 \sum_{k=1}^3 (\dots)_{jk} \mathbf{e}_j \mathbf{e}_k^T, \quad (2.69a)$$

$$\langle (\dots)_j \rangle = \sum_{j=1}^3 (\dots)_j \mathbf{e}_j. \quad (2.69b)$$

- **A3** The symmetric matrix **A3** in (2.62) can be expanded using the offset vector for the lumped mass  $\mathbf{s}_i = [s_{i_x} \ s_{i_y} \ s_{i_z}]^T$  and the modal approach (2.19) to the following form

$$\mathbf{A3} = \sum_i \text{sk}(\text{sk}(\boldsymbol{\varphi}_i) \mathbf{s}_i)^2 m_i = \sum_i \left( \text{sk} \begin{bmatrix} (s_{i_z} \boldsymbol{\Phi}_{g_{i_y} E_r} - s_{i_y} \boldsymbol{\Phi}_{g_{i_z} E_r}) \boldsymbol{\eta}_E \\ (s_{i_x} \boldsymbol{\Phi}_{g_{i_z} E_r} - s_{i_z} \boldsymbol{\Phi}_{g_{i_x} E_r}) \boldsymbol{\eta}_E \\ (s_{i_y} \boldsymbol{\Phi}_{g_{i_x} E_r} - s_{i_x} \boldsymbol{\Phi}_{g_{i_y} E_r}) \boldsymbol{\eta}_E \end{bmatrix} \right)^2 m_i. \quad (2.70)$$

Introducing the  $(3 \times q)$  matrix  $\mathbf{a}_i$  defined by

$$\mathbf{a}_i = \begin{bmatrix} \mathbf{a}_{i_1}^T & \mathbf{a}_{i_2}^T & \mathbf{a}_{i_3}^T \end{bmatrix}^T \quad (2.71)$$

with the  $(1 \times q)$  row vectors

$$\mathbf{a}_{i_1} = s_{i_z} \boldsymbol{\Phi}_{g_{i_y} E_r} - s_{i_y} \boldsymbol{\Phi}_{g_{i_z} E_r}, \quad (2.72a)$$

$$\mathbf{a}_{i_2} = s_{i_x} \boldsymbol{\Phi}_{g_{i_z} E_r} - s_{i_z} \boldsymbol{\Phi}_{g_{i_x} E_r}, \quad (2.72b)$$

$$\mathbf{a}_{i_3} = s_{i_y} \boldsymbol{\Phi}_{g_{i_x} E_r} - s_{i_x} \boldsymbol{\Phi}_{g_{i_y} E_r} \quad (2.72c)$$

in (2.73) yields

$$\mathbf{A3} = \sum_i (\text{sk}(\mathbf{a}_i \boldsymbol{\eta}_E))^2 m_i. \quad (2.73)$$

Further development of the above form gives the term **A3** in its fully generalized form:

$$\mathbf{A3} = \left\langle \boldsymbol{\eta}_E^T \widetilde{\mathbf{A3}}_{jk} \boldsymbol{\eta}_E \right\rangle \quad (2.74)$$

where the time invariant sub-matrices  $\widetilde{\mathbf{A3}}_{jk}$  are as follows:

$$\begin{aligned} \widetilde{\mathbf{A3}}_{11} &= \sum_i (-\mathbf{a}_{i_3}^T \mathbf{a}_{i_3} - \mathbf{a}_{i_2}^T \mathbf{a}_{i_2}) m_i, & \widetilde{\mathbf{A3}}_{12} &= \sum_i \mathbf{a}_{i_2}^T \mathbf{a}_{i_1} m_i, \\ \widetilde{\mathbf{A3}}_{13} &= \sum_i \mathbf{a}_{i_3}^T \mathbf{a}_{i_1} m_i, & \widetilde{\mathbf{A3}}_{22} &= \sum_i (-\mathbf{a}_{i_3}^T \mathbf{a}_{i_3} - \mathbf{a}_{i_1}^T \mathbf{a}_{i_1}) m_i, \\ \widetilde{\mathbf{A3}}_{23} &= \sum_i \mathbf{a}_{i_3}^T \mathbf{a}_{i_2} m_i, & \widetilde{\mathbf{A3}}_{33} &= \sum_i (-\mathbf{a}_{i_2}^T \mathbf{a}_{i_2} - \mathbf{a}_{i_1}^T \mathbf{a}_{i_1}) m_i \end{aligned}$$

and  $\widetilde{\mathbf{A3}}_{jk} = \widetilde{\mathbf{A3}}_{kj}^T$ .

- **A4** The non-symmetric matrix **A4** in (2.62) is given by

$$\begin{aligned} \mathbf{A4} &= \sum_i \text{sk}(\mathbf{d}_i) \text{sk}(\text{sk}(\boldsymbol{\varphi}_i) \mathbf{s}_i) m_i \\ &= \left\langle \boldsymbol{\eta}_E^T \widetilde{\mathbf{A4}}_{jk} \boldsymbol{\eta}_E \right\rangle \end{aligned} \quad (2.76)$$

with the following  $(q \times q)$  time invariant sub-matrices for  $\widetilde{\mathbf{A4}}_{jk}$

$$\begin{aligned} \widetilde{\mathbf{A4}}_{11} &= \sum_i \left( -\Phi_{g_{iz} E_t}^T \mathbf{a}_{i3} - \Phi_{g_{iy} E_t}^T \mathbf{a}_{i2} \right) m_i \quad , & \widetilde{\mathbf{A4}}_{12} &= \sum_i \Phi_{g_{iy} E_t}^T \mathbf{a}_{i1} m_i \quad , \\ \widetilde{\mathbf{A4}}_{13} &= \sum_i \Phi_{g_{iz} E_t}^T \mathbf{a}_{i1} m_i \quad , & \widetilde{\mathbf{A4}}_{21} &= \sum_i \Phi_{g_{iy} E_t}^T \mathbf{a}_{i2} m_i \quad , \\ \widetilde{\mathbf{A4}}_{22} &= \sum_i \left( -\Phi_{g_{iz} E_t}^T \mathbf{a}_{i3} - \Phi_{g_{ix} E_t}^T \mathbf{a}_{i1} \right) m_i \quad , & \widetilde{\mathbf{A4}}_{23} &= \sum_i \Phi_{g_{iz} E_t}^T \mathbf{a}_{i2} m_i \quad , \\ \widetilde{\mathbf{A4}}_{31} &= \sum_i \Phi_{g_{iz} E_t}^T \mathbf{a}_{i1} m_i \quad , & \widetilde{\mathbf{A4}}_{32} &= \sum_i \Phi_{g_{iz} E_t}^T \mathbf{a}_{i2} m_i \quad , \\ \widetilde{\mathbf{A4}}_{33} &= \sum_i \left( -\Phi_{g_{iy} E_t}^T \mathbf{a}_{i2} - \Phi_{g_{ix} E_t}^T \mathbf{a}_{i1} \right) m_i \quad . \end{aligned}$$

- **A5** The non-symmetric matrix **A5** in (2.62) can be related to the term **A4** by

$$\begin{aligned} \mathbf{A5} &= \sum_i \text{sk}(\text{sk}(\boldsymbol{\varphi}_i) \mathbf{s}_i) \text{sk}(\mathbf{d}_i) m_i \\ &= \sum_i (\text{sk}(\mathbf{d}_i) \text{sk}(\text{sk}(\boldsymbol{\varphi}_i) \mathbf{s}_i))^T m_i \\ &= (\mathbf{A4})^T \implies \widetilde{\mathbf{A5}}_{jk} = \widetilde{\mathbf{A4}}_{kj}^T \quad . \end{aligned} \quad (2.78)$$

Therefore the expression  $(\mathbf{A4} + \mathbf{A5})$  again is a symmetric matrix.

- **A6** The non-symmetric matrix **A6** in (2.62) is given by

$$\begin{aligned} \mathbf{A6} &= \sum_i \text{sk}(\mathbf{r}_i) \text{sk}(\mathbf{d}_i) m_i \\ &= \left\langle \widetilde{\mathbf{A6}}_{jk} \boldsymbol{\eta}_E \right\rangle \end{aligned} \quad (2.79)$$

with the following  $(1 \times q)$  row vectors for  $\widetilde{\mathbf{A6}}_{jk}$

$$\begin{aligned} \widetilde{\mathbf{A6}}_{11} &= \sum_i \left( -\mathbf{r}_{iz} \Phi_{g_{iz} E_t} - \mathbf{r}_{iy} \Phi_{g_{iy} E_t} \right) m_i \quad , & \widetilde{\mathbf{A6}}_{12} &= \sum_i \mathbf{r}_{iy} \Phi_{g_{ix} E_t} m_i \quad , \\ \widetilde{\mathbf{A6}}_{13} &= \sum_i \mathbf{r}_{iz} \Phi_{g_{ix} E_t} m_i \quad , & \widetilde{\mathbf{A6}}_{21} &= \sum_i \mathbf{r}_{ix} \Phi_{g_{iy} E_t} m_i \quad , \\ \widetilde{\mathbf{A6}}_{22} &= \sum_i \left( -\mathbf{r}_{iz} \Phi_{g_{iz} E_t} - \mathbf{r}_{ix} \Phi_{g_{ix} E_t} \right) m_i \quad , & \widetilde{\mathbf{A6}}_{23} &= \sum_i \mathbf{r}_{iz} \Phi_{g_{iy} E_t} m_i \quad , \\ \widetilde{\mathbf{A6}}_{31} &= \sum_i \mathbf{r}_{ix} \Phi_{g_{iz} E_t} m_i \quad , & \widetilde{\mathbf{A6}}_{32} &= \sum_i \mathbf{r}_{iy} \Phi_{g_{iz} E_t} m_i \quad , \\ \widetilde{\mathbf{A6}}_{33} &= \sum_i \left( -\mathbf{r}_{iy} \Phi_{g_{iy} E_t} - \mathbf{r}_{ix} \Phi_{g_{ix} E_t} \right) m_i \quad . \end{aligned}$$

- **A7** The non-symmetric matrix **A7** in (2.62) is given by

$$\begin{aligned} \mathbf{A7} &= \sum_i \text{sk}(\mathbf{r}_i) \text{sk}(\text{sk}(\boldsymbol{\varphi}_i) \mathbf{s}_i) m_i \\ &= \langle \widetilde{\mathbf{A7}}_{jk} \boldsymbol{\eta}_E \rangle \end{aligned} \quad (2.81)$$

with the following  $(1 \times q)$  row vectors for  $\widetilde{\mathbf{A7}}_{jk}$

$$\begin{aligned} \widetilde{\mathbf{A7}}_{11} &= \sum_i (-\mathbf{r}_{iz} \mathbf{a}_{i3} - \mathbf{r}_{iy} \mathbf{a}_{i2}) m_i \quad , & \widetilde{\mathbf{A7}}_{12} &= \sum_i \mathbf{r}_{iy} \mathbf{a}_{i1} m_i \quad , \\ \widetilde{\mathbf{A7}}_{13} &= \sum_i \mathbf{r}_{iz} \mathbf{a}_{i1} m_i \quad , & \widetilde{\mathbf{A7}}_{21} &= \sum_i \mathbf{r}_{ix} \mathbf{a}_{i2} m_i \quad , \\ \widetilde{\mathbf{A7}}_{22} &= \sum_i (-\mathbf{r}_{iz} \mathbf{a}_{i3} - \mathbf{r}_{ix} \mathbf{a}_{i1}) m_i \quad , & \widetilde{\mathbf{A7}}_{23} &= \sum_i \mathbf{r}_{iz} \mathbf{a}_{i2} m_i \quad , \\ \widetilde{\mathbf{A7}}_{31} &= \sum_i \mathbf{r}_{ix} \mathbf{a}_{i3} m_i \quad , & \widetilde{\mathbf{A7}}_{32} &= \sum_i \mathbf{r}_{iy} \mathbf{a}_{i3} m_i \quad , \\ \widetilde{\mathbf{A7}}_{33} &= \sum_i (-\mathbf{r}_{iy} \mathbf{a}_{i2} - \mathbf{r}_{ix} \mathbf{a}_{i1}) m_i \quad . \end{aligned}$$

- **A8** The non-symmetric matrix **A8** in (2.62) is given by

$$\mathbf{A8} = (\mathbf{A6})^\top = \langle \widetilde{\mathbf{A8}}_{jk} \boldsymbol{\eta}_E \rangle \implies \widetilde{\mathbf{A8}}_{jk} = \widetilde{\mathbf{A6}}_{kj} \quad . \quad (2.83)$$

Therefore  $(\mathbf{A6} + \mathbf{A8})$  again is a symmetric matrix.

- **A9** The non-symmetric matrix **A9** in (2.62) is given by

$$\mathbf{A9} = (\mathbf{A7})^\top = \langle \widetilde{\mathbf{A9}}_{jk} \boldsymbol{\eta}_E \rangle \implies \widetilde{\mathbf{A9}}_{jk} = \widetilde{\mathbf{A7}}_{kj} \quad . \quad (2.84)$$

The expression  $(\mathbf{A7} + \mathbf{A9})$  is then a symmetric matrix.

Inserting the terms **A1** (2.63) to **A9** (2.84) in equation (2.62) and defining:

$$\widetilde{\mathbf{B}}_{jk} = \widetilde{\mathbf{A2}}_{jk} + \widetilde{\mathbf{A3}}_{jk} + \widetilde{\mathbf{A4}}_{jk} + \widetilde{\mathbf{A4}}_{kj}^\top \quad \text{with} \quad \widetilde{\mathbf{B}}_{jk} = \widetilde{\mathbf{B}}_{kj}^\top \quad (q \times q) \quad \text{matrix} \quad , \quad (2.85a)$$

$$\widetilde{\mathbf{C}}_{jk} = \widetilde{\mathbf{A6}}_{jk} + \widetilde{\mathbf{A6}}_{kj} + \widetilde{\mathbf{A7}}_{jk} + \widetilde{\mathbf{A7}}_{kj} \quad \text{with} \quad \widetilde{\mathbf{C}}_{jk} = \widetilde{\mathbf{C}}_{kj} \quad (1 \times q) \quad \text{row vector} \quad (2.85b)$$

yields the final expression for the inertia tensor **J**:

$$\mathbf{J} = \sum_i \mathbf{J}_{g,i} - \mathbf{A1} - \begin{bmatrix} \boldsymbol{\eta}_E^\top \widetilde{\mathbf{B}}_{11} \boldsymbol{\eta}_E & \boldsymbol{\eta}_E^\top \widetilde{\mathbf{B}}_{12} \boldsymbol{\eta}_E & \boldsymbol{\eta}_E^\top \widetilde{\mathbf{B}}_{13} \boldsymbol{\eta}_E \\ & \boldsymbol{\eta}_E^\top \widetilde{\mathbf{B}}_{22} \boldsymbol{\eta}_E & \boldsymbol{\eta}_E^\top \widetilde{\mathbf{B}}_{23} \boldsymbol{\eta}_E \\ \text{sym} & & \boldsymbol{\eta}_E^\top \widetilde{\mathbf{B}}_{33} \boldsymbol{\eta}_E \end{bmatrix} - \begin{bmatrix} \widetilde{\mathbf{C}}_{11} \boldsymbol{\eta}_E & \widetilde{\mathbf{C}}_{12} \boldsymbol{\eta}_E & \widetilde{\mathbf{C}}_{13} \boldsymbol{\eta}_E \\ & \widetilde{\mathbf{C}}_{22} \boldsymbol{\eta}_E & \widetilde{\mathbf{C}}_{23} \boldsymbol{\eta}_E \\ \text{sym} & & \widetilde{\mathbf{C}}_{33} \boldsymbol{\eta}_E \end{bmatrix} \quad (2.86)$$

The above form may also be written in a compact expression

$$\mathbf{J} = \sum_i \mathbf{J}_{g,i} - \mathbf{A1} - \langle \boldsymbol{\eta}_E^\top \widetilde{\mathbf{B}}_{jk} \boldsymbol{\eta}_E \rangle - \langle \widetilde{\mathbf{C}}_{jk} \boldsymbol{\eta}_E \rangle \quad (2.87)$$

The time derivative  $\overset{\circ}{\mathbf{J}}$  can easily be obtained from (2.87) since the terms  $\sum_i \mathbf{J}_{g,i}$ ,  $\mathbf{A1}$ ,  $\tilde{\mathbf{B}}_{jk}$ ,  $\tilde{\mathbf{C}}_{jk}$  are time invariant. Hence  $\overset{\circ}{\mathbf{J}}$  becomes

$$\begin{aligned}\overset{\circ}{\mathbf{J}} &= -\langle \overset{\circ}{\boldsymbol{\eta}}_E^T \tilde{\mathbf{B}}_{jk} \boldsymbol{\eta}_E \rangle - \langle \boldsymbol{\eta}_E^T \tilde{\mathbf{B}}_{jk} \overset{\circ}{\boldsymbol{\eta}}_E \rangle - \langle \tilde{\mathbf{C}}_{jk} \overset{\circ}{\boldsymbol{\eta}}_E \rangle \\ &= -\langle \overset{\circ}{\boldsymbol{\eta}}_E^T (\tilde{\mathbf{B}}_{jk} + \tilde{\mathbf{B}}_{jk}^T) \boldsymbol{\eta}_E \rangle - \langle \tilde{\mathbf{C}}_{jk} \overset{\circ}{\boldsymbol{\eta}}_E \rangle \quad .\end{aligned}\quad (2.88)$$

The preceding equations for the inertia tensor and its time derivative are fully generalized, all physical values were expressed by modal coordinates and all sums over grid points are eliminated. Since all matrices, contained in the derived form, are constant they may be computed in pre-processing.

### Generalization of the $\mathbf{h}$ - Term

The  $\mathbf{h}$ -term is contained in the moment equation (2.59) and defined in (2.60) as:

$$\mathbf{h} = \sum_i \left( \bar{\mathbf{d}}_i \times \overset{\circ}{\bar{\mathbf{d}}}_i \right) m_i + \sum_i \mathbf{J}_i \overset{\circ}{\boldsymbol{\varphi}}_i \quad .$$

This term will now be analyzed.

With  $\bar{\mathbf{d}}_i = \mathbf{d}_i + \boldsymbol{\varphi}_i \times \mathbf{s}_i$  and  $\overset{\circ}{\bar{\mathbf{d}}}_i = \overset{\circ}{\mathbf{d}}_i + \overset{\circ}{\boldsymbol{\varphi}}_i \times \mathbf{s}_i$  in (2.60) the  $\mathbf{h}$ -term can be expanded to

$$\begin{aligned}\mathbf{h} &= \underbrace{\sum_i \mathbf{d}_i \times \overset{\circ}{\mathbf{d}}_i m_i}_{\mathbf{h1}} + \underbrace{\sum_i \mathbf{d}_i \times (\overset{\circ}{\boldsymbol{\varphi}}_i \times \mathbf{s}_i) m_i}_{\mathbf{h2}} + \underbrace{\sum_i (\boldsymbol{\varphi}_i \times \mathbf{s}_i) \times \overset{\circ}{\mathbf{d}}_i m_i}_{\mathbf{h3}} \\ &\quad + \underbrace{\sum_i (\boldsymbol{\varphi}_i \times \mathbf{s}_i) \times (\overset{\circ}{\boldsymbol{\varphi}}_i \times \mathbf{s}_i) m_i}_{\mathbf{h4}} + \underbrace{\sum_i \mathbf{J}_i \overset{\circ}{\boldsymbol{\varphi}}_i}_{\mathbf{h5}} \quad .\end{aligned}\quad (2.89)$$

Expansion of the preceding expression for  $\mathbf{h1}$  yields

$$\begin{aligned}\mathbf{h1} &= \begin{bmatrix} \boldsymbol{\eta}_E^T \sum_i (-\boldsymbol{\Phi}_{g_{iz} E_t}^T \boldsymbol{\Phi}_{g_{iy} E_t} + \boldsymbol{\Phi}_{g_{iy} E_t}^T \boldsymbol{\Phi}_{g_{iz} E_t}) m_i \overset{\circ}{\boldsymbol{\eta}}_E \\ \boldsymbol{\eta}_E^T \sum_i (+\boldsymbol{\Phi}_{g_{iz} E_t}^T \boldsymbol{\Phi}_{g_{ix} E_t} - \boldsymbol{\Phi}_{g_{ix} E_t}^T \boldsymbol{\Phi}_{g_{iz} E_t}) m_i \overset{\circ}{\boldsymbol{\eta}}_E \\ \boldsymbol{\eta}_E^T \sum_i (-\boldsymbol{\Phi}_{g_{iy} E_t}^T \boldsymbol{\Phi}_{g_{ix} E_t} + \boldsymbol{\Phi}_{g_{ix} E_t}^T \boldsymbol{\Phi}_{g_{iy} E_t}) m_i \overset{\circ}{\boldsymbol{\eta}}_E \end{bmatrix} \\ &= \langle \boldsymbol{\eta}_E^T \widetilde{\mathbf{h1}}_j \overset{\circ}{\boldsymbol{\eta}}_E \rangle\end{aligned}\quad (2.90)$$

note that  $\widetilde{\mathbf{h1}}_j = -\widetilde{\mathbf{h1}}_j^T$ .

The expanded term  $\mathbf{h2}$  may be expressed by

$$\begin{aligned}\mathbf{h2} &= - \begin{bmatrix} \overset{\circ}{\boldsymbol{\eta}}_E^T \sum_i (-\mathbf{a}_{i3}^T \boldsymbol{\Phi}_{g_{iy} E_t} + \mathbf{a}_{i2}^T \boldsymbol{\Phi}_{g_{iz} E_t}) m_i \boldsymbol{\eta}_E \\ \overset{\circ}{\boldsymbol{\eta}}_E^T \sum_i (+\mathbf{a}_{i3}^T \boldsymbol{\Phi}_{g_{ix} E_t} - \mathbf{a}_{i1}^T \boldsymbol{\Phi}_{g_{iz} E_t}) m_i \boldsymbol{\eta}_E \\ \overset{\circ}{\boldsymbol{\eta}}_E^T \sum_i (-\mathbf{a}_{i2}^T \boldsymbol{\Phi}_{g_{ix} E_t} + \mathbf{a}_{i1}^T \boldsymbol{\Phi}_{g_{iy} E_t}) m_i \boldsymbol{\eta}_E \end{bmatrix} \\ &= - \langle \overset{\circ}{\boldsymbol{\eta}}_E^T \widetilde{\mathbf{h2}}_j \boldsymbol{\eta}_E \rangle \quad .\end{aligned}\quad (2.91)$$



The term  $\mathbf{h3}$  can be written in a similar structure

$$\mathbf{h3} = \langle \boldsymbol{\eta}_E^T \widetilde{\mathbf{h3}}_j \overset{\circ}{\boldsymbol{\eta}}_E \rangle \quad \text{with} \quad \widetilde{\mathbf{h3}}_j = \widetilde{\mathbf{h2}}_j \quad . \quad (2.92)$$

Expansion of the expression for  $\mathbf{h4}$  yields

$$\mathbf{h4} = \langle \boldsymbol{\eta}_E^T \widetilde{\mathbf{h4}}_j \overset{\circ}{\boldsymbol{\eta}}_E \rangle \quad (2.93)$$

with

$$\begin{aligned} \widetilde{\mathbf{h4}}_1 &= \sum_i [+(\Phi_{g_{iz}E_r}^T \mathbf{s}_x - \Phi_{g_{ix}E_r}^T \mathbf{s}_z)(\Phi_{g_{ix}E_r} \mathbf{s}_y - \Phi_{g_{iy}E_r} \mathbf{s}_x) \\ &\quad -(\Phi_{g_{ix}E_r}^T \mathbf{s}_y - \Phi_{g_{iy}E_r}^T \mathbf{s}_x)(\Phi_{g_{iz}E_r} \mathbf{s}_x - \Phi_{g_{ix}E_r} \mathbf{s}_z)] m_i \quad , \\ \widetilde{\mathbf{h4}}_2 &= \sum_i [+(\Phi_{g_{ix}E_r}^T \mathbf{s}_y - \Phi_{g_{iy}E_r}^T \mathbf{s}_x)(\Phi_{g_{iy}E_r} \mathbf{s}_z - \Phi_{g_{iz}E_r} \mathbf{s}_y) \\ &\quad -(\Phi_{g_{iy}E_r}^T \mathbf{s}_z - \Phi_{g_{iz}E_r}^T \mathbf{s}_y)(\Phi_{g_{ix}E_r} \mathbf{s}_y - \Phi_{g_{iy}E_r} \mathbf{s}_x)] m_i \quad , \\ \widetilde{\mathbf{h4}}_3 &= \sum_i [+(\Phi_{g_{iy}E_r}^T \mathbf{s}_z - \Phi_{g_{iz}E_r}^T \mathbf{s}_y)(\Phi_{g_{iz}E_r} \mathbf{s}_x - \Phi_{g_{ix}E_r} \mathbf{s}_z) \\ &\quad -(\Phi_{g_{iz}E_r}^T \mathbf{s}_x - \Phi_{g_{ix}E_r}^T \mathbf{s}_z)(\Phi_{g_{iy}E_r} \mathbf{s}_z - \Phi_{g_{iz}E_r} \mathbf{s}_y)] m_i \end{aligned}$$

note that  $\widetilde{\mathbf{h4}}_j = -\widetilde{\mathbf{h4}}_j^T$ .

The term  $\mathbf{h5}$  can be written as follows

$$\mathbf{h5} = \sum_i \mathbf{J}_i \overset{\circ}{\boldsymbol{\varphi}}_i = \underbrace{\sum_i \mathbf{J}_i \Phi_{g_i E_r}}_{\widetilde{\mathbf{h5}}} \overset{\circ}{\boldsymbol{\eta}}_E \quad . \quad (2.94)$$

With the preceding expressions the  $\mathbf{h}$ -term can finally be written in the following form

$$\mathbf{h} = -\langle \overset{\circ}{\boldsymbol{\eta}}_E^T \widetilde{\mathbf{h2}}_j \boldsymbol{\eta}_E \rangle + \langle \boldsymbol{\eta}_E^T (\widetilde{\mathbf{h1}}_j + \widetilde{\mathbf{h2}}_j + \widetilde{\mathbf{h4}}_j) \overset{\circ}{\boldsymbol{\eta}}_E \rangle + \widetilde{\mathbf{h5}} \overset{\circ}{\boldsymbol{\eta}}_E \quad (2.95)$$

and the time derivative  $\overset{\circ}{\mathbf{h}}$ -term

$$\overset{\circ}{\mathbf{h}} = \langle \overset{\circ}{\boldsymbol{\eta}}_E^T (\widetilde{\mathbf{h1}}_j + \widetilde{\mathbf{h4}}_j) \overset{\circ}{\boldsymbol{\eta}}_E \rangle - \langle \overset{\circ\circ}{\boldsymbol{\eta}}_E^T \widetilde{\mathbf{h2}}_j \boldsymbol{\eta}_E \rangle + \langle \boldsymbol{\eta}_E^T (\widetilde{\mathbf{h1}}_j + \widetilde{\mathbf{h2}}_j + \widetilde{\mathbf{h4}}_j) \overset{\circ\circ}{\boldsymbol{\eta}}_E \rangle + \widetilde{\mathbf{h5}} \overset{\circ\circ}{\boldsymbol{\eta}}_E \quad . \quad (2.96)$$

The term (2.95) and its time derivative (2.96) will be used in the moment equation (2.59). All matrices in (2.95) and (2.96) can now be computed in pre-processing. During simulation only a multiplication with generalized coordinates is required.

### 2.4.3 Elastic Equation

The third equation in Lagrange's equations is the elastic equation (2.21c). Hereby the following derivatives are needed

$$\frac{d'}{dt} \left\{ \frac{\partial \mathcal{L}}{\partial \dot{\boldsymbol{\eta}}_E} \right\} = \frac{d'}{dt} \left\{ \frac{\partial T_{\text{kin}}}{\partial \dot{\boldsymbol{\eta}}_E} - \frac{\partial T_{\text{pot}}}{\partial \dot{\boldsymbol{\eta}}_E} \right\} , \quad (2.97a)$$

$$\frac{\partial \mathcal{L}}{\partial \boldsymbol{\eta}_E} = \frac{\partial T_{\text{kin}}}{\partial \boldsymbol{\eta}_E} - \frac{\partial T_{\text{pot}}}{\partial \boldsymbol{\eta}_E} . \quad (2.97b)$$

The generalized force  $\mathbf{Q}_E$  in (2.21c) is obtained from (2.53) as

$$\mathbf{Q}_E = \boldsymbol{\Phi}_{gE}^T \mathbf{P}_g . \quad (2.98)$$

With the expression for the kinetic energy (2.40) and the  $\mathbf{h}$ -term (2.95) the derivative  $\frac{\partial T_{\text{kin}}}{\partial \dot{\boldsymbol{\eta}}_E}$  (2.97a) becomes

$$\frac{\partial T_{\text{kin}}}{\partial \dot{\boldsymbol{\eta}}_E} = \frac{\partial}{\partial \dot{\boldsymbol{\eta}}_E} \left\{ \frac{1}{2} \mathbf{V}_b^T \mathbf{V}_b m + \frac{1}{2} \boldsymbol{\Omega}_b^T \mathbf{J} \boldsymbol{\Omega}_b + \frac{1}{2} \dot{\boldsymbol{\eta}}_E^T \mathbf{M}_{EE} \dot{\boldsymbol{\eta}}_E + \boldsymbol{\Omega}_b^T \mathbf{h} \right\} \quad (2.99)$$

$$= \mathbf{M}_{EE} \dot{\boldsymbol{\eta}}_E + \frac{\partial}{\partial \dot{\boldsymbol{\eta}}_E} \left\{ \boldsymbol{\Omega}_b^T \mathbf{h} \right\} \quad (2.100)$$

where the  $\mathbf{h}$ -term (2.95) may be written in the following form

$$\mathbf{h} = \sum_{j=1}^3 \left( -\dot{\boldsymbol{\eta}}_E^T \widetilde{\mathbf{h}}_2 \boldsymbol{\eta}_E + \boldsymbol{\eta}_E^T (\widetilde{\mathbf{h}}_1 + \widetilde{\mathbf{h}}_2 + \widetilde{\mathbf{h}}_4) \dot{\boldsymbol{\eta}}_E \right) \mathbf{e}_j + \widetilde{\mathbf{h}}_5 \dot{\boldsymbol{\eta}}_E . \quad (2.101)$$

Then the derivative (2.99) can be expressed as follows

$$\begin{aligned} \frac{\partial T_{\text{kin}}}{\partial \dot{\boldsymbol{\eta}}_E} &= \mathbf{M}_{EE} \dot{\boldsymbol{\eta}}_E \\ &+ \frac{\partial}{\partial \dot{\boldsymbol{\eta}}_E} \left\{ \sum_{j=1}^3 \left( -\dot{\boldsymbol{\eta}}_E^T \widetilde{\mathbf{h}}_2 \boldsymbol{\eta}_E + \boldsymbol{\eta}_E^T (\widetilde{\mathbf{h}}_1 + \widetilde{\mathbf{h}}_2 + \widetilde{\mathbf{h}}_4) \dot{\boldsymbol{\eta}}_E \right) \boldsymbol{\Omega}_b^T \mathbf{e}_j + \boldsymbol{\Omega}_b^T \widetilde{\mathbf{h}}_5 \dot{\boldsymbol{\eta}}_E \right\} \end{aligned} \quad (2.102)$$

applying the differentiation  $\frac{\partial}{\partial \dot{\boldsymbol{\eta}}_E}$  in (2.102) yields

$$\frac{\partial T_{\text{kin}}}{\partial \dot{\boldsymbol{\eta}}_E} = \mathbf{M}_{EE} \dot{\boldsymbol{\eta}}_E + \sum_{j=1}^3 \underbrace{\left( \widetilde{\mathbf{h}}_1^T - \widetilde{\mathbf{h}}_2^T + \widetilde{\mathbf{h}}_2^T + \widetilde{\mathbf{h}}_4^T \right)}_{\widetilde{\mathbf{h}}_j} \boldsymbol{\eta}_E \boldsymbol{\Omega}_b^T \mathbf{e}_j + \widetilde{\mathbf{h}}_5^T \boldsymbol{\Omega}_b \quad (2.103)$$

where the term

$$\widetilde{\mathbf{h}}_j = \widetilde{\mathbf{h}}_1^T - \widetilde{\mathbf{h}}_2^T + \widetilde{\mathbf{h}}_2^T + \widetilde{\mathbf{h}}_4^T \quad (2.104)$$

is introduced to simplify the expression.

Next the derivative of the potential energy (2.97a) is considered. It simply becomes

$$\frac{\partial T_{\text{pot}}}{\partial \dot{\boldsymbol{\eta}}_E} = 0 \quad . \quad (2.105)$$

The additional derivative  $\frac{d'}{dt}$  applied on (2.103) yields

$$\frac{d'}{dt} \left\{ \frac{\partial \mathcal{L}}{\partial \dot{\boldsymbol{\eta}}_E} \right\} = \mathbf{M}_{EE} \ddot{\boldsymbol{\eta}}_E + \sum_{j=1}^3 \tilde{\mathbf{h}}_j \left( \dot{\boldsymbol{\eta}}_E \boldsymbol{\Omega}_b^T + \boldsymbol{\eta}_E \dot{\boldsymbol{\Omega}}_b^T \right) \mathbf{e}_j + \tilde{\mathbf{h}}_5^T \dot{\boldsymbol{\Omega}}_b \quad . \quad (2.106)$$

The derivative  $\frac{\partial T_{\text{kin}}}{\partial \boldsymbol{\eta}_E}$  (2.97b) is considered next

$$\begin{aligned} \frac{\partial T_{\text{kin}}}{\partial \boldsymbol{\eta}_E} &= \frac{\partial}{\partial \boldsymbol{\eta}_E} \left\{ \frac{1}{2} \mathbf{V}_b^T \mathbf{V}_b m + \frac{1}{2} \boldsymbol{\Omega}_b^T \mathbf{J} \boldsymbol{\Omega}_b + \frac{1}{2} \dot{\boldsymbol{\eta}}_E^T \mathbf{M}_{EE} \dot{\boldsymbol{\eta}}_E + \boldsymbol{\Omega}_b^T \mathbf{h} \right\} \\ &= \frac{1}{2} \frac{\partial}{\partial \boldsymbol{\eta}_E} \{ \boldsymbol{\Omega}_b^T \mathbf{J} \boldsymbol{\Omega}_b \} + \frac{\partial}{\partial \boldsymbol{\eta}_E} \{ \boldsymbol{\Omega}_b^T \mathbf{h} \} \end{aligned} \quad (2.107)$$

where the first term can be written as follows

$$\begin{aligned} \frac{\partial}{\partial \boldsymbol{\eta}_E} \{ \boldsymbol{\Omega}_b^T \mathbf{J} \boldsymbol{\Omega}_b \} &= - \frac{\partial}{\partial \boldsymbol{\eta}_E} \sum_{j=1}^3 \sum_{k=1}^3 \left( \boldsymbol{\eta}_E^T \tilde{\mathbf{B}}_{jk} \boldsymbol{\eta}_E + \tilde{\mathbf{C}}_{jk} \boldsymbol{\eta}_E \right) (\boldsymbol{\Omega}_b^T \mathbf{e}_j \mathbf{e}_k^T \boldsymbol{\Omega}_b) \\ &= - \sum_{j=1}^3 \sum_{k=1}^3 \left( (\tilde{\mathbf{B}}_{jk} + \tilde{\mathbf{B}}_{jk}^T) \boldsymbol{\eta}_E + \tilde{\mathbf{C}}_{jk}^T \right) (\boldsymbol{\Omega}_b^T \mathbf{e}_j \mathbf{e}_k^T \boldsymbol{\Omega}_b) \end{aligned} \quad (2.108)$$

and the second term is given by

$$\begin{aligned} \frac{\partial}{\partial \boldsymbol{\eta}_E} \{ \boldsymbol{\Omega}_b^T \mathbf{h} \} &= \frac{\partial}{\partial \boldsymbol{\eta}_E} \left\{ \sum_{j=1}^3 \left( - \dot{\boldsymbol{\eta}}_E^T \tilde{\mathbf{h}}_{2j} \boldsymbol{\eta}_E + \boldsymbol{\eta}_E^T (\tilde{\mathbf{h}}_{1j} + \tilde{\mathbf{h}}_{2j} + \tilde{\mathbf{h}}_{4j}) \dot{\boldsymbol{\eta}}_E \right) \boldsymbol{\Omega}_b^T \mathbf{e}_j + \boldsymbol{\Omega}_b^T \tilde{\mathbf{h}}_5 \dot{\boldsymbol{\eta}}_E \right\} \\ &= \sum_{j=1}^3 \underbrace{\left( \tilde{\mathbf{h}}_{1j} - \tilde{\mathbf{h}}_{2j}^T + \tilde{\mathbf{h}}_{2j} + \tilde{\mathbf{h}}_{4j} \right)}_{\tilde{\mathbf{h}}_j^T} \dot{\boldsymbol{\eta}}_E \boldsymbol{\Omega}_b^T \mathbf{e}_j \quad . \end{aligned} \quad (2.109)$$

The derivative  $\frac{\partial T_{\text{pot}}}{\partial \boldsymbol{\eta}_E}$  (2.97b) becomes

$$\frac{\partial T_{\text{pot}}}{\partial \boldsymbol{\eta}_E} = \mathbf{K}_{EE} \boldsymbol{\eta}_E \quad . \quad (2.110)$$

Incorporating the preceding derivatives into the elastic equations of motion yields

$$\begin{aligned}
& \mathbf{M}_{EE} \ddot{\boldsymbol{\eta}}_E + \mathbf{K}_{EE} \boldsymbol{\eta}_E \\
& + \sum_{j=1}^3 \tilde{\mathbf{h}}_j \left( \dot{\boldsymbol{\eta}}_E \boldsymbol{\Omega}_b^T + \boldsymbol{\eta}_E \dot{\boldsymbol{\Omega}}_b^T \right) \mathbf{e}_j + \tilde{\mathbf{h}}_5^T \dot{\boldsymbol{\Omega}}_b \\
& + \frac{1}{2} \sum_{j=1}^3 \sum_{k=1}^3 \left( (\tilde{\mathbf{B}}_{jk} + \tilde{\mathbf{B}}_{jk}^T) \boldsymbol{\eta}_E + \tilde{\mathbf{C}}_{jk}^T \right) \boldsymbol{\Omega}_b^T \mathbf{e}_j \mathbf{e}_k^T \boldsymbol{\Omega}_b \\
& - \sum_{j=1}^3 \tilde{\mathbf{h}}_j^T \dot{\boldsymbol{\eta}}_E \boldsymbol{\Omega}_b^T \mathbf{e}_j = \boldsymbol{\Phi}_{gE}^T \mathbf{P}_g \quad . \quad (2.111)
\end{aligned}$$

So far, structural damping has been neglected since physical damping can not be provided for industrial aeroelastic models. It is therefore common practice to introduce damping via the diagonal modal damping matrix [5]:

$$\mathbf{B}_{EE} = 2 \begin{bmatrix} \ddots & & \\ & \zeta_i & \\ & & \ddots \end{bmatrix} (\mathbf{M}_{EE} \mathbf{K}_{EE})^{1/2} \quad (2.112)$$

with the modal damping parameter  $\zeta_i$ . These parameters are available from ground vibration tests of the airframe.

Introduction of (2.112) in (2.111) yields the final form of the elastic equation with generalized coupling terms:

$$\begin{aligned}
& \mathbf{M}_{EE} \ddot{\boldsymbol{\eta}}_E + \mathbf{B}_{EE} \dot{\boldsymbol{\eta}}_E + \mathbf{K}_{EE} \boldsymbol{\eta}_E \\
& + \underbrace{\left( \sum_{j=1}^3 \tilde{\mathbf{h}}_j \boldsymbol{\eta}_E \mathbf{e}_j^T + \tilde{\mathbf{h}}_5^T \right)}_{\text{due to angular acc. of the body frame}} \dot{\boldsymbol{\Omega}}_b + \underbrace{2 \sum_{j=1}^3 \tilde{\mathbf{h}}_j \dot{\boldsymbol{\eta}}_E \mathbf{e}_j^T \boldsymbol{\Omega}_b}_{\text{Coriolis term}} \\
& + \frac{1}{2} \sum_{j=1}^3 \sum_{k=1}^3 \underbrace{\left( (\tilde{\mathbf{B}}_{jk} + \tilde{\mathbf{B}}_{jk}^T) \boldsymbol{\eta}_E + \tilde{\mathbf{C}}_{jk}^T \right)}_{\text{centrifugal loading on the elastic modes}} \boldsymbol{\Omega}_b^T \mathbf{e}_j \mathbf{e}_k^T \boldsymbol{\Omega}_b = \boldsymbol{\Phi}_{gE}^T \mathbf{P}_g \quad . \quad (2.113)
\end{aligned}$$

## 2.5 Validation of the Modal Form

In the previous sections the equations of motion are derived. Inertial coupling terms, contained in the moment and the elastic equation, are derived in a fully generalized form. The generalized form of the coupling terms is now validated by comparison with the physical form.

All modal coupling components are also included in the modal form of the inertia tensor and the h-term. Therefore the physical form of the inertia tensor and h-term can be used to validate the generalization process. Table 2.1 summarizes the respective equations.

	inertia tensor	h-term
equation in physical form	(2.33)	(2.60)
equation in generalized form	(2.87)	(2.95)

**Table 2.1:** Equations for physical and modal form of the inertia tensor and the h-term

The physical and modal forms are numerically compared for test cases. The results are given in Appendix B. It is found that errors are of the order of the machine accuracy.

## 2.6 Inertially Uncoupled Equations of Motion

Inertially decoupled equations of motion as derived by Waszak [69] can be obtained from the inertially coupled equations of motion by introducing additional assumptions in the formulation:

**Assumption 6.** *The inertia tensor of the aircraft  $J$  is constant, i.e. the inertia forces act in the undeformed condition.*

**Assumption 7.** *The inertial cross coupling between the overall and the elastic motion represented by the term  $\mathbf{h} = \sum_i (\bar{\mathbf{d}}_i \times \dot{\bar{\mathbf{d}}}_i) m_i + \sum_i \mathbf{J}_i \dot{\varphi}_i$  (2.60) is small and may be neglected.*

The equations (2.56), (2.59), (2.113) then simplify to:

$$m \left[ \overset{\circ}{\mathbf{V}}_b + \boldsymbol{\Omega}_b \times \mathbf{V}_b - \mathbf{T}_{be} \mathbf{g}_e \right] = (\boldsymbol{\Phi}_{gR}^T)_t \mathbf{P}_g \quad , \quad (2.114a)$$

$$\mathbf{J} \overset{\circ}{\boldsymbol{\Omega}}_b + \boldsymbol{\Omega}_b \times \mathbf{J} \boldsymbol{\Omega}_b = (\boldsymbol{\Phi}_{gR}^T)_r \mathbf{P}_g \quad \text{with} \quad \mathbf{J} = \text{const} \quad , \quad (2.114b)$$

$$\mathbf{M}_{EE} \overset{\circ\circ}{\boldsymbol{\eta}}_E + \mathbf{B}_{EE} \overset{\circ}{\boldsymbol{\eta}}_E + \mathbf{K}_{EE} \boldsymbol{\eta}_E = \boldsymbol{\Phi}_{gE}^T \mathbf{P}_g \quad . \quad (2.114c)$$

## 2.7 Application to a Beam Model

A beam model example will be used to demonstrate the effect of the internal coupling on the simulation of an elastic system and to show the capability of the presented equations of motion.

Consider a simple plain model as shown in Figure 2.4 consisting of two massless Euler-Bernoulli beams (length  $l_0$ , cross section  $A$ , Young's modulus  $E$ , geometric moments of inertia  $I$ ) attached to a central mass ( $m_2, J_2$ ). Two additional masses are located at each end of the beam ( $m_1, J_1; m_3, J_3$ ). All model data is given in Appendix C (element properties Tables C.1, C.2 and respective mass and stiffness matrices (C.2),(C.3)). A modal damping parameter  $\zeta = 0.05$ , (2.112) is included in the formulation.

The body fixed coordinate frame  $b$  is located in the center of gravity (location of mass  $m_2$ ) where the  $y$ -axis is aligned with the elastic axis of the undeformed beams. The body fixed frame  $b$  is aligned with the inertial reference frame  $e$  in the initial condition. In this simple planar example the kinematic equations (2.5) are given by  $\dot{\phi} = p$ .

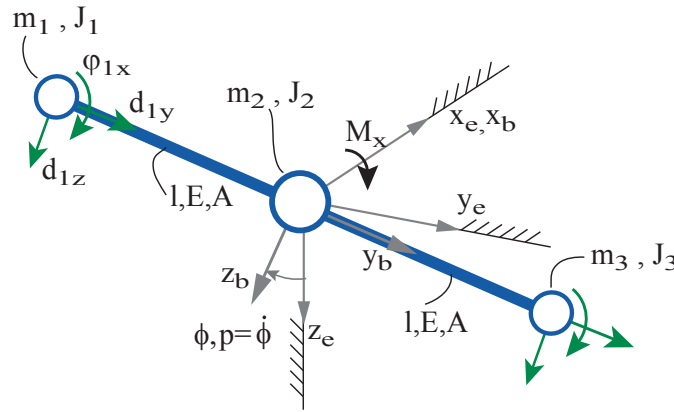


**Figure 2.4:** Structural model for the simple example

The elastic deformation for the planar example is then given by the displacement vector

$$\mathbf{u}_g = \begin{bmatrix} d_{1y} & d_{1z} & \varphi_{1x} & d_{2y} & d_{2z} & \varphi_{2x} & d_{3y} & d_{3z} & \varphi_{3x} \end{bmatrix}$$

and expressed by generalized coordinates  $\boldsymbol{\eta}_E$  using the modal approach (2.19),  $\mathbf{u}_g = \boldsymbol{\Phi}_{gE} \boldsymbol{\eta}_E$ . The elastic modes shapes  $\boldsymbol{\Phi}_{gE}$  are obtained from a free-free modal analysis of the FE-model ((C.2),(C.3)) of the Euler-Bernoulli beams. The numerical values of  $\boldsymbol{\Phi}_{gE}$  are given in (C.4).

The system is subjected to an external moment  $M_x$  applied at the central mass. Its variation

with time is given by

$$M_x(t) = \begin{cases} 20 \text{ Nm} : & 0\text{s} \leq t < 0.5\text{s} \\ 0 \text{ Nm} : & t \geq 0.5\text{s} \end{cases} . \quad (2.115)$$

Then the simulation is performed using:

- Internally coupled equations of motion ((2.56), (2.59), (2.113)).
- Internally uncoupled equations of motion ((2.114)).
- An analytical reference solution for the quasi-steady situation implying that the elastic velocity and acceleration are zero, see Figure 2.5.

Note that equations ((2.56), (2.59), (2.113)) can be simplified for the planar example to a moment equation

$$\begin{aligned} & \left( (J_1 + J_2 + J_3) + (m_1 + m_3)l_0^2 - \boldsymbol{\eta}_E^T \widetilde{\mathbf{A}}\mathbf{2}_{11}\boldsymbol{\eta}_E - 2\widetilde{\mathbf{A}}\mathbf{6}_{11}\boldsymbol{\eta}_E \right) \dot{p} \\ & - \left( \overset{\circ}{\boldsymbol{\eta}}_E^T (\widetilde{\mathbf{A}}\mathbf{2}_{11} + \widetilde{\mathbf{A}}\mathbf{2}_{11}^T)\boldsymbol{\eta}_E + 2\widetilde{\mathbf{A}}\mathbf{6}_{11} \overset{\circ}{\boldsymbol{\eta}}_E \right) p \\ & + \overset{\circ}{\boldsymbol{\eta}}_E^T \widetilde{\mathbf{h}}\mathbf{1}_1 \overset{\circ}{\boldsymbol{\eta}}_E + \boldsymbol{\eta}_E^T \widetilde{\mathbf{h}}\mathbf{1}_1 \overset{\circ\circ}{\boldsymbol{\eta}}_E + \widetilde{\mathbf{h}}\mathbf{5}_1 \overset{\circ}{\boldsymbol{\eta}}_E = M_x \end{aligned}$$

and an elastic equation

$$\begin{aligned} & \mathbf{M}_{EE} \overset{\circ\circ}{\boldsymbol{\eta}}_E + \mathbf{B}_{EE} \overset{\circ}{\boldsymbol{\eta}}_E + \mathbf{K}_{EE}\boldsymbol{\eta}_E \\ & + \left( \widetilde{\mathbf{h}}\mathbf{1}_1^T \boldsymbol{\eta}_E + \widetilde{\mathbf{h}}\mathbf{5}_1^T \right) \dot{p} + 2\widetilde{\mathbf{h}}\mathbf{1}_1^T \overset{\circ}{\boldsymbol{\eta}}_E p + \frac{1}{2} \left( (\widetilde{\mathbf{A}}\mathbf{2}_{11} + \widetilde{\mathbf{A}}\mathbf{2}_{11}^T)\boldsymbol{\eta}_E + 2\widetilde{\mathbf{A}}\mathbf{6}_{11}^T \right) p^2 = \boldsymbol{\Phi}_{g_{2x}E_r}^T M_x . \end{aligned}$$

The kinematic equations (2.5) simplify to

$$\dot{\phi} = p .$$

### 2.7.1 Discussion of the Beam Model

Figure 2.6(a) depicts the time history of the applied moment and the resulting angular velocity of the body frame. Due to the rotation of the system the total inertia tensor increases resulting in a slightly decreased rotational velocity obtained by the inertially coupled formulation. Equation (2.124) is used to compute the analytical solution.

The trajectories of the left grid point (node 1) are shown in Figure 2.6(b). The inertial observer sees a perfect circular trajectory for the uncoupled equations and a slightly increased radius for the coupled equations caused by the elongation of the beams. At  $t = 2\text{s}$  the node (uncoupled equations) is in an advanced position due to the higher rotational velocity of the

A simple analytical solution for the elongation can be derived for the quasi-steady situation considering a beam subjected to an axial force.

The centrifugal force of a mass rotating with angular velocity  $p$  at the distance  $l_0 + \Delta l$  of the rotation center is given by

$$F_{\text{centr}} = m_1 p^2 (l_0 + \Delta l) \quad . \quad (2.116)$$

The beam element stress is then given by the force per area and by the Young's modulus  $E$  and the strain  $\epsilon$ :

$$\sigma = \frac{F_{\text{centr}}}{A} = E\epsilon \quad . \quad (2.117)$$

The strain is the elastic elongation  $\Delta l$  per initial length  $l_0$ :

$$\epsilon = \frac{\Delta l}{l_0} \quad . \quad (2.118)$$

With (2.117) and (2.118) the centrifugal force is:

$$F_{\text{centr}} = EA \frac{\Delta l}{l_0} \quad . \quad (2.119)$$

Combining (2.116) and (2.119) one obtains for the elongation

$$\Delta l = \frac{mp^2 l_0^2}{EA - ml_0 p^2} \quad . \quad (2.120)$$

The rotational momentum of the system is given by

$$H_r = \int_0^t M(t) dt = Jp \quad , \quad (2.121)$$

where the total inertia simply is

$$J = J_1 + J_2 + J_3 + 2m_1(l_0 + \Delta l)^2 \quad . \quad (2.122)$$

With (2.122) and (2.120) in (2.121) the equation for the rotational velocity is

$$H_r = (J_1 + J_2 + J_3)p + 2m_1 \left[ l_0 + \frac{mp^2 l_0^2}{EA - ml_0 p^2} \right]^2 p \quad (2.123)$$

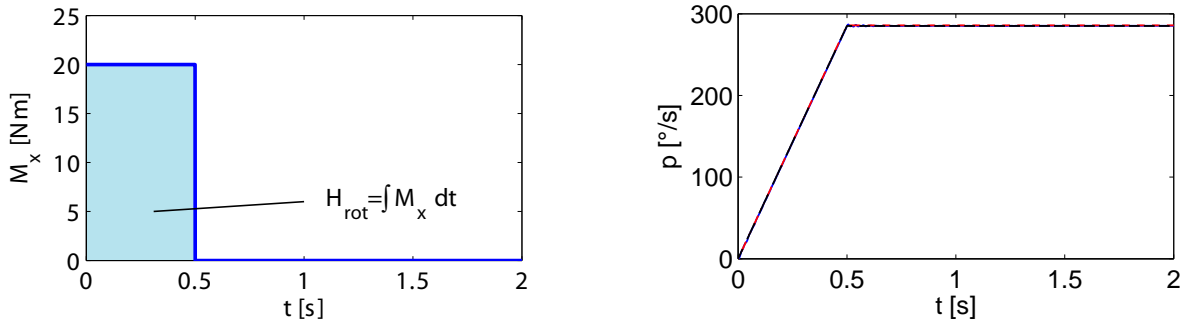
or in polynomial form

$$\begin{aligned} & [(J_1 + J_2 + J_3) m_1^2 l_0^2] p^5 - [m_1^2 l_0^2 H_r] p^4 - [2(J_1 + J_2 + J_3) EA m_1 l_0] p^3 \\ & + [2 H_r EA m_1 l_0] p^2 + [E^2 A^2 (J_1 + J_2 + J_3 + 2m_1 l_0^2)] p - [H_r E^2 A^2] = 0 \quad . \quad (2.124) \end{aligned}$$

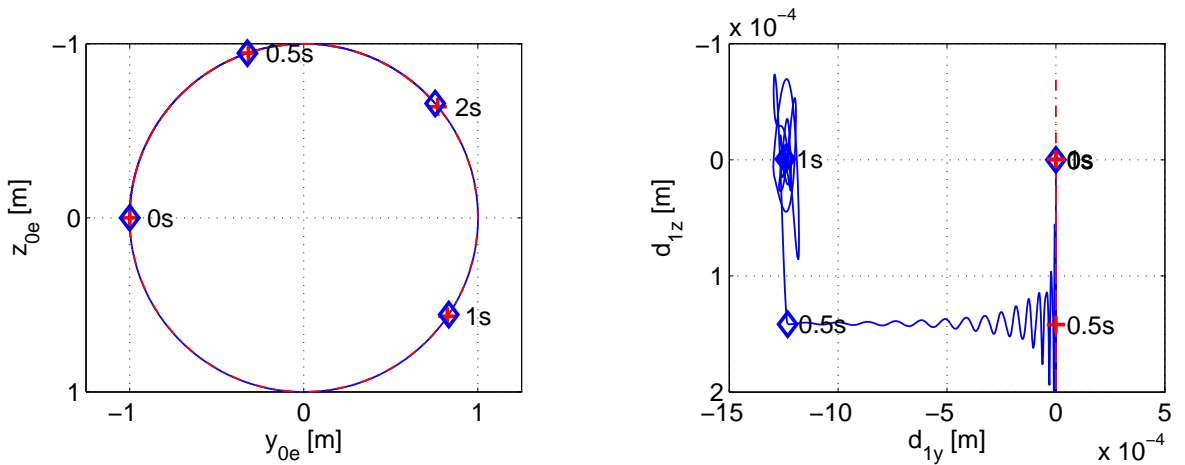
For  $t = 2\text{s}$  one obtains from (2.124) the physically relevant solution:  $p = 285.2^\circ/\text{s}$ . Equation (2.120) yields the elastic elongation of the beam element:  $\underline{\underline{\Delta l = 1.2\text{ mm}}}$ .

**Figure 2.5:** Quasi-steady One Dimensional Analytical Solution

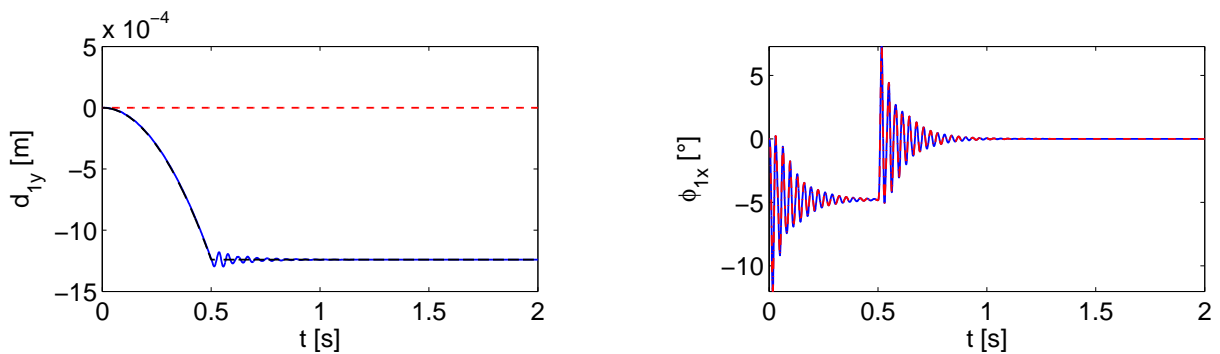




(a) Left: Applied external Moment. Right: Angular velocity of body frame (— coupled; - - - uncoupled; - - - quasi-steady)



(b) Trajectories of left node (Grid Point 1). Left: Inertial observer; Right: Observer moving with the body frame. ( $\diamond$  coupled;  $\cdot$  - + - uncoupled)



(c) Displacements at left node (Grid Point 1); (— coupled; - - - uncoupled; - - - quasi-steady)

**Figure 2.6:** Simulation Results for the Beam Model

body frame. The moving observer clearly notices the change in the radial coordinate caused by the centrifugal force. Elastic displacements are depicted in Figure 2.6(c).

Looking at the local rotation of the node (Figure 2.6(c)), both uncoupled and coupled equations, yield identical results since the rotation is primarily driven by the applied moment. However, looking at the elongation of the beam the inertially coupled equations yield an elongation varying around the analytical solution for the quasi-steady situation (2.120). Ap-

parently uncoupled equations are not capable of representing the elastic elongation due to the rotation of the body frame. This simple example shows the necessity of the inertial coupling terms for a physically correct solution.

## 2.8 Summary of the Results

The equations of motion for an elastic aircraft in flight are derived using Lagrange's equations in terms of quasi-coordinates. The equations are given for a system with discrete masses, rotational degrees of freedom and offsets of masses from grid points. Therefore available data from FE-models used in industrial loads and aeroelastic analysis can be incorporated directly.

The equations include all inertial coupling terms. The inertia tensor for the deformed aircraft and the additional  $h$ -term provide the coupling of the moment equation with the elastic equation. The forces from angular accelerations of the body frame, Coriolis forces and the centrifugal loading on the elastic modes provide the coupling of the elastic equation with the moment equation.

All coupling terms are cast into a generalized matrix form where all sums over grid points are eliminated for computational efficiency. The modal form is validated by the comparison with the physical form. The required matrices can be assembled in pre-processing from available FE-data (only the physical mass matrix and the free vibration mode shapes are needed). Operations during simulation are thus reduced to multiplications with generalized coordinates.

### Equations of Motion

Force equation (2.56):

$$m \left[ \overset{\circ}{\mathbf{V}}_b + \boldsymbol{\Omega}_b \times \mathbf{V}_b - \mathbf{T}_{be} \mathbf{g}_e \right] = (\boldsymbol{\Phi}_{gR}^T)_t \mathbf{P}_g \quad .$$

Moment equation (2.59):

$$\mathbf{J} \overset{\circ}{\boldsymbol{\Omega}}_b + \boldsymbol{\Omega}_b \times \mathbf{J} \boldsymbol{\Omega}_b + \overset{\circ}{\mathbf{J}} \boldsymbol{\Omega}_b + \overset{\circ}{\mathbf{h}} + \boldsymbol{\Omega}_b \times \mathbf{h} = (\boldsymbol{\Phi}_{gR}^T)_r \mathbf{P}_g \quad ,$$

with:  $\mathbf{J}$  (2.87),  $\overset{\circ}{\mathbf{J}}$  (2.88),  $\mathbf{h}$  (2.95),  $\overset{\circ}{\mathbf{h}}$  (2.96).

Elastic equation (2.113):

$$\begin{aligned} & \mathbf{M}_{EE} \overset{\circ\circ}{\boldsymbol{\eta}}_E + \mathbf{B}_{EE} \overset{\circ}{\boldsymbol{\eta}}_E + \mathbf{K}_{EE} \boldsymbol{\eta}_E \\ & + \left( \sum_{j=1}^3 \tilde{\mathbf{h}}_j \boldsymbol{\eta}_E \mathbf{e}_j^T + \tilde{\mathbf{h}}\mathbf{5}^T \right) \overset{\circ}{\boldsymbol{\Omega}}_b + 2 \sum_{j=1}^3 \tilde{\mathbf{h}}_j \overset{\circ}{\boldsymbol{\eta}}_E \mathbf{e}_j^T \boldsymbol{\Omega}_b \\ & + \frac{1}{2} \sum_{j=1}^3 \sum_{k=1}^3 \left( (\tilde{\mathbf{B}}_{jk} + \tilde{\mathbf{B}}_{jk}^T) \boldsymbol{\eta}_E + \tilde{\mathbf{C}}_{jk}^T \right) \boldsymbol{\Omega}_b^T \mathbf{e}_j \mathbf{e}_k^T \boldsymbol{\Omega}_b = \boldsymbol{\Phi}_{gE}^T \mathbf{P}_g \quad , \end{aligned}$$

with:  $\tilde{\mathbf{h}}_j$  (2.104),  $\tilde{\mathbf{h}}\mathbf{5}$  (2.94),  $\tilde{\mathbf{B}}_{jk}$ ,  $\tilde{\mathbf{C}}_{jk}$  (2.85).

Kinematic equations (2.5):

$$\begin{aligned} \dot{\boldsymbol{\Theta}} &= \mathbf{D}^{-1} \boldsymbol{\Omega}_b \quad , \\ \dot{\mathbf{R}}_{0e} &= \mathbf{T}_{be}^{-1} \mathbf{V}_b \quad . \end{aligned}$$

State space form:

$$\begin{aligned} \dot{\mathbf{x}} &= f(\mathbf{x}, \mathbf{P}_g) \quad , \\ \text{with: } \mathbf{x}^T &= \left[ \mathbf{R}_{0e}^T \quad \boldsymbol{\Theta}^T \quad \mathbf{V}_b^T \quad \boldsymbol{\Omega}_b^T \quad \boldsymbol{\eta}_E^T \quad \overset{\circ}{\boldsymbol{\eta}}_E^T \right] \quad . \end{aligned}$$

**Assumption 1.** *The aircraft is described as a collection of lumped mass elements, with an associated mass and inertia tensor.*

**Assumption 2.** *Linear elastic theory applies.*

**Assumption 3.** *Local translational and rotational elastic deformations with respect to the reference shape are small.*

**Assumption 4.** *Orthogonal mode shapes resulting from a free-free modal analysis are available. The deformation of the airplane may be written as a linear combination of the mode shapes, i.e. the modal approach will be used.*

**Assumption 5.** *Gravity is constant over the airframe.*

**Figure 2.7:** Summary of the Equations of Motion

### 3 Equations of Structural Loads

Flight loads analysis is concerned with the determination of loads acting on the airframe in flight due to maneuvering or atmospheric turbulence. Prior to the computations of loads a simulation is performed based on generalized differential equations resulting in trajectories for the generalized coordinates. In the previous chapter the underlying generalized equations of motion are derived. Hereby, the generalized approach based on Lagrange's equations in terms of quasi-coordinates is chosen for simplicity and efficiency.

Now the task is the calculation of loads at local structural points based on the known trajectories of generalized coordinates. This recovery of loads requires the formulation of the dynamic equilibrium of forces at the nodal level. Therefore the principle of momentum is necessary for the derivation of the loads equation.

Loads computation considering aeroelastic effects is already described in Bisplinghoff [8]. It is shown that the methods for the loads computation can be divided into two main groups. Firstly, approaches that recover the loads directly from the structural deformation (modal displacements) and secondly, approaches based on the principle of momentum, hence the equilibrium of forces (force summation). Convergence studies of the force summation and mode displacement methods [47, 8, 28, 45] show a superior convergence behavior (as a function of the number of modes taken into account) of the force summation method. Therefore it is desirable to derive a force summation method suitable for inertially coupled equations of motion, derived in Chapter 2.

In this chapter the two approaches (based on modal displacements and the summation of forces) will be applied to the results from the inertially coupled equations of motion. A new force summation method, consistent to the assumptions made during the equation development is formulated.

### 3.1 Deformation Approach

The deformation approach or Mode Displacement Method (MDM) [8, 15, 17, 28, 45, 14, 47] directly recovers the elastic nodal forces from the elastic deformation of the airframe. Figure 3.1 depicts the nodal displacements and the elastic interconnection.

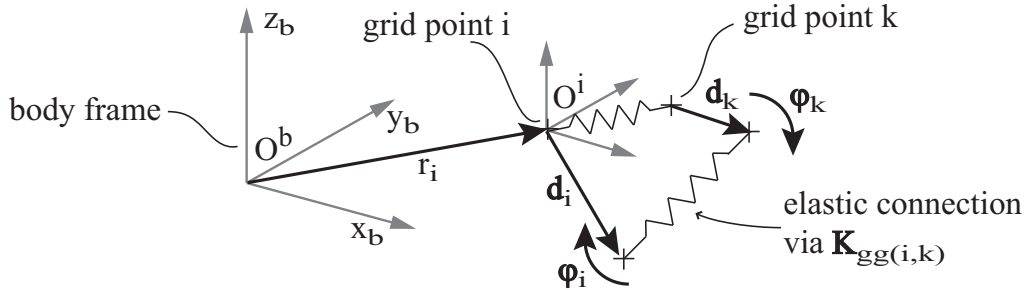


**Figure 3.1:** Translational elastic deformation  $\mathbf{d}_i$  and rotational elastic deformation  $\varphi_i$  at grid point i and its elastic connection

The elastic displacements (2.17) are multiplied with the physical stiffness matrix (2.41), representing the elastic connection to other grid points, to yield the elastic forces:

$$\mathbf{L}^{\text{MDM}} = \mathbf{K}_{gg} \begin{bmatrix} \vdots \\ \mathbf{d}_i \\ \varphi_i \\ \vdots \end{bmatrix} = \mathbf{K}_{gg} \mathbf{u}_g \quad . \quad (3.1)$$

The physical displacements at each grid point  $\mathbf{d}_i, \varphi_i$  (Figure 3.1) are recovered from the generalized displacements using the modal approach (2.19). With the modal approach the Mode Displacement Method can be written as follows:

$$\begin{aligned} \mathbf{L}^{\text{MDM}} &= \mathbf{K}_{gg} \mathbf{\Phi}_{gE} \boldsymbol{\eta}_E \\ &= \mathbf{K}_{gE} \boldsymbol{\eta}_E \quad . \end{aligned} \quad (3.2)$$

The Mode Displacement Method only requires modal elastic displacements. It contains no assumption regarding inertial coupling and can therefore be applied to the inertially coupled and uncoupled equations of motion or to aeroelastic systems in the above form. For the inertially coupled equations of motion, derived in the present thesis, generalized displacements  $\boldsymbol{\eta}_E$  are given by the elastic equation (2.113).

## 3.2 Momentum Approach

The momentum approach is used to derive a force summation method (FSM) from first principles. First the general formulation is derived using the assumptions made for the inertially coupled equations of motion. As a spin-off result the Force Summation Method for inertially uncoupled equations of motion (2.114) and the known formulation for aeroelastic systems [8] will be formulated based on the general formulation.

### 3.2.1 General Formulation

In order to derive the loads equation for a free flying flexible aircraft with inertially coupled equations of motion one has to start with the principle of momentum, also known as method of Newton Euler.

The equations of Newton-Euler are given by [22]:

$$\frac{d}{dt} \begin{bmatrix} \mathbf{H}_{t,i} \\ \mathbf{H}_{r,i} \end{bmatrix} = \begin{bmatrix} \mathbf{F}_i \\ \mathbf{M}_i \end{bmatrix} \quad (3.3)$$

where  $\mathbf{H}_{t,i}$ ,  $\mathbf{H}_{r,i}$  denotes the translational and the rotational momentum vector and  $\mathbf{F}_i$ ,  $\mathbf{M}_i$  are the total forces and moments with respect to the location of the mass  $i$ .

The linear and angular momentum of the lumped mass  $i$  (left hand side of (3.3)) may be written as follows [22]

$$\begin{bmatrix} \mathbf{H}_{t,i} \\ \mathbf{H}_{r,i} \end{bmatrix} = \begin{bmatrix} m_i \mathbf{I} & \mathbf{0} \\ \mathbf{0} & \mathbf{J}_i \end{bmatrix} \begin{bmatrix} \dot{\mathbf{R}}_i \\ \dot{\boldsymbol{\Omega}}_i \end{bmatrix} \quad (3.4)$$

where the velocity  $\dot{\mathbf{R}}_i$  and the rotational velocity  $\dot{\boldsymbol{\Omega}}_i$  of the lumped mass  $i$  is defined in (2.14) and (2.16). The time derivative of the momentum (3.4) is given by:

$$\frac{d}{dt} \begin{bmatrix} \mathbf{H}_{t,i} \\ \mathbf{H}_{r,i} \end{bmatrix} = \begin{bmatrix} m_i \ddot{\mathbf{R}}_i \\ \mathbf{J}_i (\dot{\boldsymbol{\Omega}}_b + \ddot{\boldsymbol{\varphi}}_i) + \text{sk}(\boldsymbol{\Omega}_b) \mathbf{J}_i (\boldsymbol{\Omega}_b + \dot{\boldsymbol{\varphi}}_i) \end{bmatrix} \quad (3.5)$$

The resulting force and moment at the grid point  $\mathbf{F}_i$ ,  $\mathbf{M}_i$  (right hand side of (3.3)) is expanded to elastic forces  $\mathbf{P}_{g,i}^{el}$ , gravity forces  $\mathbf{G}_i$ , and other external forces  $\mathbf{P}_{gt,i}$ :

$$\begin{bmatrix} \mathbf{F}_i \\ \mathbf{M}_i \end{bmatrix} = \begin{bmatrix} \mathbf{P}_{gt,i} \\ \mathbf{P}_{gr,i} \end{bmatrix} + \begin{bmatrix} \mathbf{P}_{gt,i}^{el} \\ \mathbf{P}_{gr,i}^{el} \end{bmatrix} + \begin{bmatrix} \mathbf{0} \\ -\text{sk}(\mathbf{s}_i) (\mathbf{P}_{gt,i} + \mathbf{P}_{gt,i}^{el}) \end{bmatrix} + \begin{bmatrix} \mathbf{G}_i \\ \mathbf{0} \end{bmatrix} \quad (3.6)$$

Figure 3.2 depicts the respective forces and moments. Note that  $\mathbf{s}_i$  represents the mass offset (see Figure 3.2). Therefore the term  $-\text{sk}(\mathbf{s}_i) (\mathbf{P}_{gt,i} + \mathbf{P}_{gt,i}^{el})$  is the moment due to the forces

$\mathbf{P}_{gt,i} + \mathbf{P}_{gt,i}^{el}$  acting at the grid point location with respect to the location of the mass element.

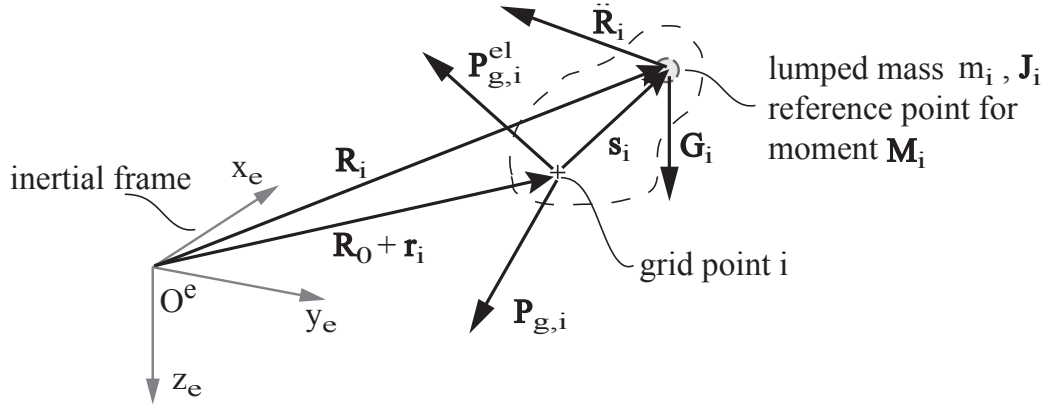


**Figure 3.2:** External and elastic forces at a grid point  $i$

With the external forces (3.6) and the time derivative of the momentum (3.5) the equations of Newton Euler (3.3) can be written in the following form:

$$\begin{aligned} \begin{bmatrix} m_i \ddot{\mathbf{R}}_i \\ \mathbf{J}_i(\dot{\boldsymbol{\Omega}}_b + \ddot{\boldsymbol{\varphi}}_i) + \text{sk}(\boldsymbol{\Omega}_b) \mathbf{J}_i(\boldsymbol{\Omega}_b + \dot{\boldsymbol{\varphi}}_i) \end{bmatrix} &= \begin{bmatrix} \mathbf{P}_{gt,i} \\ \mathbf{P}_{gr,i} \end{bmatrix} + \begin{bmatrix} \mathbf{P}_{gt,i}^{el} \\ \mathbf{P}_{gr,i}^{el} \end{bmatrix} \\ &+ \begin{bmatrix} \mathbf{0} \\ -\text{sk}(\mathbf{s}_i)(\mathbf{P}_{gt,i} + \mathbf{P}_{gt,i}^{el}) \end{bmatrix} + \begin{bmatrix} \mathbf{G}_i \\ \mathbf{0} \end{bmatrix} . \end{aligned} \quad (3.7)$$

Further development of the above equation yields:

$$\begin{aligned} \begin{bmatrix} m_i \ddot{\mathbf{R}}_i \\ \mathbf{J}_i(\dot{\boldsymbol{\Omega}}_b + \ddot{\boldsymbol{\varphi}}_i) + \text{sk}(\boldsymbol{\Omega}_b) \mathbf{J}_i(\boldsymbol{\Omega}_b + \dot{\boldsymbol{\varphi}}_i) \end{bmatrix} &= \begin{bmatrix} \mathbf{I} & \mathbf{0} \\ -\text{sk}(\mathbf{s}_i) & \mathbf{I} \end{bmatrix} \left( \begin{bmatrix} \mathbf{P}_{gt,i} \\ \mathbf{P}_{gr,i} \end{bmatrix} + \begin{bmatrix} \mathbf{P}_{gt,i}^{el} \\ \mathbf{P}_{gr,i}^{el} \end{bmatrix} \right) + \begin{bmatrix} \mathbf{G}_i \\ \mathbf{0} \end{bmatrix} \\ \Leftrightarrow \begin{bmatrix} \mathbf{I} & \mathbf{0} \\ \text{sk}(\mathbf{s}_i) & \mathbf{I} \end{bmatrix} \begin{bmatrix} m_i \ddot{\mathbf{R}}_i \\ \mathbf{J}_i(\dot{\boldsymbol{\Omega}}_b + \ddot{\boldsymbol{\varphi}}_i) + \text{sk}(\boldsymbol{\Omega}_b) \mathbf{J}_i(\boldsymbol{\Omega}_b + \dot{\boldsymbol{\varphi}}_i) \end{bmatrix} &= \begin{bmatrix} \mathbf{P}_{gt,i} \\ \mathbf{P}_{gr,i} \end{bmatrix} + \begin{bmatrix} \mathbf{P}_{gt,i}^{el} \\ \mathbf{P}_{gr,i}^{el} \end{bmatrix} + \begin{bmatrix} \mathbf{I} & \mathbf{0} \\ \text{sk}(\mathbf{s}_i) & \mathbf{I} \end{bmatrix} \begin{bmatrix} \mathbf{G}_i \\ \mathbf{0} \end{bmatrix} \\ \Leftrightarrow \begin{bmatrix} m_i \ddot{\mathbf{R}}_i \\ m_i \text{sk}(\mathbf{s}_i) \ddot{\mathbf{R}}_i + \mathbf{J}_i(\dot{\boldsymbol{\Omega}}_b + \ddot{\boldsymbol{\varphi}}_i) + \text{sk}(\boldsymbol{\Omega}_b) \mathbf{J}_i(\boldsymbol{\Omega}_b + \dot{\boldsymbol{\varphi}}_i) \end{bmatrix} &= \begin{bmatrix} \mathbf{P}_{gt,i} \\ \mathbf{P}_{gr,i} \end{bmatrix} + \begin{bmatrix} \mathbf{P}_{gt,i}^{el} \\ \mathbf{P}_{gr,i}^{el} \end{bmatrix} + \begin{bmatrix} m_i \mathbf{I} & \mathbf{0} \\ m_i \text{sk}(\mathbf{s}_i) & \mathbf{I} \end{bmatrix} \begin{bmatrix} \mathbf{T}_{be} \mathbf{g}_e \\ \mathbf{0} \end{bmatrix} \end{aligned} \quad (3.8)$$

where the gravitational force on the mass element  $i$  is expressed by (2.43)

$$\mathbf{G}_i = m_i \mathbf{T}_{be} \mathbf{g}_e . \quad (3.9)$$

The expression (3.8) is now solved for the resulting elastic forces acting from the grid point  $i$  on the elastically connected grid points, hence:

$$\mathbf{L}_i = - \begin{bmatrix} \mathbf{P}_{gt,i}^{el} \\ \mathbf{P}_{gr,i}^{el} \end{bmatrix} . \quad (3.10)$$

The preliminary form of the Force Summation Method then becomes:

$$\mathbf{L}_{g,i}^{\text{FSM}} = \begin{bmatrix} \mathbf{P}_{gt,i} \\ \mathbf{P}_{gr,i} \end{bmatrix} - \begin{bmatrix} m_i \mathbf{I} & \mathbf{0} \\ m_i \text{sk}(\mathbf{s}_i) & \mathbf{J}_i \end{bmatrix} \begin{bmatrix} \ddot{\mathbf{R}}_i - \mathbf{T}_{be} \mathbf{g}_e \\ \overset{\circ}{\mathbf{\Omega}}_b + \overset{\circ\circ}{\dot{\varphi}}_i \end{bmatrix} - \begin{bmatrix} \mathbf{0} \\ \text{sk}(\mathbf{\Omega}_b) \mathbf{J}_i \end{bmatrix} (\mathbf{\Omega}_b + \overset{\circ}{\dot{\varphi}}_i) . \quad (3.11)$$

At this point of the derivation the difference between the two ways of computing loads can be explained. In the above form  $\mathbf{L}^{\text{FSM}}$  are elastic forces obtained by the summation of forces, whereas  $\mathbf{L}^{\text{MDM}}$  in (3.2) are elastic forces obtained directly from modal displacements. It is obvious that both formulations would yield identical loads when all mode shapes are taken into account. However, a modal order reduction is applied to the generalized equations of motion, i.e. the modal approach only contains a sub-set of all elastic mode shapes. Then the two methods yield different loads and the question of the convergence behavior as a function of the number of modes arises. As already noted convergence studies [47, 8, 28, 45] show a superior convergence behavior for the force summation method. The main reason for this is that the force summation method incorporates the distributed external force vector. Hereby modes that are not included in the modal approach are accounted for quasi-statically, since inertia forces vanish for a quasi-static deformation. Furthermore, the FSM directly accounts for the loads from overall motion, whereas the MDM recovers the loads only from the trajectories of generalized elastic coordinates.

The translational inertial acceleration of the local mass element  $m_i$  in (3.11) is given by differentiation of (2.14) as follows:

$$\begin{aligned} \ddot{\mathbf{R}}_i &= \overset{\circ}{\mathbf{V}}_b + \mathbf{\Omega}_b \times \mathbf{V}_b \\ &+ \overset{\circ\circ}{\dot{\mathbf{d}}}_i + 2\mathbf{\Omega}_b \times \overset{\circ}{\dot{\mathbf{d}}}_i \\ &+ \mathbf{\Omega}_b \times \mathbf{\Omega}_b \times (\bar{\mathbf{r}}_i + \bar{\mathbf{d}}_i) + \overset{\circ}{\mathbf{\Omega}}_b \times (\bar{\mathbf{r}}_i + \bar{\mathbf{d}}_i) . \end{aligned} \quad (3.12)$$

Separation into contributions from the rigid body motion and the elastic deformation yields:

$$\begin{aligned} \ddot{\mathbf{R}}_i &= \underbrace{\overset{\circ}{\mathbf{V}}_b + \text{sk}(\mathbf{\Omega}_b) \mathbf{V}_b}_{\text{acceleration at c.g.}} + (\text{sk}(\mathbf{\Omega}_b)^2 + \text{sk}(\overset{\circ}{\mathbf{\Omega}}_b)) \bar{\mathbf{r}}_i \\ &\quad \underbrace{+ \overset{\circ\circ}{\dot{\mathbf{d}}}_i + 2\text{sk}(\mathbf{\Omega}_b) \overset{\circ}{\dot{\mathbf{d}}}_i + (\text{sk}(\mathbf{\Omega}_b)^2 + \text{sk}(\overset{\circ}{\mathbf{\Omega}}_b)) \bar{\mathbf{d}}_i}_{\text{elastic contribution}} . \end{aligned} \quad (3.13)$$

Table 3.1 gives a detailed description of the acceleration terms.



Term in (3.13)	Type of acceleration
$\ddot{\mathbf{R}}_i$	total acceleration at a mass element
$\overset{\circ}{\mathbf{V}}_b + \text{sk}(\mathbf{\Omega}_b)\mathbf{V}_b$	acceleration at the c.g.
$\text{sk}(\mathbf{\Omega}_b)^2\bar{\mathbf{r}}_i$	centripetal acceleration (rigid contribution)
$\text{sk}(\overset{\circ}{\mathbf{\Omega}}_b)\bar{\mathbf{r}}_i$	acceleration due to offset from the c.g. (rigid contribution)
$\overset{\circ\circ}{\bar{\mathbf{d}}}_i$	elastic acceleration
$2\text{sk}(\mathbf{\Omega}_b)\overset{\circ}{\bar{\mathbf{d}}}_i$	coriolis acceleration
$\text{sk}(\mathbf{\Omega}_b)^2\overset{\circ}{\bar{\mathbf{d}}}_i$	centripetal acceleration (elastic contribution)
$\text{sk}(\overset{\circ}{\mathbf{\Omega}}_b)\overset{\circ}{\bar{\mathbf{d}}}_i$	acceleration due to offset from the c.g. (elastic contribution)

**Table 3.1:** Components of total acceleration of mass element

Elastic displacements, velocities and accelerations are now expressed using the modal approach (2.19):

$$\bar{\mathbf{d}}_i = \mathbf{d}_i + \boldsymbol{\varphi}_i \times \mathbf{s}_i = \begin{bmatrix} \mathbf{I} & -\text{sk}(\mathbf{s}_i) \end{bmatrix} \boldsymbol{\Phi}_{g_iE} \boldsymbol{\eta}_E \quad , \quad (3.14a)$$

$$\overset{\circ}{\bar{\mathbf{d}}}_i = \overset{\circ}{\mathbf{d}}_i + \overset{\circ}{\boldsymbol{\varphi}}_i \times \mathbf{s}_i = \begin{bmatrix} \mathbf{I} & -\text{sk}(\mathbf{s}_i) \end{bmatrix} \boldsymbol{\Phi}_{g_iE} \overset{\circ}{\boldsymbol{\eta}}_E \quad , \quad (3.14b)$$

$$\overset{\circ\circ}{\bar{\mathbf{d}}}_i = \overset{\circ\circ}{\mathbf{d}}_i + \overset{\circ\circ}{\boldsymbol{\varphi}}_i \times \mathbf{s}_i = \begin{bmatrix} \mathbf{I} & -\text{sk}(\mathbf{s}_i) \end{bmatrix} \boldsymbol{\Phi}_{g_iE} \overset{\circ\circ}{\boldsymbol{\eta}}_E \quad . \quad (3.14c)$$

Introduction of (3.13) and (3.14) in (3.11) yields the Force Summation Method:

$$\begin{aligned} \mathbf{L}_{g,i}^{\text{FSM}} = & \begin{bmatrix} \mathbf{P}_{gt,i} \\ \mathbf{P}_{gr,i} \end{bmatrix} - \begin{bmatrix} m_i\mathbf{I} & \mathbf{0} \\ m_i\text{sk}(\mathbf{s}_i) & \mathbf{J}_i \end{bmatrix} \\ & \left\{ \begin{bmatrix} \mathbf{I} & -\text{sk}(\mathbf{s}_i) \\ \mathbf{0} & \mathbf{I} \end{bmatrix} \begin{bmatrix} \mathbf{I} & -\text{sk}(\mathbf{r}_i) \\ \mathbf{0} & \mathbf{I} \end{bmatrix} \begin{bmatrix} \overset{\circ}{\mathbf{V}}_b + \text{sk}(\mathbf{\Omega}_b)\mathbf{V}_b \\ \overset{\circ}{\mathbf{\Omega}}_b \end{bmatrix} + \begin{bmatrix} \text{sk}(\mathbf{\Omega}_b)^2\bar{\mathbf{r}}_i \\ \mathbf{0} \end{bmatrix} \right. \\ & + \begin{bmatrix} \mathbf{I} & -\text{sk}(\mathbf{s}_i) \\ \mathbf{0} & \mathbf{I} \end{bmatrix} \boldsymbol{\Phi}_{g_iE} \overset{\circ\circ}{\boldsymbol{\eta}}_E + \begin{bmatrix} -\mathbf{T}_{be}\mathbf{g}_e \\ \mathbf{0} \end{bmatrix} \\ & + \begin{bmatrix} 2\text{sk}(\mathbf{\Omega}_b) \\ \mathbf{0} \end{bmatrix} \begin{bmatrix} \mathbf{I} & -\text{sk}(\mathbf{s}_i) \end{bmatrix} \boldsymbol{\Phi}_{g_iE} \overset{\circ}{\boldsymbol{\eta}}_E \\ & \left. + \begin{bmatrix} \text{sk}(\mathbf{\Omega}_b)^2 + \text{sk}(\overset{\circ}{\mathbf{\Omega}}_b) \\ \mathbf{0} \end{bmatrix} \begin{bmatrix} \mathbf{I} & -\text{sk}(\mathbf{s}_i) \end{bmatrix} \boldsymbol{\Phi}_{g_iE} \boldsymbol{\eta}_E \right\} \\ & - \begin{bmatrix} \mathbf{0} \\ \text{sk}(\mathbf{\Omega}_b)\mathbf{J}_i \end{bmatrix} \left( \mathbf{\Omega}_b + \boldsymbol{\Phi}_{g_iE_r} \overset{\circ}{\boldsymbol{\eta}}_E \right) \quad . \quad (3.15) \end{aligned}$$

With the expressions (see also Appendix A.1)

$$\begin{bmatrix} m_i\mathbf{I} & \mathbf{0} \\ m_i\text{sk}(\mathbf{s}_i) & \mathbf{J}_i \end{bmatrix} \begin{bmatrix} \mathbf{I} & -\text{sk}(\mathbf{s}_i) \\ \mathbf{0} & \mathbf{I} \end{bmatrix} = \begin{bmatrix} m_i\mathbf{I} & -m_i\text{sk}(\mathbf{s}_i) \\ m_i\text{sk}(\mathbf{s}_i) & \mathbf{J}_{g,i} \end{bmatrix} = \mathbf{M}_{gg,i} \quad ,$$

$$\underbrace{\begin{bmatrix} m_i \mathbf{I} & -m_i \text{sk}(\mathbf{s}_i) \\ m_i \text{sk}(\mathbf{s}_i) & \mathbf{J}_{g,i} \end{bmatrix}}_{\mathbf{M}_{gg,i}} \underbrace{\begin{bmatrix} \mathbf{I} & -\text{sk}(\mathbf{r}_i) \\ \mathbf{0} & \mathbf{I} \end{bmatrix}}_{\Phi_{gR,i}} = \underbrace{\begin{bmatrix} m_i \mathbf{I} & -m_i \text{sk}(\mathbf{r}_i + \mathbf{s}_i) \\ m_i \text{sk}(\mathbf{s}_i) & \mathbf{J}_{g,i} - m_i \text{sk}(\mathbf{s}_i) \text{sk}(\mathbf{r}_i) \end{bmatrix}}_{\mathbf{M}_{gR,i}}$$

the Force Summation Method can be written in a more compact form:

$$\begin{aligned} \mathbf{L}_{g,i}^{\text{FSM}} = & \begin{bmatrix} \mathbf{P}_{gt,i} \\ \mathbf{P}_{gr,i} \end{bmatrix} - \mathbf{M}_{gR,i} \left\{ \begin{aligned} & \begin{bmatrix} \dot{\mathbf{V}}_b + \text{sk}(\Omega_b) \mathbf{V}_b - \mathbf{T}_{bc} \mathbf{g}_c \\ \dot{\Omega}_b \end{bmatrix} + \begin{bmatrix} \text{sk}(\Omega_b)^2 \bar{\mathbf{r}}_i \\ 0 \end{bmatrix} \\ & + \underbrace{\begin{bmatrix} 2\text{sk}(\Omega_b) \\ \mathbf{0} \end{bmatrix} \begin{bmatrix} \mathbf{I} & -\text{sk}(\mathbf{s}_i) \end{bmatrix} \Phi_{gE} \dot{\boldsymbol{\eta}}_E}_{\text{inertial coupling term A}} \\ & + \underbrace{\begin{bmatrix} \text{sk}(\Omega_b)^2 + \text{sk}(\dot{\Omega}_b) \\ \mathbf{0} \end{bmatrix} \begin{bmatrix} \mathbf{I} & -\text{sk}(\mathbf{s}_i) \end{bmatrix} \Phi_{gE} \boldsymbol{\eta}_E}_{\text{inertial coupling term B}} \end{aligned} \right\} \\ & - \begin{bmatrix} \mathbf{0} \\ \text{sk}(\Omega_b) \mathbf{J}_i \end{bmatrix} \left( \Omega_b + \underbrace{\Phi_{gE} \dot{\boldsymbol{\eta}}_E}_{\text{inertial coupling term C}} \right) - \mathbf{M}_{gE,i} \ddot{\boldsymbol{\eta}}_E \end{aligned} \quad (3.16)$$

where the trajectories for  $\mathbf{V}_b, \dot{\mathbf{V}}_b, \Omega_b, \dot{\Omega}_b$  and  $\boldsymbol{\eta}_E, \dot{\boldsymbol{\eta}}_E, \ddot{\boldsymbol{\eta}}_E$  are obtained from simultaneous integration of the force equation (2.56), the moment equation (2.59) and from the elastic equation of motion (2.113).

### Discussion of the Force Summation Method

The Force Summation Method (3.16), derived in the previous section, is based on the same assumption as the equations of motion. The present form may therefore be used for the recovery of local forces and moments over the airframe, based on the simulation results of the equations of motion (2.56), (2.59) and (2.113).

The terms denoted by A,B,C in (3.16) represent the inertial coupling between the rigid and the elastic motion. Inertial coupling terms are already discussed for the equations of motion. Due to the half generalized form of the Force Summation Method compared to the generalized form of the elastic equation the inertial coupling terms cannot be related directly. However, it can be seen that A and B represent the coriolis term and the centrifugal loading. The term C represents the effect of the variable inertia tensor in the moment equation. Note that it should be possible to derive a generalized form similar to the equations of motion from the force summation method. For practical reasons, pointed out for the development of the equations of motion, the validation will only be performed numerically.

### 3.2.2 Inertially Uncoupled Formulation

Inertially uncoupled equations of motion (2.114) can be derived from the equations of motion including inertial coupling by introducing two additional assumptions (Assumption 6 and 7, on page 37) during the equation development. The same can be done for the loads equation. Starting with the general formulation of the loads equation including inertial coupling (3.16) a consistent formulation for inertially decoupled equations of motion can be obtained by introducing the same additional assumptions.

Application of the first additional assumption (Assumption 6, *The inertia tensor of the aircraft  $J$  is constant*) to (3.16) eliminates the inertial coupling term C. Application of the second additional assumption (Assumption 7, *The inertial cross coupling between the overall and the elastic motion is small and may be neglected*) eliminates the terms A and B. The Force Summation Method for the inertially uncoupled equations of motion then becomes

$$\mathbf{L}_g^{\text{FSM}} = \mathbf{P}_g - \mathbf{M}_{gR} \begin{bmatrix} \overset{\circ}{\mathbf{V}}_b + \text{sk}(\overset{\circ}{\boldsymbol{\Omega}}_b)\mathbf{V}_b - \mathbf{T}_{be}\mathbf{g}_e \\ \overset{\circ}{\boldsymbol{\Omega}}_b \end{bmatrix} - \mathbf{M}_{gE} \overset{\circ\circ}{\boldsymbol{\eta}}_E \quad . \quad (3.17)$$

### 3.2.3 Linearized Formulation

Aeroelastic equations of motion assume that the rigid body displacements are small and gravity is usually neglected [8]. The force summation method for an aeroelastic system [28, 45, 27] is obtained by solving the half generalized aeroelastic equation of motion for the elastic forces.

The Force Summation Method can also be obtained from the nonlinear decoupled formulation (3.17) by replacing the nonlinear rigid body acceleration term:

$$\begin{bmatrix} \overset{\circ}{\mathbf{V}}_b + \text{sk}(\overset{\circ}{\boldsymbol{\Omega}}_b)\mathbf{V}_b - \mathbf{T}_{be}\mathbf{g}_e \\ \overset{\circ}{\boldsymbol{\Omega}}_b \end{bmatrix}$$

with the acceleration expressed by a set of rigid body modes (2.51) and respective generalized accelerations  $\overset{\circ\circ}{\boldsymbol{\eta}}_R$  and neglecting gravity. The linearized formulation can then be written as follows [28, 45, 27]:

$$\mathbf{L}_g^{\text{FSM}} = \mathbf{P}_g - \mathbf{M}_{gR} \overset{\circ\circ}{\boldsymbol{\eta}}_R - \mathbf{M}_{gE} \overset{\circ\circ}{\boldsymbol{\eta}}_E \quad . \quad (3.18)$$

Note that the above form is the simplest form of the force summation method. However, it is common practice to also account for linearized Euler terms  $\text{sk}(\overset{\circ}{\boldsymbol{\Omega}}_b)\mathbf{V}_b$  and gravity terms  $\mathbf{T}_{be}\mathbf{g}_e$  in the same form as it is done in linearized equations of motion [10, 64].

### 3.3 Integrated Shear Loads

The previous expressions for the nodal loads  $\mathbf{L}_g^{\text{FSM}}$  yield local forces and moments at each grid point. The actual structural loading at a certain position in the airframe is then obtained by virtually cutting the structure at the desired point and summing all local forces and moments from the grid points that are cut free. Figure 3.3 depicts the cut  $j$  defined by the position vector  $\mathbf{r}_{c,j}$  and the set of grid points  $\Gamma_j$  contributing to the cut load.

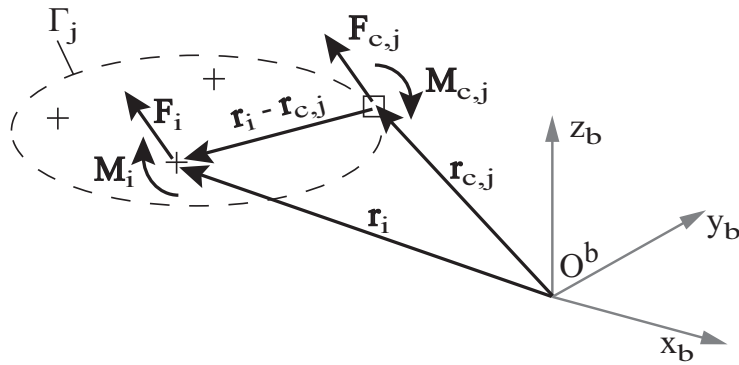


**Figure 3.3:** Transformation of Nodal Loads to Cut Loads

The transformation from nodal to cut loads is then performed using the transformation matrix  $\mathbf{T}_{cg}$

$$\mathbf{L}_c^{\text{FSM}} = \mathbf{T}_{cg} \mathbf{L}_g^{\text{FSM}} \quad (3.19)$$

defined by

$$\mathbf{T}_{cg,ji} = \begin{cases} \begin{bmatrix} \mathbf{I} & \mathbf{0} \\ \text{sk}(\mathbf{r}_i - \mathbf{r}_{c,j}) & \mathbf{I} \end{bmatrix}; & i \in \Gamma_j \\ \begin{bmatrix} \mathbf{0} & \mathbf{0} \\ \mathbf{0} & \mathbf{0} \end{bmatrix}; & i \notin \Gamma_j \end{cases} . \quad (3.20)$$

Equation (3.19) simply sums all local forces and moments contained in the set  $\Gamma_j$  and adds the moments induced by the local forces, using the lever arm  $\mathbf{r}_i - \mathbf{r}_{c,j}$ , to the moment at the cut station.

### 3.4 Validation of the General Formulation

Elastic forces contained in the generalized equations of motion and the loads equation cannot be compared directly. The generalized equations of motion yield elastic forces on the elastic modes where the loads equation yields elastic forces at nodal coordinates. A symbolic generalization of the loads equation is complicated and unnecessary. For validation of the loads equation the loads are transformed from the physical into the modal space by pre-multiplication with the elastic mode shapes:

$$\mathbf{L}_E^{\text{FSM}} = \mathbf{\Phi}_{gE}^{\text{T}} \mathbf{L}_g^{\text{FSM}} \quad . \quad (3.21)$$

The respective generalized loads are then compared numerically. Trajectories from simulation are depicted in the Appendix D. It is found that the conventional loads equation for the decoupled equations of motion is not consistent with the equations of motion with inertial coupling (as one would expect) whereas the previously derived loads equation (3.16) is consistent to the coupled formulation.

### 3.5 Summary of the Results

The Force Summation Method for an elastic aircraft in flight is derived based on the principle of momentum. The new formulation is suitable for the computation of loads in combination with inertially coupled equations of motions. The underlying assumptions are the same as for the development of the equations of motion.

The new formulation is validated using generalized elastic forces from the equation of motion. Consistency of the equation of motion and the loads equation is shown.

The present force summation method is given for a system with discrete masses, rotational degrees of freedom and mass offsets. Available data from industrial FE-models used in loads and aeroelastics can be incorporated directly. The input to the half-generalized form in terms of states corresponds to the simulation results of the inertially coupled equations of motion.

### Equations of Structural Loads

Force Summation Method for inertially coupled equations of motion (3.16):

$$\mathbf{L}_{g,i}^{\text{FSM}} = \begin{bmatrix} \mathbf{P}_{gt,i} \\ \mathbf{P}_{gr,i} \end{bmatrix} - \mathbf{M}_{gR,i} \left\{ \begin{aligned} & \begin{bmatrix} \dot{\mathbf{V}}_b + \text{sk}(\mathbf{\Omega}_b)\mathbf{V}_b - \mathbf{T}_{be}\mathbf{g}_e \\ \dot{\mathbf{\Omega}}_b \end{bmatrix} + \begin{bmatrix} \text{sk}(\mathbf{\Omega}_b)^2\bar{\mathbf{r}}_i \\ \mathbf{0} \end{bmatrix} \\ & + \begin{bmatrix} 2\text{sk}(\mathbf{\Omega}_b) \\ \mathbf{0} \end{bmatrix} \begin{bmatrix} \mathbf{I} & -\text{sk}(\mathbf{s}_i) \end{bmatrix} \mathbf{\Phi}_{g_iE} \dot{\boldsymbol{\eta}}_E \\ & + \begin{bmatrix} \text{sk}(\mathbf{\Omega}_b)^2 + \text{sk}(\dot{\mathbf{\Omega}}_b) \\ \mathbf{0} \end{bmatrix} \begin{bmatrix} \mathbf{I} & -\text{sk}(\mathbf{s}_i) \end{bmatrix} \mathbf{\Phi}_{g_iE} \boldsymbol{\eta}_E \end{aligned} \right\} \\ - \begin{bmatrix} \mathbf{0} \\ \text{sk}(\mathbf{\Omega}_b)\mathbf{J}_i \end{bmatrix} \left( \mathbf{\Omega}_b + \mathbf{\Phi}_{g_iE_r} \dot{\boldsymbol{\eta}}_E \right) - \mathbf{M}_{gE,i} \ddot{\boldsymbol{\eta}}_E \quad ,$$

with  $\mathbf{V}_b, \dot{\mathbf{V}}_b$  from (2.56),  $\mathbf{\Omega}_b, \dot{\mathbf{\Omega}}_b$  from (2.59) and  $\boldsymbol{\eta}_E, \dot{\boldsymbol{\eta}}_E, \ddot{\boldsymbol{\eta}}_E$  from (2.113).

Transformation of nodal loads to integrated loads (3.19):

$$\mathbf{L}_c^{\text{FSM}} = \mathbf{T}_{cg} \mathbf{L}_g^{\text{FSM}} \quad .$$

The underlying assumptions are the same as for the development of the equations of motion:

**Assumption 1.** *The aircraft is described as a collection of lumped mass elements, with an associated mass and inertia tensor.*

**Assumption 2.** *Linear elastic theory applies.*

**Assumption 3.** *Local translational and rotational elastic deformations with respect to the reference shape are small.*

**Assumption 4.** *Orthogonal mode shapes resulting from a free-free modal analysis are available. The deformation of the airplane may be written as a linear combination of the mode shapes, i.e. the modal approach will be used.*

**Assumption 5.** *Gravity is constant over the airframe.*

**Figure 3.4:** Summary of the Equations of Structural Loads

## 4 Modelling of External Forces

For the derivation of the equations of motion (Chapter 2) and the equation of structural loads (Chapter 3) the vector of nonconservative external forces  $\mathbf{P}_g$  is introduced.

The modelling of the external forces will now be put in concrete terms. External forces acting on the airframe of the free flying flexible aircraft are aerodynamic loads imposed by fluid motion and propulsion forces. Landing gear forces additionally arise during touch down and taxiing.

Distributed aerodynamic forces require a different modelling strategy than other locally applied external forces. Therefore the external forces will be grouped into aerodynamic forces caused by motion, control inputs and atmospheric disturbance and caused by other external forces including propulsion forces, gear forces, etc. The vector of external forces can then be written as follows

$$\mathbf{P}_g = \mathbf{P}_g^{\text{aero}} + \mathbf{P}_g^{\text{oext}} \quad . \quad (4.1)$$

The following sections focus on these two groups of external forces.

### 4.1 Aerodynamic Forces

The presented EOM represent the aircraft flight mechanics as well as structural dynamics of the airframe. Therefore the following requirements for the aerodynamic model arise:

- validity for large rigid body motion, i.e. large angles of attack and sideslip,
- provision for unsteady aerodynamic forces,
- forces must be available in distributed form for the recovery of structural loads (EOL),
- computational efficiency for rapid time domain simulation,
- incorporation of available aerodynamic modules.

As for the EOM based on available structural models, the aerodynamic forces are obtained from the integration of available data. Aerodynamic models for flight mechanics and ma-

neuver loads calculation are database driven modules providing quasi-steady aerodynamic forces over the airframe as a function of the flight condition and the quasi-steady deformation of the airframe. They are based on table look-ups and application rules which are valid in a wide range of flight points. Nonlinear effects and corrections for the quasi-steady deformation of the airframe are considered. Linear structural dynamic models used in dynamic response and gust loads calculation commonly use the doublet lattice method (DLM). This method provides unsteady aerodynamic lift forces on an airframe in oscillatory motion in the frequency domain.

Both methods have their limitations. Database models do not represent unsteady effects from the dynamic deformation. The DLM is a linear method that is adapted to experimental and flight test data in industrial applications in order to improve steady results at a given flight point [51]. However, the method is not accounting for large rigid body motions and drag. Therefore the aerodynamic models have to be integrated into a model that fulfills the requirements. In the following, the quasi-flexible forces from modules based on databases and the provision of forces from the DLM are described. Then the integration of the two models is considered and the handling of overlaps between the models is addressed.

### 4.1.1 Quasi-Flexible Aerodynamic Forces

An industrial aerodynamic database is used providing distributed aerodynamic forces as a function of the flight condition. The aerodynamic module is based on the “Données Aérodynamiques” database [1]. The database incorporates table look-ups and application rules obtained from CFD calculations, wind tunnel tests and flight test results. The database-driven aerodynamic loads can include nonlinearities, like for instance cross coupling terms of the angle of attack and the angle of side slip  $\alpha\beta$ , or  $\beta^2$ . These forces are quasi-steady including the effect of angular rates and the lag effect on the horizontal tail. Aeroelastic effects are accounted for quasi-statically via so-called flex-factors that primarily depend on the vertical load factor  $n_z$  and the dynamic pressure  $q_\infty$  [1, 16]. The aerodynamic forces from database will be denoted by:

$$\mathbf{P}_g^{\text{qf}} = \mathbf{P}_g^{\text{qf}}(n_z, q_\infty, \dots) \quad . \quad (4.2)$$

The quasi-flexible correction has to be kept in mind for subsequent coupling of the database loads with the aerodynamic loads from the doublet lattice method because the quasi-static deformation is also represented by the DLM loads.



### 4.1.2 Flexible Aerodynamic Forces

#### The Doublet Lattice Method

The Doublet-Lattice Method (DLM) [2, 25, 9] is widely used for flutter and dynamic response analysis of aircraft at subsonic speeds. The DLM solves a linear boundary value problem for harmonically oscillating lifting surfaces. It is equivalent to the Vortex-Lattice Method at zero reduced frequency [25].

The DLM provides unsteady aerodynamic loads in the frequency domain. The method is based on linearized aerodynamic potential theory. A small perturbation approach is applied to the acceleration potential separating it into a steady part and an unsteady part for harmonic oscillatory motion. Since the acceleration potential is proportional to the pressure change [8], modelling of the wake is not necessary. This reduces the computing effort and also largely simplifies the model generation compared to time domain approaches where wake modelling is essential. However, the DLM is limited to harmonic rigid body motion and to elastic deformation described by superposition of harmonic oscillations.

For application of the DLM, the airplane is discretized as small panels. Figure 4.1 shows an example of an industrial aerodynamic DLM mesh.

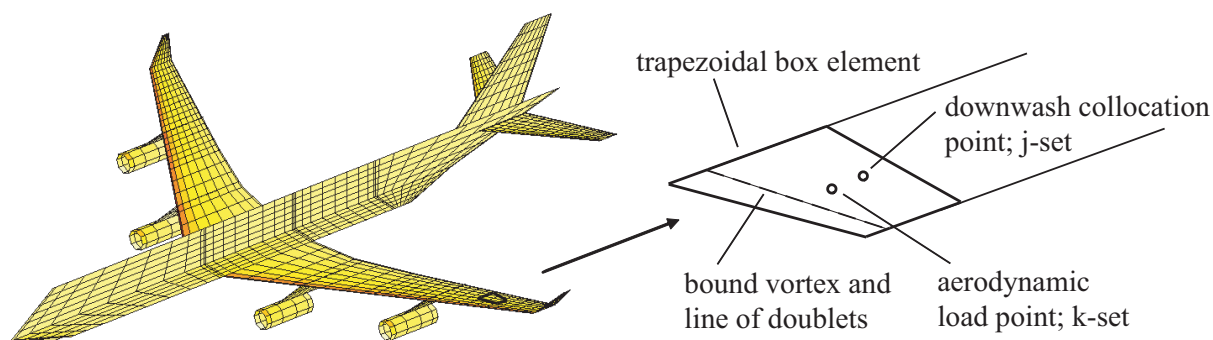


**Figure 4.1:** DLM Aerodynamic model – Steady flow effects are represented by a horseshoe vortex with the bound vortex at quarter chord line of box. Oscillatory increments are represented by a distribution of acceleration potential doublets of uniform strength

The DLM yields the matrix of aerodynamic influence coefficient (AIC) that relates control point forces to deflections. The AIC depends on Mach number  $Ma$  and reduced frequency  $k$  and is denoted by  $\mathbf{Q}_{jj}$ . The subscript  $j$  refers to the set of aerodynamic control points located at 75% box chord (see Figure 4.1). Where a so-called “set” denotes the collection of a specific type of points in a single vector. The integration matrix  $\mathbf{S}_{kj}$  and the substantial

differentiation matrix  $\mathbf{D}_{jk}$  transform the AIC matrix to the aerodynamic loading point set located at the box center [51]

$$\mathbf{Q}_{kk} = \mathbf{S}_{kj} \mathbf{Q}_{jj}(Ma, k) \mathbf{D}_{jk} \quad . \quad (4.3)$$

### Interconnection of Aerodynamic and Structural Grid

In general the loading points of the aerodynamic mesh ( $k$ -set) do not coincidence with the structural grid ( $g$ -set). In order to translate the forces on the aerodynamic mesh into forces at the structural grid an interpolation matrix  $\mathbf{T}_{kg}$  is used [51]. This matrix interconnects aerodynamic and structural model based upon the theory of splines. The aerodynamic influence coefficients can then be written as follows

$$\mathbf{Q}_{gE} = \mathbf{T}_{kg}^T \mathbf{S}_{kj} \mathbf{Q}_{jj} \mathbf{D}_{jk} \mathbf{T}_{kg} \mathbf{\Phi}_{gE} \quad (4.4)$$

where the right-multiplication with the elastic mode shapes  $\mathbf{\Phi}_{gE}$  yields a half generalized form of the AIC matrix.

### Transformation of Aerodynamic Forces into the Time Domain

For time domain simulation a rational function approximation (RFA) is employed in order to transform the aerodynamic forces from the frequency into the Laplace domain. To this end various RFA approaches have been developed [29, 53]. A comparison of the approximation methods is presented in [60]. After approximation the AIC matrix is written in the following form:

$$\mathbf{Q}_{gE}(s) = \mathbf{A}_{gE_0} + \mathbf{A}_{gE_1} \frac{\bar{c}}{V} s + \mathbf{A}_{gE_2} \frac{\bar{c}^2}{V^2} s^2 + \mathbf{D}_{gE} \left( s\mathbf{I} - \frac{V}{\bar{c}} \mathbf{R}_E \right)^{-1} \mathbf{E}_E s \quad , \quad (4.5)$$

note that the relation between the Laplace variable  $s$  and the reduced frequency  $k$  is given by  $k = \frac{\bar{c}}{V} \text{Im}(s)$ .

The aerodynamic forces due to elastic deformation are obtained by multiplication of (4.5) with the elastic mode shapes and the dynamic pressure:

$$\begin{aligned} \mathbf{P}_g^{\text{DLM}}(s) &= q_\infty \mathbf{Q}_{gE}(s) \boldsymbol{\eta}_E(s) \\ &= q_\infty \left( \mathbf{A}_{gE_0} + \mathbf{A}_{gE_1} \frac{\bar{c}}{V} s + \mathbf{A}_{gE_2} \frac{\bar{c}^2}{V^2} s^2 \right) \boldsymbol{\eta}_E + q_\infty \mathbf{D}_{gE} \left( s\mathbf{I} - \frac{V}{\bar{c}} \mathbf{R}_E \right)^{-1} \mathbf{E}_E s \boldsymbol{\eta}_E \\ &= q_\infty \left( \mathbf{A}_{gE_0} + \mathbf{A}_{gE_1} \frac{\bar{c}}{V} s + \mathbf{A}_{gE_2} \frac{\bar{c}^2}{V^2} s^2 \right) \boldsymbol{\eta}_E + q_\infty \mathbf{D}_{gE} \mathbf{x}_{LE} \end{aligned} \quad (4.6)$$

where the vector of aerodynamic lag states  $\mathbf{x}_{LE}$  is given by:

$$s \mathbf{x}_{LE} = \frac{V}{\bar{c}} \mathbf{R}_E \mathbf{x}_{LE} + \mathbf{E}_E s \boldsymbol{\eta}_E \quad . \quad (4.7)$$

Laplace transformation of (4.6) yields the DLM aerodynamic forces in the time domain:

$$\mathbf{P}_g^{\text{DLM}} = q_\infty \left\{ \mathbf{A}_{gE_0} \boldsymbol{\eta}_E + \mathbf{A}_{gE_1} \frac{\bar{c}}{V} \overset{\circ}{\boldsymbol{\eta}}_E + \mathbf{A}_{gE_2} \frac{\bar{c}^2}{V^2} \overset{\circ\circ}{\boldsymbol{\eta}}_E + \mathbf{D}_{gE} \mathbf{x}_{LE} \right\} \quad (4.8)$$

with

$$\overset{\circ}{\mathbf{x}}_{LE} = \frac{V}{\bar{c}} \mathbf{R}_E \mathbf{x}_{LE} + \mathbf{E}_E \overset{\circ}{\boldsymbol{\eta}}_E \quad . \quad (4.9)$$

### 4.1.3 Integration of the Aerodynamic Models

In the following section the integration of the quasi-flexible database loads with the DLM-aerodynamics is described.

The task is to find the best combination of the two aerodynamic models (Table 4.1). Hereby the problem of the handling of overlaps between the models has to be considered.

Database loads ( $\mathbf{P}_g^{\text{qf}}$ (4.2))	DLM-loads ( $\mathbf{P}_g^{\text{DLM}}$ (4.8))
based on CFD, experimental and flight mechanics data	based on linear potential theory
nonlinear	linear
quasi-steady	unsteady
quasi-flexible corrections	fully flexible model

**Table 4.1:** Characteristics of the aerodynamic models

Database loads account for quasi-flexible effects whereas the DLM yields fully flexible loads. Therefore the quasi-flexible contribution has to be eliminated either in database loads or in DLM loads. Database loads are adapted to flight test, CFD calculation and experimental data. Therefore it is not favorable to touch the database loads after these adaptations in order to remove the corrections for the quasi-flexible deformation. Instead, the quasi-flexible effects will be eliminated in the DLM loads. This directly leads to the concept of the residualized model approach.

The residualized model approach, accounting for the integration of generalized aerodynamic models, was developed by Winther [71] (see also Ref. [31, 70, 33, 48]). In the frame of this work the RM-approach is extended for application to a distributed quasi-flexible model and its integration with an unsteady aerodynamic model. Figure 4.2 depicts the basic steps.

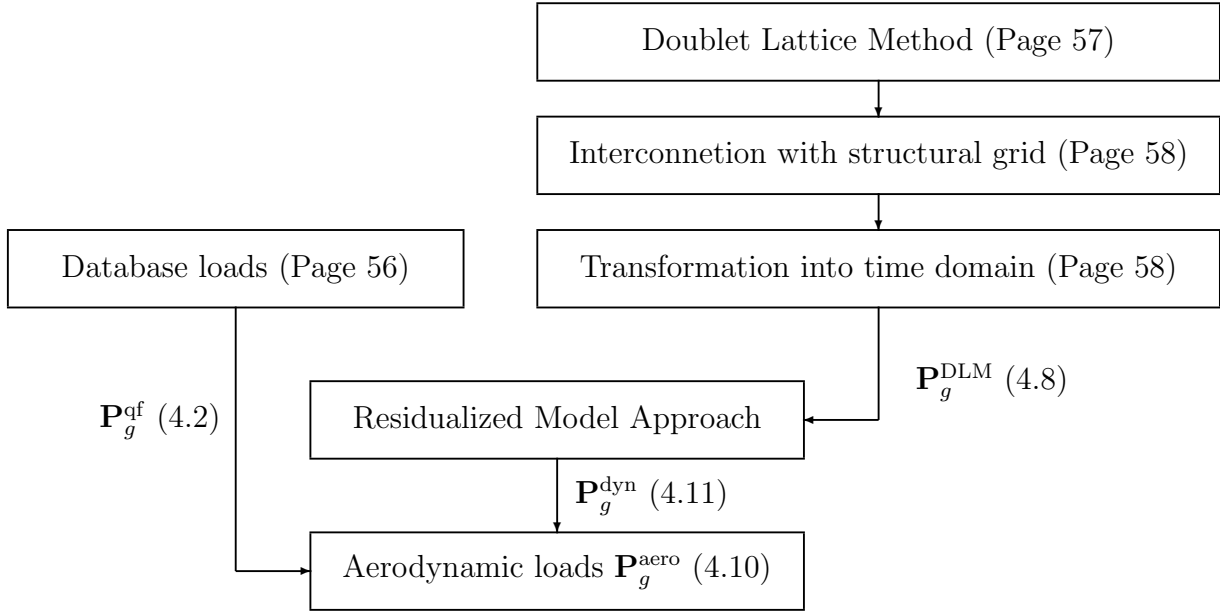


**Figure 4.2:** Principal steps for modelling the aerodynamic loads

First, the aerodynamic forces  $\mathbf{P}_g^{\text{aero}}$  from (4.1) will be written as superposition of the quasi-flexible forces  $\mathbf{P}_g^{\text{qf}}$  from (4.2) and a dynamic increment  $\mathbf{P}_g^{\text{dyn}}$ :

$$\mathbf{P}_g^{\text{aero}} = \mathbf{P}_g^{\text{qf}} + \mathbf{P}_g^{\text{dyn}} \quad . \quad (4.10)$$

The dynamic increment  $\mathbf{P}_g^{\text{dyn}}$  is then obtained from the unsteady aerodynamic forces  $\mathbf{P}_g^{\text{DLM}}$  by elimination of the quasi-flexible contribution. The key assumption hereby is

**Assumption 8.** *The quasi-flexible effects in the database loads  $\mathbf{P}_g^{\text{qf}}$  are equivalent to the statically residualised aerodynamic forces from the DLM, i.e.  $\overset{\circ}{\boldsymbol{\eta}}_E = 0, \overset{\circ\circ}{\boldsymbol{\eta}}_E = 0$ .*

Elimination of the quasi flexible contribution in (4.8) yields:

$$\begin{aligned} \mathbf{P}_g^{\text{dyn}} &= \mathbf{P}_g^{\text{DLM}}(\boldsymbol{\eta}_E, \overset{\circ}{\boldsymbol{\eta}}_E, \overset{\circ\circ}{\boldsymbol{\eta}}_E) - \mathbf{P}_g^{\text{DLM}}(\boldsymbol{\eta}_{E_0}) \\ &= q_\infty \left\{ A_{gE_0}(\boldsymbol{\eta}_E - \boldsymbol{\eta}_{E_0}) + A_{gE_1} \frac{\bar{c}}{V} \dot{\boldsymbol{\eta}}_E + A_{gE_2} \frac{\bar{c}^2}{V^2} \ddot{\boldsymbol{\eta}}_E + D_{gEXL_E} \right\} \end{aligned} \quad (4.11)$$

where  $\boldsymbol{\eta}_{E_0}$  is the quasi flexible modal deformation. Note that  $\mathbf{P}_g^{\text{dyn}}$  no longer depends on the absolute elastic deformation  $\boldsymbol{\eta}_E$  but on the incremental elastic deformation  $\boldsymbol{\eta}_E - \boldsymbol{\eta}_{E_0}$ .

With (4.1) and (4.10) in (2.113) one obtains the following form for the elastic equation:

$$\begin{aligned}
& \mathbf{M}_{EE} \overset{\circ}{\ddot{\boldsymbol{\eta}}}_E + \mathbf{K}_{EE} \boldsymbol{\eta}_E + \sum_{j=1}^3 \tilde{\mathbf{h}}_j \left( \overset{\circ}{\boldsymbol{\eta}}_E \boldsymbol{\Omega}_b^T + \boldsymbol{\eta}_E \overset{\circ}{\boldsymbol{\Omega}}_b^T \right) \mathbf{e}_j + \tilde{\mathbf{h}}_5^T \overset{\circ}{\boldsymbol{\Omega}}_b \\
& \quad + \frac{1}{2} \sum_{j=1}^3 \sum_{k=1}^3 \left( (\tilde{\mathbf{B}}_{jk} + \tilde{\mathbf{B}}_{jk}^T) \boldsymbol{\eta}_E + \tilde{\mathbf{C}}_{jk}^T \right) \boldsymbol{\Omega}_b^T \mathbf{e}_j \mathbf{e}_k^T \boldsymbol{\Omega}_b - \sum_{j=1}^3 \tilde{\mathbf{h}}_j^T \overset{\circ}{\boldsymbol{\eta}}_E \boldsymbol{\Omega}_b^T \mathbf{e}_j \\
& = \boldsymbol{\Phi}_{gE}^T \left( \mathbf{P}_g^{\text{qf}} + q_\infty \left\{ A_{gE_0} (\boldsymbol{\eta}_E - \boldsymbol{\eta}_{E_0}) + A_{gE_1} \frac{\bar{c}}{V} \dot{\boldsymbol{\eta}}_E + A_{gE_2} \frac{\bar{c}^2}{V^2} \ddot{\boldsymbol{\eta}}_E + D_{gE} \mathbf{x}_{LE} \right\} + \mathbf{P}_g^{\text{oext}} \right) .
\end{aligned} \tag{4.12}$$

The elastic modes in (4.12) can now be residualized. This requires the following steps:

1. Residualization of the flexible modes, hence  $\overset{\circ}{\boldsymbol{\eta}}_E = 0, \overset{\circ\circ}{\boldsymbol{\eta}}_E = 0$ .
2. Elimination of inertial coupling terms during residualization for consistency with quasi-steady database aerodynamics. Inertial coupling is not accounted for in the computation of flex factors [46].

Application of the above steps to (4.12) yields the quasi-flexible modes

$$\boldsymbol{\eta}_{E_0} = \mathbf{K}_{EE}^{-1} \boldsymbol{\Phi}_{gE}^T (\mathbf{P}_g^{\text{qf}} + \mathbf{P}_g^{\text{oext}}) . \tag{4.13}$$

With (4.13) and (4.11) the incremental dynamic forces are fully described and may be combined with the quasi-flexible forces (4.10):

$$\mathbf{P}_g^{\text{aero}} = \mathbf{P}_g^{\text{qf}} + \mathbf{P}_g^{\text{dyn}}$$

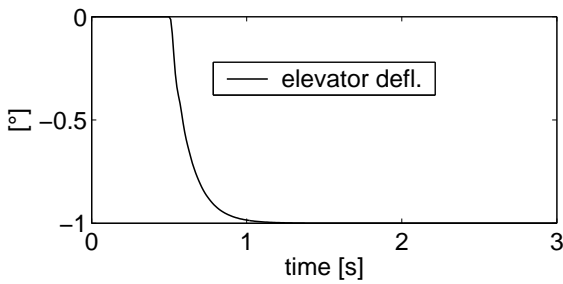
where  $\mathbf{P}_g^{\text{qf}}$  is given by (4.2) and  $\mathbf{P}_g^{\text{dyn}}$  is obtained from (4.11) with (4.13).

## Illustrative Example

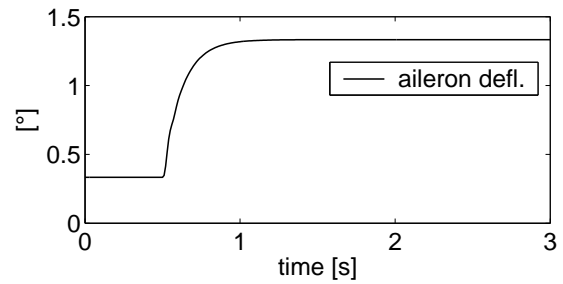
An elevator and aileron input will be considered to illustrate the quasi-flexible and dynamic contribution to the total aerodynamic forces. The control surface deflection for the two example maneuvers is shown in Figure 4.3. The airplane is trimmed at horizontal flight using the horizontal stabilizer, aileron, rudder and thrust setting. Note that the elevator is not deflected in the trim condition due to trimming with the horizontal stabilizer, whereas the ailerons are deflected.

The integrated vertical forces and moments due to the respective inputs are depicted in Figures 4.4 and 4.5. The elevator input causes a gradual change in wing bending. The vertical force and the pitching moment are well represented by the quasi-flexible aerodynamics, see Figure 4.4(a) and 4.5(a). The situation is different for the aileron input. Asymmetric wing

bending is excited causing the significant difference in the roll moment between the quasi-flexible and the full flexible aerodynamics, see Figure 4.4(b) and 4.5(b).

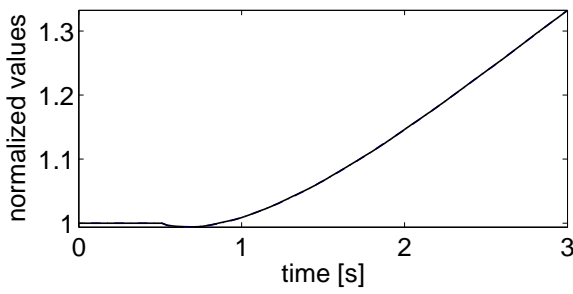


(a) Input for longitudinal maneuver

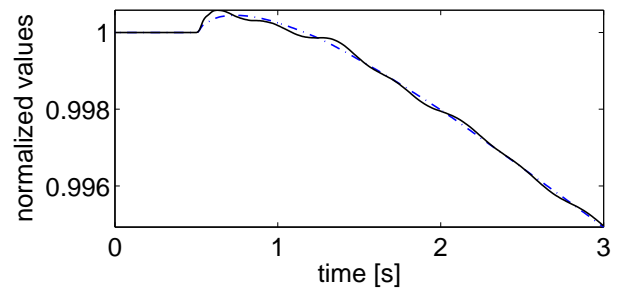


(b) Input for lateral maneuver

**Figure 4.3:** Control surface deflection for the example case

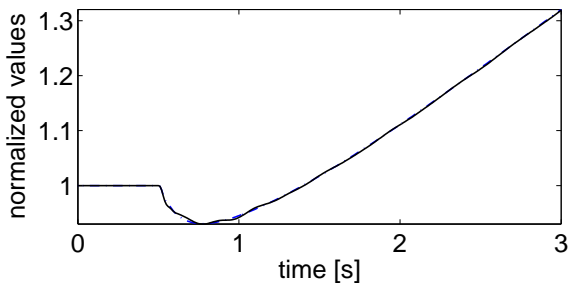


(a) Elevator input, vertical aerodynamic force

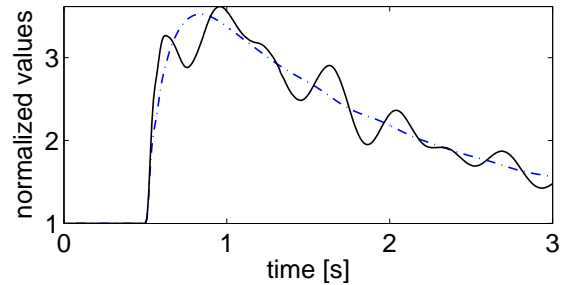


(b) Aileron input, vertical aerodynamic force

**Figure 4.4:** Integrated aerodynamic forces (—  $\mathbf{P}_g^{\text{aero}}$  total aerodynamic force, - · -  $\mathbf{P}_g^{\text{qf}}$  quasi flexible contribution)



(a) Elevator input, pitching moment



(b) Aileron input, rolling moment

**Figure 4.5:** Integrated aerodynamic moments over the airplane (—  $\mathbf{P}_g^{\text{aero}}$  total aerodynamic force, - · -  $\mathbf{P}_g^{\text{qf}}$  quasi flexible contribution)

## 4.2 Other External Forces

Propulsion and landing gear forces are nonconservative forces applied locally at the airframe. The concentrated characteristic and the significant magnitude have to be considered in the modelling approach. The local external forces are therefore modelled as follower forces. Follower forces account for a directional change of the force vector due to elastic deformation of the structure [6, 5].

Figure 4.6 depicts the geometric situation. The force vector  $\mathbf{F}_i$  is applied at the endpoint of the offset vector  $\mathbf{f}_i$  describing a rigid connection to the grid point.

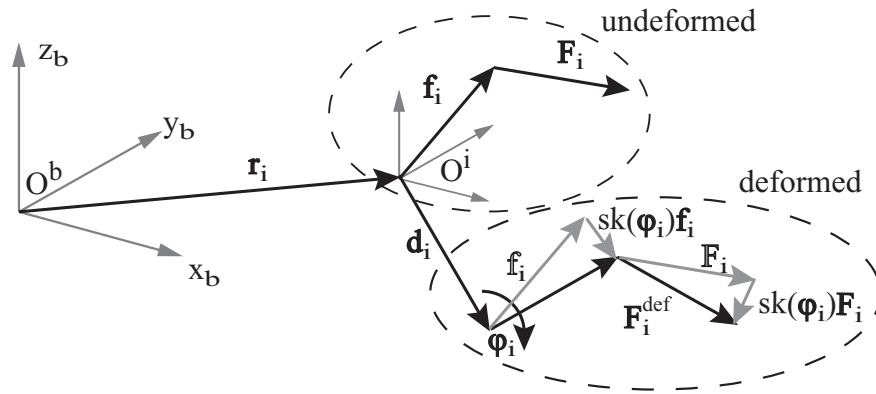


**Figure 4.6:** Local follower force in undeformed and deformed condition

By inspection of Figure 4.6 the external forces in the deformed condition can be written as follows [6]

$$\mathbf{P}_{g,i}^{\text{prop}} = \begin{bmatrix} \mathbf{F}_i^{\text{def}} \\ \mathbf{M}_i^{\text{def}} \end{bmatrix} = \begin{bmatrix} \mathbf{I} + \text{sk}(\boldsymbol{\varphi}_i) \\ \text{sk}(\mathbf{d}_i + (\mathbf{I} + \text{sk}(\boldsymbol{\varphi}_i))\mathbf{f}_i) \end{bmatrix} \mathbf{F}_i^{\text{undef}} \quad (4.14)$$

where the translation and angular elastic deformations  $\mathbf{d}_i, \boldsymbol{\varphi}_i$  are obtained from the modal approach (2.19)

$$\begin{bmatrix} \mathbf{d}_i \\ \boldsymbol{\varphi}_i \end{bmatrix} = \begin{bmatrix} \boldsymbol{\Phi}_{g_i E_t} \\ \boldsymbol{\Phi}_{g_i E_r} \end{bmatrix} \boldsymbol{\eta}_E = \boldsymbol{\Phi}_{g_i E} \boldsymbol{\eta}_E \quad .$$

The magnitude of the local forces is obtained from the respective landing gear and engine model. Hereby the engine model may vary from a simple scaling of the thrust setting to a detailed thermodynamic engine model.

### 4.3 Summary

The vector of nonconservative external forces  $\mathbf{P}_g$  includes the aerodynamic forces and all other external forces as for example propulsion and landing gear forces.

The modelling of aerodynamic forces is tailored towards integration of industrial aerodynamic models. For time domain simulation of a free flying flexible aircraft the nonlinear aerodynamic database has to be combined with an aerodynamic model for the unsteady aerodynamic forces. The nonlinear quasi-flexible model is required for the representation of flight mechanical aerodynamic effects whereas the unsteady aerodynamic model affects structural dynamics.

The presented form for the aerodynamic model integration is an extension to the RM-approach. The combination of the aerodynamic model is based on the residualization of the unsteady aerodynamic forces, leaving the nonlinear quasi-flexible aerodynamics unchanged. This is favorable since the database loads have been adapted to experimental and flight test data.

Local forces (engine forces etc.) are modelled as follower forces. Aerodynamic and other external forces are now described and complete the right hand side of the equations of motion.



# 5 Simulation

The objective of this chapter is to describe the implementation of the equations of motion and equations of loads and to present simulation results for a free flying flexible transport aircraft.

The first section describes the simulation environment including its sub-models and the basic data flow. Then two trim cases are considered and inertial coupling effects are analyzed. Next a roll maneuver is studied serving as a relevant test case for time domain simulation and loads analysis. The influence of the inertial coupling terms on nodal and integrated structural loads is worked out. Furthermore, the combination of the new force summation method (Chapter 3) with data from an uncoupled simulation is shown.

## 5.1 Simulation Model

### 5.1.1 Data Preparation

A finite element model of a commercial transport aircraft is available. The model contains mass data, stiffness data and the DLM aerodynamic model input for the finite element program MSC.NASTRAN. NASTRAN is a general purpose finite element analysis computer program that addresses a wide range of analysis types such as statics, dynamics and aeroelasticity. The program modules are controlled by an internal language, the so-called Direct Matrix Abstraction Program (DMAP).

The overall data flow in pre-processing is depicted in Figure 5.1. The mass information is retrieved from a mass database. A structural finite element (FE) model may be used to provide airframe structural masses but other nonstructural masses such as payload or fuel are not modelled. Therefore the mass database is used gathering the actual masses for a specific loading case from the structural and nonstructural masses. All masses in a specific structural region are then combined into a lumped mass. These lumped mass elements are attached to a structural grid point and represent the aircraft mass model.

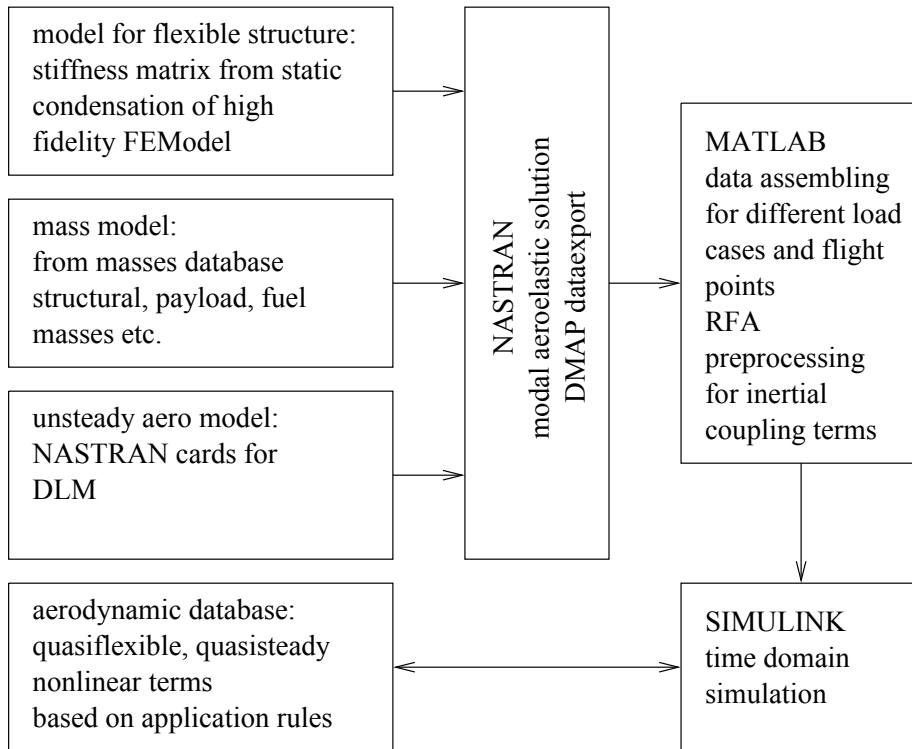


**Figure 5.1:** Data flowchart for data preparation

The stiffness matrix is obtained from a high fidelity GVT-adapted<sup>1</sup> structural FE-model (shell model). For a loads analysis the stiffness matrix is statically condensed using Guyan reduction [20] to nodes where the mass data is provided. Note that for a lumped mass model for which the reduction is performed to nodes where lumped masses are provided the Guyan reduction is an exact method since all eliminated degrees of freedom are massless [44].

The unsteady aerodynamic model consists of the aerodynamic panels for the DLM method. It basically represents the projected surfaces of the airplane.

With this data a NASTRAN dynamic aeroelastic analysis is performed. This includes settings for the working point and parameters for the solution sequence (number of mode shapes, mach number, reduced frequencies etc). The NASTRAN run assembles all stiffness, mass and aerodynamic model data, performs a free-free modal analysis and generates the AIC matrices. The resulting data is written to file via a DMAP<sup>2</sup> alter. The output data contains:

- geometrical information for structural and aerodynamic grid,
- mass and stiffness matrix,
- free-free mode shapes,

<sup>1</sup>The ground vibration test (GVT) provides data for the validation of analytical structural dynamics by measuring structural frequency response functions [30].

<sup>2</sup>MSC.Nastran DMAP (Direct Matrix Abstraction Program). A programming language for writing customized applications and input-output modules.

- AIC matrix from DLM,
- structural and aerodynamic grid interconnection matrix (spline),
- loads monitor stations.

The NASTRAN data is then converted into a file format that is readable from the numerical computing environment MATLAB. This environment allows easy matrix manipulation, data processing and implementation of algorithms. In MATLAB the unsteady aerodynamic forces are approximated using a rational function approximation (RFA). The VarLoads<sup>3</sup> pre-processing translates all information into a modular data structure and was developed for an effective calculation of load loops. Hereby the complete model data is cast in a data tree based on MATLAB structural arrays. It includes the sub-models for each discipline such as an unsteady aerodynamic sub-model for each flight condition and a modal model for every mass configuration.

The inertially coupled equations of motion require the provision of the inertial coupling terms. All coupling terms are generalized i.e. they consist of constant matrices that are combined with generalized coordinates (2.59, 2.113). The constant matrices are assembled for every mass configuration in pre-processing and stored in the data structure.

For the computation of integrated loads from nodal loads the integration matrix (3.20) is required. It only depends on the location of the structural grids. The load integration matrix is therefore stored in the general model data component.

The aerodynamic database is introduced via a MATLAB interface. The quasi-flexible aerodynamic forces can then be directly accessed during simulation.

### 5.1.2 Simulation Environment

The equations of motion (EOM Chapter 2), equations of loads (EOL Chapter 3) and the external forces (Chapter 4) are implemented in the VarLoads simulation environment. This industrial simulation environment is based on MATLAB-SIMULINK and is suitable for easy implementation of new sub-models. An overview of this environment is presented in the following beginning with the top level. It consists of the flexible aircraft model, simulation inputs and outputs, flight control system etc. Then the flexible aircraft sub-model is highlighted. It is of primary interest for this work and consists of the equations of motion and the external forces. Finally the EOM sub-model is explained. It contains the implementation of

---

<sup>3</sup> Variable Loads Environment. Consists of MATLAB pre-processing and SIMULINK simulation environment [24]

the inertially coupled EOM.

### Top Level of Simulation Environment

The top level of the simulation model is depicted in Figure 5.2. Hereby the aircraft model is the core sub-model of the simulation environment.

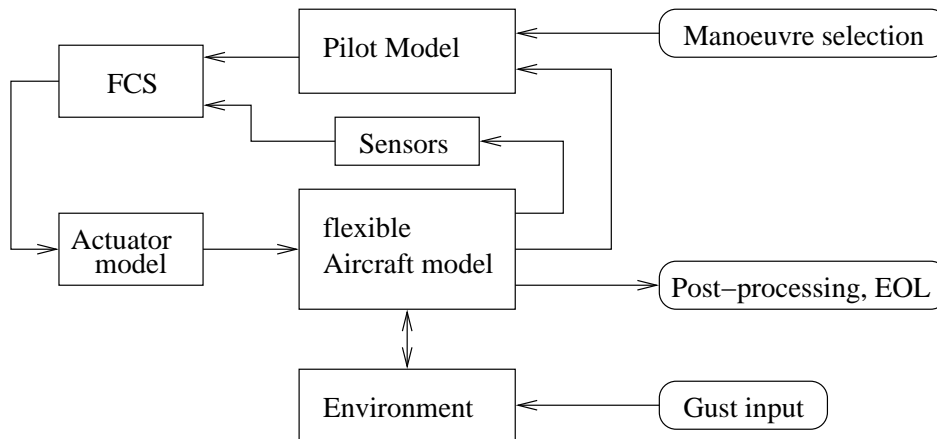


**Figure 5.2:** Feedback interconnection of the aircraft model and systems (top-level of model)

Other peripheral top level components are the pilot model, the flight control system (FCS), actuator models, an environment model, etc.

Inputs to the simulation can either be maneuver or gust inputs. Maneuver inputs are sent to the pilot model. The pilot model simulates the pilot's reaction to the aircraft states. Pilot commands are then sent to the flight control system (FCS). The FCS provides the control laws and yields commanded control surface and propulsion settings. They are translated by the actuator model into control surface deflections connected to the aerodynamic model. The gust input (continuous turbulence, 1-cos gust) is connected to the atmospheric model providing atmospheric disturbances for the aircraft model.

Furthermore, the top level contains the interface to the post-processing routines. They include the loads recovery and the output of requested simulation results.

### Aircraft Model

The aircraft model is of special interest in the present work, since it contains the EOM (Page 43) and the model for the external forces derived in the previous chapters. Figure 5.3 shows the dataflow within the aircraft model.

Control surface deflections, gust input and propulsion setting are the inputs to the aerodynamic and propulsion model. The external forces are combined into the total non-conservative external forces and drive the equations of motion. Note that the RM-approach (4.11) realized in the aerodynamic sub-model (Figure 4.13) requires the feedback of propulsion forces in order to compute the quasi-steady deformation (4.13).

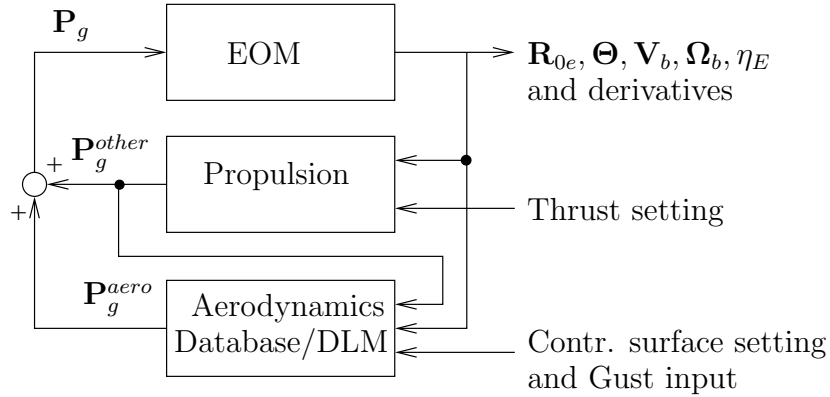


**Figure 5.3:** Information flowchart within the aircraft model

The outputs of the aircraft model are all flight mechanical and elastic states, as well as the total external force distribution  $\mathbf{P}_g$ . The distributed external forces are subsequently required for the computation of structural loads.

### Equations of Motion Environment

The implementation of the inertially coupled EOM is depicted in Figure 5.4. The force and moments equations are driven by the total external forces and moments. The elastic equation is driven by the generalized external forces. It can be seen that the inertial coupling requires the feedback of the elastic modes to the moment equation and the feedback of the angular rates to the elastic equation.

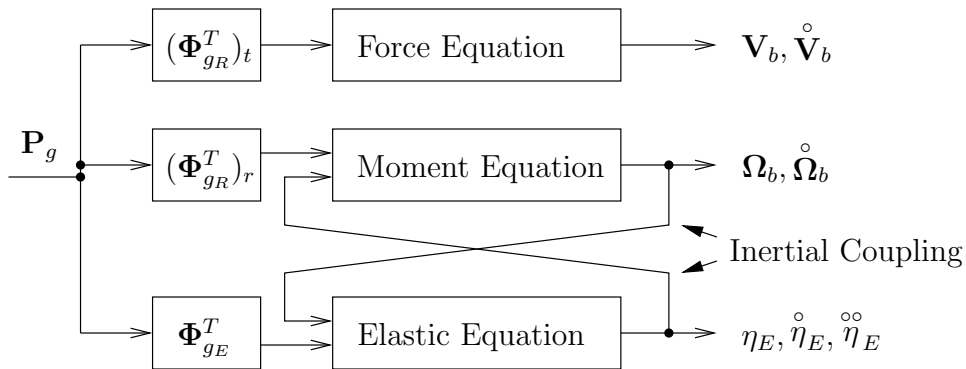


**Figure 5.4:** Information flowchart for inertially coupled equations of motion

### 5.1.3 Post-Processing

The recovery of structural loads is performed in the post-processing, based on the computed trajectories. Therefore the algebraic equation EOL (3.16) is implemented. All data is available from simulation and the computation of loads is straight forward. Furthermore requested output data is collected and stored for other external tools.

## 5.2 Trimming

The trimming process is concerned with the determination of the complete state vector  $\mathbf{x}$  and the input vector  $\mathbf{u}$  for a given physically meaningful initial condition. Hereby the initial condition may vary from a quasi-steady flight condition (e.g. horizontal flight, coordinated turn) to a general transient flight condition (e.g. accelerated flight, pull-up condition).

For trimming and simulation the equations of motions ((2.56),(2.59),(2.113)) and the kinematic equations (2.5) have to be cast in the following form:

$$\begin{aligned}\dot{\mathbf{x}} &= f(\mathbf{x}, \mathbf{u}) \quad f \in \mathbb{R}^n, \mathbf{x} \in \mathbb{R}^n, u \in \mathbb{R}^k \\ \mathbf{y} &= g(\mathbf{x}, \mathbf{u}) \quad g \in \mathbb{R}^m \quad ,\end{aligned}\tag{5.1}$$

where  $\mathbf{x}$  denotes the vector of the system states

$$\begin{aligned}\mathbf{x}^T &= \begin{bmatrix} \mathbf{R}_{0e}^T & \boldsymbol{\Theta}^T & \mathbf{V}_b^T & \boldsymbol{\Omega}_b^T & \boldsymbol{\eta}_E^T & \dot{\boldsymbol{\eta}}_E^T \end{bmatrix} \\ &= \begin{bmatrix} x_{0e} & y_{0e} & z_{0e} & | & \phi & \theta & \psi & | & u & v & w & | & p & q & r & | & \boldsymbol{\eta}_E^T & \dot{\boldsymbol{\eta}}_E^T \end{bmatrix} \quad ,\end{aligned}\tag{5.2}$$

$\mathbf{u}$  is the input vector containing the control surface deflections (control surfaces that are used for trimming only) and the trust setting

$$\mathbf{u}^T = \begin{bmatrix} i_H & \xi & \zeta & \delta_F \end{bmatrix}\tag{5.3}$$

and  $\mathbf{y}$  is the output vector (outputs that are relevant for trimming only)

$$\mathbf{y}^T = \begin{bmatrix} Ma & \alpha & \beta & n_z \end{bmatrix} \quad .\tag{5.4}$$

In this set of equations (5.1) the elements of  $\dot{\mathbf{x}}$  and  $\mathbf{y}$  are  $n + m$  unknown values, whereas  $\mathbf{x}$  and  $\mathbf{u}$  are  $n + k$  known values from the control inputs and integration of  $\dot{\mathbf{x}}$  respectively. To start a simulation the complete state vector  $\mathbf{x}$  and input vector  $\mathbf{u}$  have to be known for the first evaluation of (5.1).

A special case for the initial condition is the static equilibrium of the system. Mathematically, the problem of finding a static equilibrium is formulated as solving  $\mathbf{x}$  from the first equations,

such that  $\dot{\mathbf{x}}$  is zero. For aircraft simulation, initial conditions are only partially static. For example, due to the velocity of the aircraft it is not possible that the derivatives of the position  $\dot{x}_{0e}, \dot{y}_{0e}$  are identical zero. Furthermore the initial condition for aircraft simulation is often defined as a mixture of specific values of some entries in  $\mathbf{x}$  and  $\mathbf{u}$  and some entries in  $\mathbf{y}$  and  $\dot{\mathbf{x}}$ . Hereby the known elements of  $\mathbf{y}$  and  $\dot{\mathbf{x}}$  are referred to as the trim requirements and the unknown elements of  $\mathbf{x}$  and  $\mathbf{u}$  are the so-called trim variables.

Since the above set of equations (5.1) hereby still has to be satisfied, it is important that the balance between the numbers of unknown variables and equations is retained. The known values in  $\mathbf{x}, \mathbf{u}, \dot{\mathbf{x}}, \mathbf{y}$  will be collected in a vector  $\mathbf{v}$ . The remaining unknown elements in  $\mathbf{x}, \mathbf{u}, \dot{\mathbf{x}}, \mathbf{y}$  are combined in a vector  $\mathbf{w}$  in order to completely define a trim condition. Of course, most of the unknowns  $\mathbf{w}$  will no longer occur on the left hand side, so that the set of equations has to be solved numerically. In the frame of this work, this is referred to as the trimming problem. To this end a variety of nonlinear equation solvers are available. Here the routine TRIMEX, based on the nonlinear equation solver from MINPACK-1 is used. Due to the nonlinearity of (5.1) the trim point corresponding to a given vector  $\mathbf{v}$  may not be unique. Therefore it is important to specify initial values for the unknown variables so that the trim algorithm yields the appropriate solution.

For the analysis of the inertially coupled equations of motion trim conditions with significant angular rates are of interest. Two trim conditions are considered in the following. One that imposes high centrifugal forces on the structure, a so-called high roll rate condition, and one that leads to a significant wing bending, a pull-up condition. The latter also serves as the initial condition for subsequent simulation.

### (a) High Roll Rate Condition

The roll condition is specified by defining the desired values of the position  $x_{0e}, y_{0e}, z_{0e}$ , the roll attitude  $\phi$ , the desired roll rate  $p$  and the Mach number  $Ma$ . The trim condition is further characterized by zero translational and angular accelerations and a steady state structural deformation (derivative of the generalized elastic coordinates equals zero). The complete vector of given values for the roll rate trim condition is as follows

$$\begin{aligned} \mathbf{v}^T &= \left[ x_{0e} \quad y_{0e} \quad z_{0e} \quad \phi \quad p \quad q \quad r \quad \dot{y}_{0e} \quad \dot{z}_{0e} \quad \dot{u} \quad \dot{v} \quad \dot{w} \quad \dot{p} \quad \dot{q} \quad \dot{r} \quad \dot{\boldsymbol{\eta}}_E^T \quad \dot{\boldsymbol{\eta}}_E^T \quad Ma \right] \\ &= \left[ 0 \quad 0 \quad -12400\text{m} \quad 0 \quad 0.52\text{s}^{-1} \quad 0 \quad 0 \quad 0 \quad 0 \quad 0 \quad 0 \quad 0 \quad 0 \quad 0 \quad 0 \quad \mathbf{0}^T \quad \mathbf{0}^T \quad 0.8 \right] . \end{aligned} \quad (5.5)$$

The control surface deflections  $i_H, \xi, \zeta$  and thrust setting  $\delta_F$  are the free variables which are

used to establish the trim condition. With the remaining unknown variables (e.g. values for the velocity component  $\dot{x}_{0e}$ , the derivatives of the euler angles  $\dot{\phi}, \dot{\theta}, \dot{\psi}$ , etc.) the complete vector of unknown variables for the roll rate condition becomes

$$\mathbf{w}^T = \left[ \theta \quad \psi \mid u \quad v \quad w \mid \boldsymbol{\eta}_E^T \quad \dot{\boldsymbol{\eta}}_E^T \mid \dot{x}_{0e} \mid \dot{\phi} \quad \dot{\theta} \quad \dot{\psi} \mid i_H \quad \xi \quad \zeta \quad \delta_F \mid \alpha \quad \beta \quad n_z \right] . \quad (5.6)$$

Note that for the selection of the elements in  $\mathbf{v}$  and  $\mathbf{w}$  it is important to consider that the trim variables must have an influence on the trim requirements. Otherwise the free values cannot be used to establish the trim condition, i.e. the trim problem is not set up properly.<sup>4</sup>

### (b) Pull-Up Condition

The second trim condition is a wings level pull-up with a vertical load factor of  $n_z = 1.67g$ . This trim condition imposes a large wing bending and is often required for aircraft certification. The vector of given values defines the initial position, the orientation and a steady state deformation as follows

$$\begin{aligned} \mathbf{v}^T &= \left[ x_{0e} \quad y_{0e} \quad z_{0e} \quad \phi \mid p \mid \dot{y}_{0e} \quad \dot{z}_{0e} \mid \dot{u} \quad \dot{v} \quad \dot{w} \mid \dot{p} \quad \dot{q} \quad \dot{r} \mid \boldsymbol{\eta}_E^T \quad \ddot{\boldsymbol{\eta}}_E^T \mid Ma \quad \beta \quad n_z \right] \\ &= \left[ 0 \quad 0 \quad -12400\text{m} \mid 0 \mid 0 \mid 0 \quad 0 \mid 0 \quad 0 \quad 0 \mid 0 \quad 0 \mid \mathbf{0}^T \quad \mathbf{0}^T \mid 0.8 \quad 0 \quad 1.67 \right] . \end{aligned} \quad (5.7)$$

The corresponding unknown free values that can control the given values then become

$$\mathbf{w}^T = \left[ \theta \quad \psi \mid u \quad v \quad w \mid q \quad r \mid \boldsymbol{\eta}_E^T \quad \dot{\boldsymbol{\eta}}_E^T \mid \dot{x}_{0e} \mid \dot{\phi} \quad \dot{\theta} \quad \dot{\psi} \mid i_H \quad \xi \quad \zeta \quad \delta_F \mid \alpha \right] . \quad (5.8)$$

### Trim Results

A selection of characteristic values for the above trim cases are given in Table 5.1. Note that the roll condition has a nonzero angle of sideslip due to setting the yaw rate to zero. A zero angle of sideslip could be achieved by selecting the yaw rate to be an independent variable.

Figure 5.5 shows the deformed airframe and the inertia ellipsoid located at the center of gravity. The ellipsoid radii are aligned with the principal axes of inertia. The inertia ellipsoid may be considered as a surface of constant rotational kinetic energy for an arbitrary rigid body rotation [73].

<sup>4</sup>Trim variables that have no influence on any trim requirement and linear dependencies of trim variables or trim requirements result in singular values of zero of the sensitivity (Jacobian) matrix. The corresponding singular vectors show the trim requirements and trim variables that lead to the rank deficiency.



	(a) Roll	(b) Pull up
$\alpha$ [°]	0.3	6.3
$\beta$ [°]	2.7	0.0
$p$ [°/s]	30	0.0
$q$ [°/s]	0.0	1.5
$r$ [°/s]	0.0	0.0
$\phi$ [°]	0.0	0.0
$\theta$ [°]	0.3	6.3
$\psi$ [°]	-2.7	0.0
$n_z$ [-]	0.36	1.67

**Table 5.1:** Selection of characteristic values of the high roll rate trim condition (a), and the pull-up condition (b).

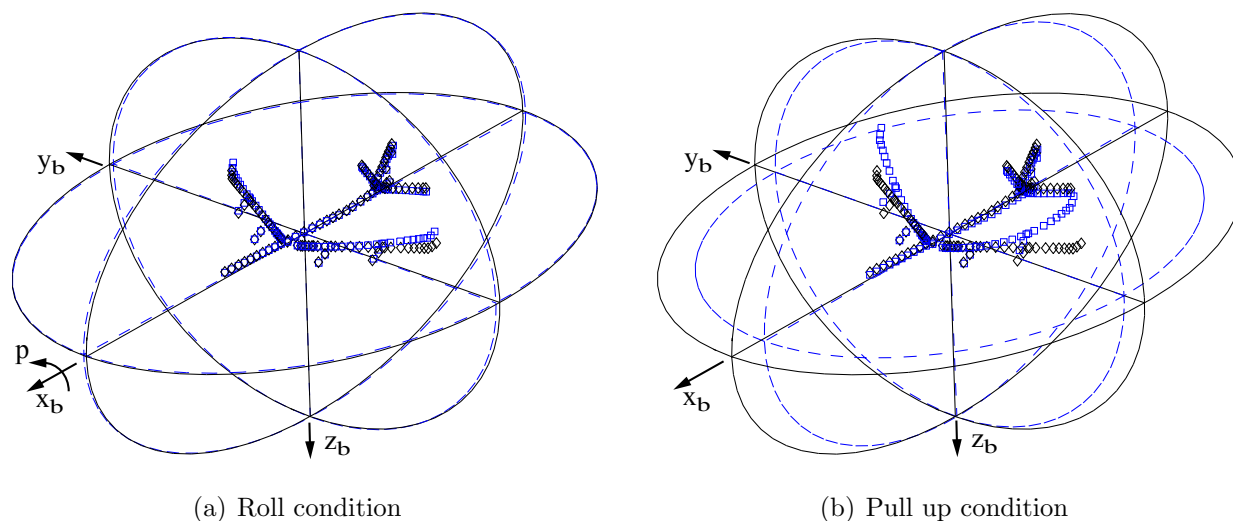


**Figure 5.5:** Inertia ellipsoid in undeformed ( $\diamond$ —) and deformed ( $\square$  - - -) condition (deformation scaled up)

The roll condition yields a small unsymmetrical structural deformation. The inertia tensor in deformed condition is therefore changed in the off-diagonal elements compared to the undeformed configuration. This results in a small change in the orientation of the principal axes of inertia. The pull up conditions show a more significant variation between the undeformed and the deformed configuration due to the higher angle of attack. Here it can be noticed that roll and pitch inertia decrease due to the symmetric wing bending. The inertially coupled equations of motion account for this change in inertia since the moment equations incorporates the inertia tensor of the actual deformation.

## Elastic Deformation

The effect of inertial coupling on local structural deformation will be further analyzed for the high roll rate condition. A trim solution is obtained using uncoupled and inertially coupled equations of motion. Figure 5.6 depicts the deformation obtained from the two trim calculations. The aileron deflection (Right up, left down) causes the left wing to bend more upward. The roll motion induces an additional upward airflow at the right stabilizer and a downward airflow at the left stabilizer resulting in an opposite stabilizer deformation and in fuselage torsion.

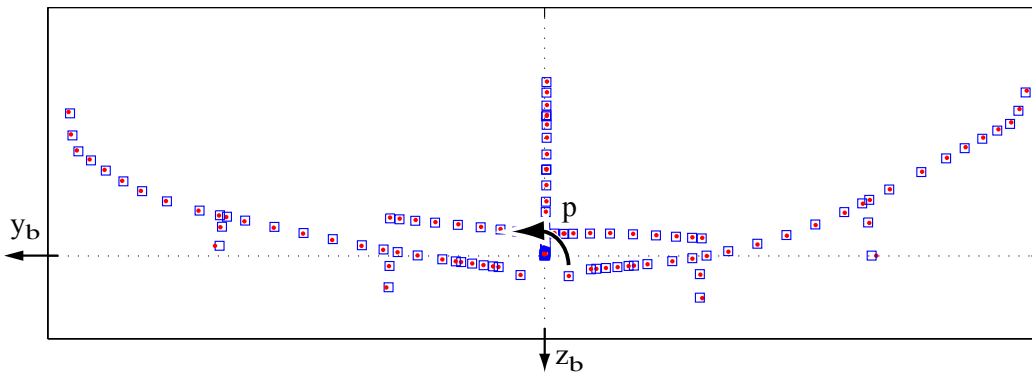


**Figure 5.6:** Comparison of trim deformations for the high-roll-rate trim condition (a), computed with uncoupled ( $\square$ ) and inertially coupled ( $\bullet$ ) equations of motion (front view, deformation scaled up)

The wing bending is closely represented by uncoupled and coupled EOM. However, a difference can be noticed at the engine grids. The roll rate causes the engines to displace outward due to centrifugal forces contained in the inertially coupled formulation. An outward displacement of the engines can also be noticed in case of the uncoupled EOM. In this case it is a result of the wing bending and no direct effect of the centrifugal forces.

## 5.3 Dynamic Maneuver

A dynamic maneuver will be considered in this section. The trim results for the pull-up and high-roll-rate condition showed the quasi-static effect of inertial coupling on the elastic deformation and the inertia tensor. Here a dynamic maneuver is considered as a test case to analyze the influence on time domain simulation and recovery of dynamic loads. The FAR 25 roll-maneuver is a standard maneuver in the development of transport aircraft. It combines the pull-up condition with the high roll rate and high roll acceleration conditions. Figure 5.7 shows the motion of the airplane for the roll maneuver, as seen by an inertial observer and depicts the respective aileron deflection.

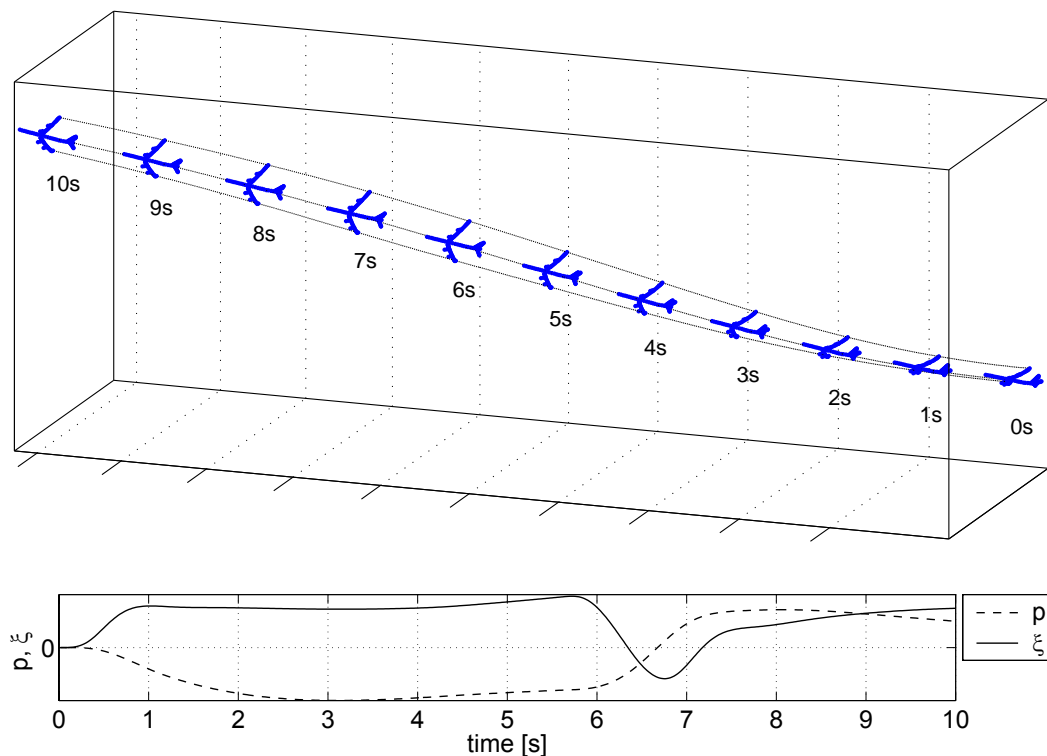


**Figure 5.7:** View on 1.67g roll maneuver with time histories of the roll rate  $p$  and the aileron deflection  $\xi$

The initial condition  $t = 0$  of the roll maneuver is the horizontal pull-up trimmed at a vertical load factor of  $n_z = 1.67g$  (trim condition (b), Section 5.2, Table 5.1). Then rolling is initiated by the pilot model via the ailerons until a high roll rate condition ( $t=3s$ ) and a high bank angle is reached. Next, opposite aileron deflection is applied, resulting in a high roll deceleration condition ( $t=6.5s$ ). The bank angle decreases and the airplane starts to roll back to a wings level flight.

In the following the effect of inertial coupling will be analyzed. The dynamic maneuver is simulated using inertially decoupled and coupled EOM. Kinetic energy terms are considered first, then the influence on flight mechanical and elastic states are depicted. After discussion of the airplane motion, dynamic loads of the airframe are shown.

### 5.3.1 Energy Terms

The derivation of the equations of motion is based on the Lagrange's equations. Hereby the formulation of the energy terms is one of the basic steps. The kinetic energy contains the cross coupling terms between rigid body and elastic motion. A decoupled formulation neglects these terms. It is therefore desirable to study the influence of inertial coupling in the kinetic energy first.

From Equation (2.40) the nodal kinetic energy in the translational coupling term becomes  $\mathbf{\Omega}_b^T(\bar{\mathbf{d}}_i \times \dot{\bar{\mathbf{d}}}_i)m_i$ . The term is evaluated for each node during the roll maneuver. The maximum value is depicted in Figure 5.8, where the sphere radii indicate the magnitude of the kinetic energy. The highest values can be noticed at the outer engine nodes. The maximum values are reached at about  $t \approx 6s$ . At this time the roll rate has reached a high value, see Figure 5.7. Elastic displacements and velocities are depicted for the same time step. It can be seen that both vectors are not collinear or even close to collinearity. Collinearity is often assumed for the development of inertially uncoupled formulations.

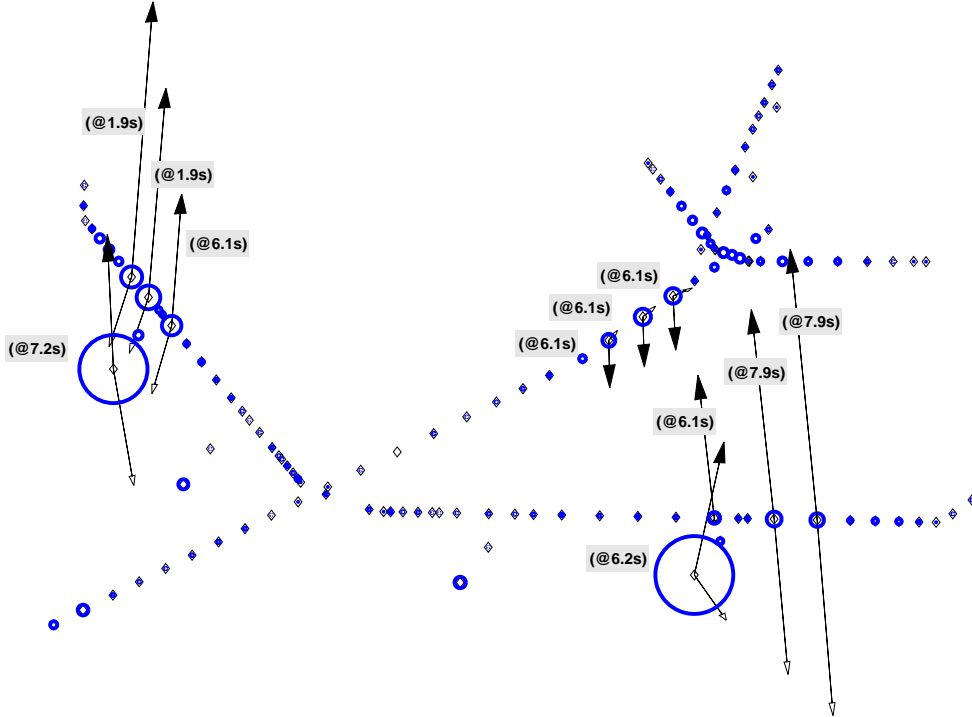


**Figure 5.8:** Kinetic energy of the translational inertial coupling term. Sphere radii illustrate the maximum values. The respective elastic deformation is depicted by  $\blacktriangleright$ , the velocity by  $\blacktriangleright$

### 5.3.2 Flight Mechanical States

The effect of the inertial coupling on flight mechanical states  $\mathbf{R}_{0e}$ ,  $\mathbf{\Theta}$ ,  $\mathbf{V}_b$ ,  $\mathbf{\Omega}_b$  will be considered next. Flight mechanical states are obtained from the force and moment equations (2.56), (2.59) and the kinematic equations (2.5). The moment equation (2.59) accounts for variation of the inertia tensor of the vehicle via feedback of the modal elastic states (see Figure 5.4) and contains the additional  $\mathbf{h}$ -term. Figure 5.9 depicts the variation of the inertia tensor with time. The effect on the diagonal elements as well as the main off-diagonal term  $J_{xz}$  is noticeable but small. Especially the small off-diagonal elements  $J_{xy}$  and  $J_{yz}$  change

significantly with elastic deformation due to the un-symmetric deformation.

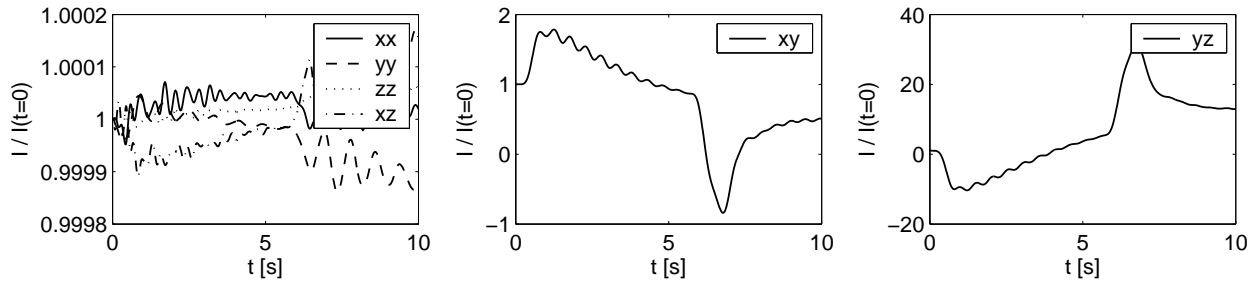


**Figure 5.9:** Time variation of the inertia tensor  $\mathbf{J}$

The angular velocity of the body frame  $\boldsymbol{\Omega}_b = [p, q, r]^T$  and the Euler angles  $\boldsymbol{\Theta} = [\phi, \theta, \psi]^T$  obtained from inertially coupled and decoupled EOM are depicted in Figure 5.10. The roll acceleration  $\dot{p}$  reaches a slightly higher value at its first maximum in case of the coupled simulation. The differences in angular rates and Euler angles are less than 0.5%.

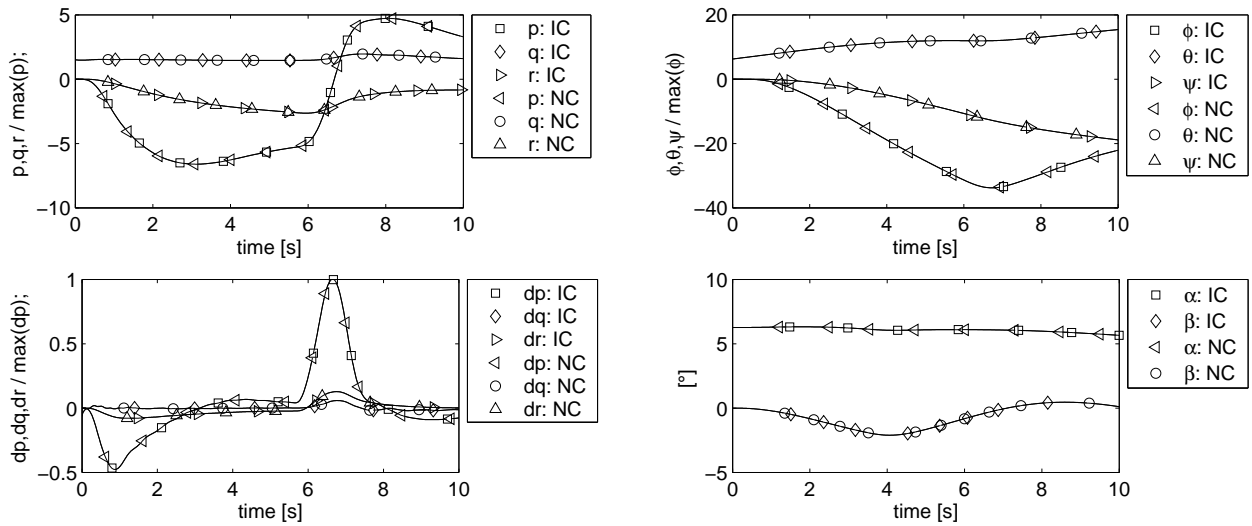


**Figure 5.10:** Flight mechanical states. (IC: with inertial coupling, NC: without inertial coupling)

However the small inertial coupling effects are of no practical relevance for the flight mechanical states. These effects increase for maneuvers with higher angular rates or structural models with higher flexibility, especially if simulation times are longer.

### 5.3.3 Modal Elastic States

The elastic equation (2.113) completes the EOM in addition to the force and moment equation. It yields the generalized elastic coordinates or modal states. They will now be analyzed and compared to those obtained from the uncoupled formulation.

Selected characteristic modes are shown in Figure 5.11. It can be noticed that there is either close agreement or a significant difference in the time history of generalized coordinates. The first mode and the second mode are good examples for those modes that are not affected by the EOM type. Modes number seven and nine are highly affected modes.

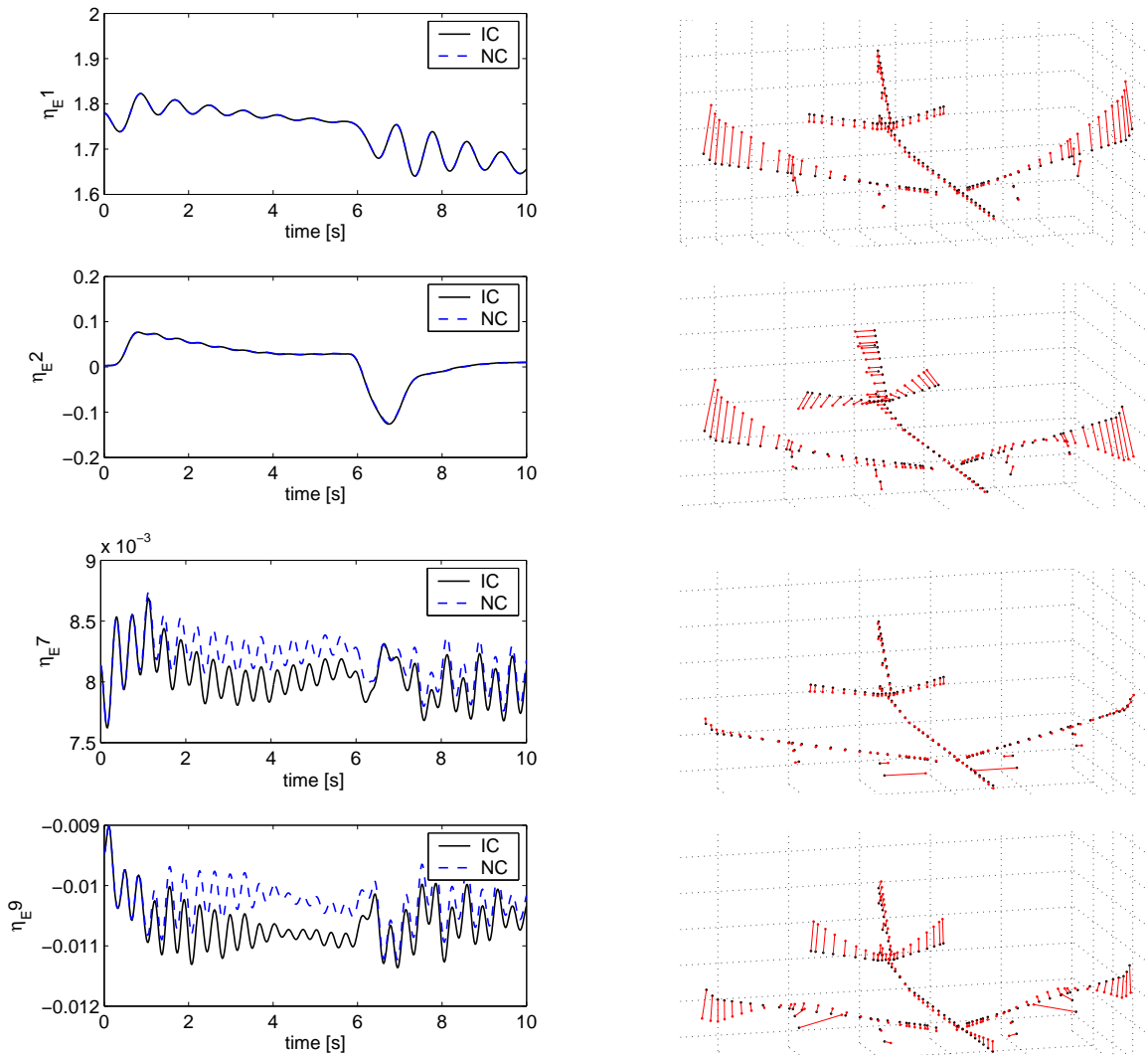


**Figure 5.11:** Time history of selected generalized elastic coordinates and the corresponding mode shape (IC: with inertial coupling, NC: without inertial coupling)

The first mode and the second mode represent a low frequency symmetric and asymmetric wing bending mode. They are mainly driven by the aerodynamic forces due to control surface deflection and airplane motion. The asymmetric wing bending therefore correlates with the aileron deflection (Figure 5.7) and the roll rate (Figure 5.10).

The seventh and ninth mode are good examples of modes being affected by inertial coupling. They represent lateral inner and outer engine modes. The time histories from both simulations are identical up to about  $t = 1$  s. Then a low frequency offset occurs. This can be explained by the centrifugal forces that cause an outward displacement of the engines

when the roll rate builds up, represented by the respective engine modes. At  $t = 6.5s$  the maximum roll angle is reached and the roll rate is zero. At this point modal time histories agree. Then the opposite roll rate increases, causing again an outward displacement of the engines.

The contribution of the inertial coupling terms to the elastic equation (2.113) involves the coriolis, centrifugal and angular acceleration terms. Each term yields generalized forces, Figure 5.12 shows the time histories. It can be noticed that the centrifugal term increases with roll rate. At  $t = 6.5s$  the roll rate is zero but roll acceleration is high. At this time the angular acceleration term becomes important. The coriolis term varies with the velocity of the generalized coordinates and the roll rate but is about an order smaller than the other coupling terms.

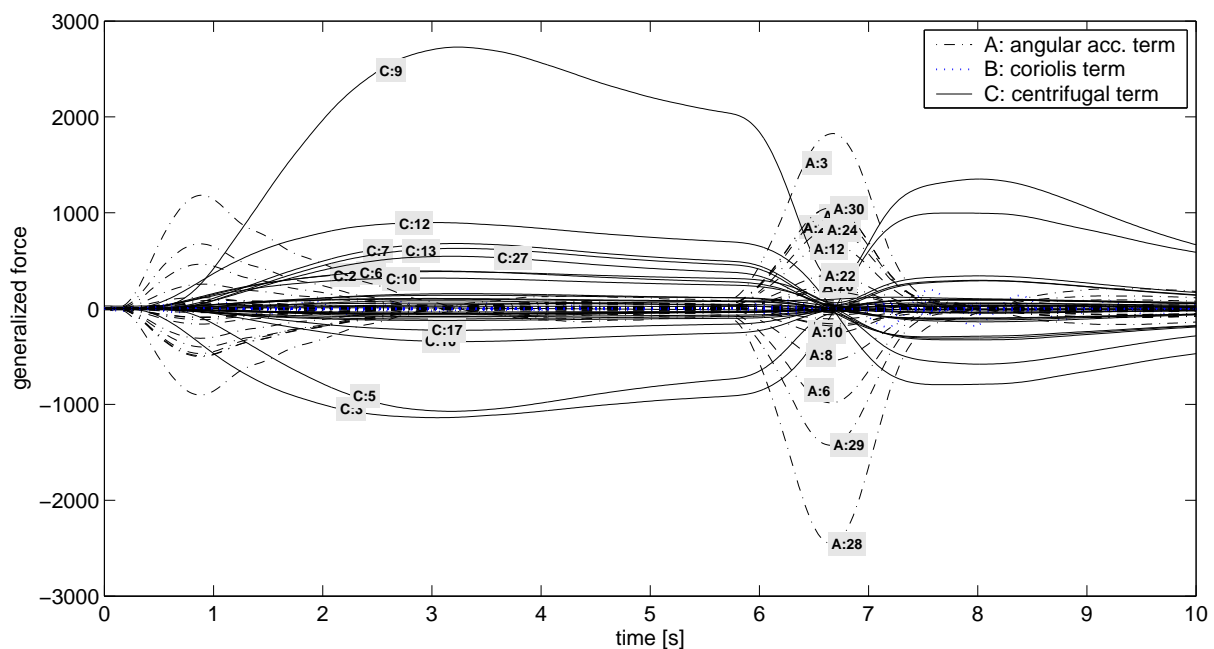


**Figure 5.12:** Generalized forces of the inertial coupling terms. The numbers denote the respective generalized coordinate

For the given roll maneuver the inertial coupling effects primarily result from centrifugal forces at the engines. A high roll rate, offset of engines from the fuselage and large concentrated engine masses lead to prominent inertial coupling terms at the location of the engines.

### 5.3.4 Structural Loads

The equations of structural loads (3.16) are used to compute elastic forces at nodes of the structural model. Recalling the equations for the kinetic energy (2.24) it is obvious that inertial coupling has a significant influence at nodes where elastic deformation and large local masses are present. For a conventional transport aircraft engines are therefore significantly subjected to inertial coupling effects.

The lateral nodal forces at the left outer engine pylon node (Figure 5.13) show the correlation of the roll rate and acceleration with structural loads. The main differences in lateral loads are encountered at the time where maximum roll rate is reached.

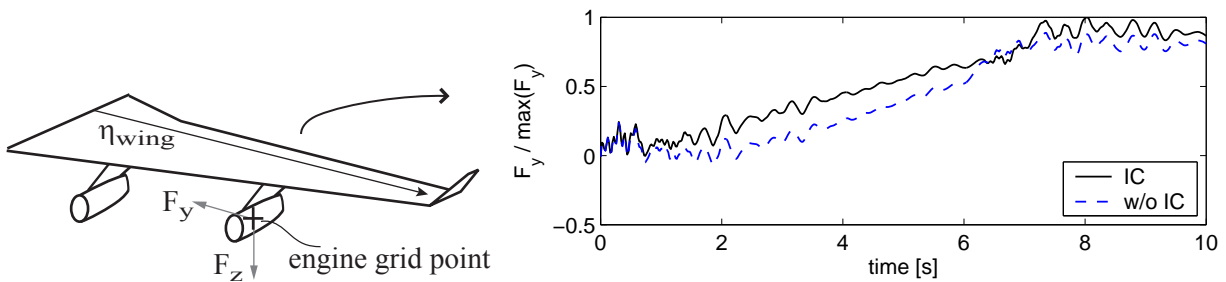


**Figure 5.13:** Nodal lateral force at left engine grid point

Integrated shear loads will be studied next. A loads envelope for the left wing due to the given maneuver is depicted in Figure 5.14. The distributed minimum and maximum integrated shear loads are obtained from simulation with inertially uncoupled and coupled equations of motion.

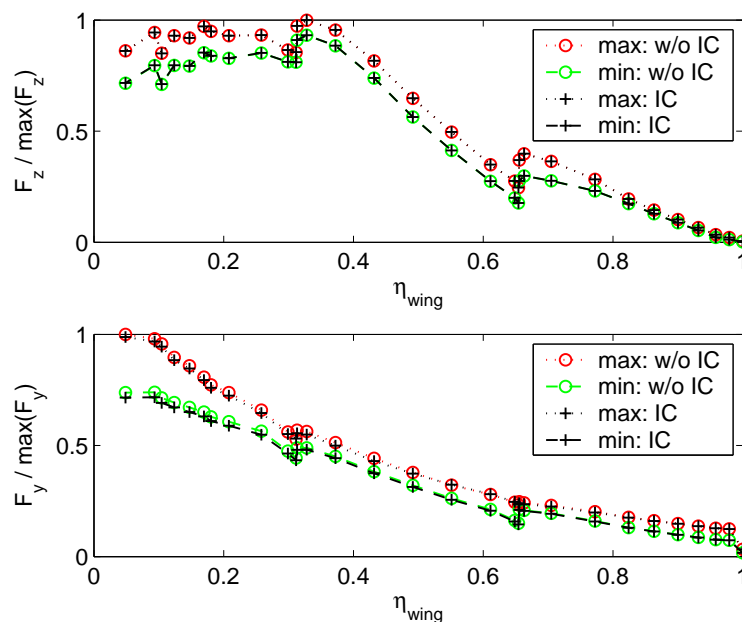


**Figure 5.14:** Envelope of test maneuver - integrated shear loads



The vertical shear forces  $F_z$  are not noticeably influenced by inertial coupling effects since aerodynamic forces, gravity forces and inertial forces are the driving forces for the shear loads. The situation is different for lateral loads  $F_y$ , see Figure 5.14. Aerodynamic components are small and inertial coupling forces, e.g. centrifugal forces are significant in the lateral direction. Especially the outer engine, located at  $\eta_{wing} = 0.65$ , causes a difference between coupled and uncoupled simulation.

Figure 5.15 depicts an overview of the maximum differences for coupled and uncoupled simulation. As previously shown, engines and pylons cause the main differences in lateral forces. Lateral forces also affect the local moments due to offset of the mass element to the grid points. The high differences in local moments  $M_z$  are caused by this modelling aspect.

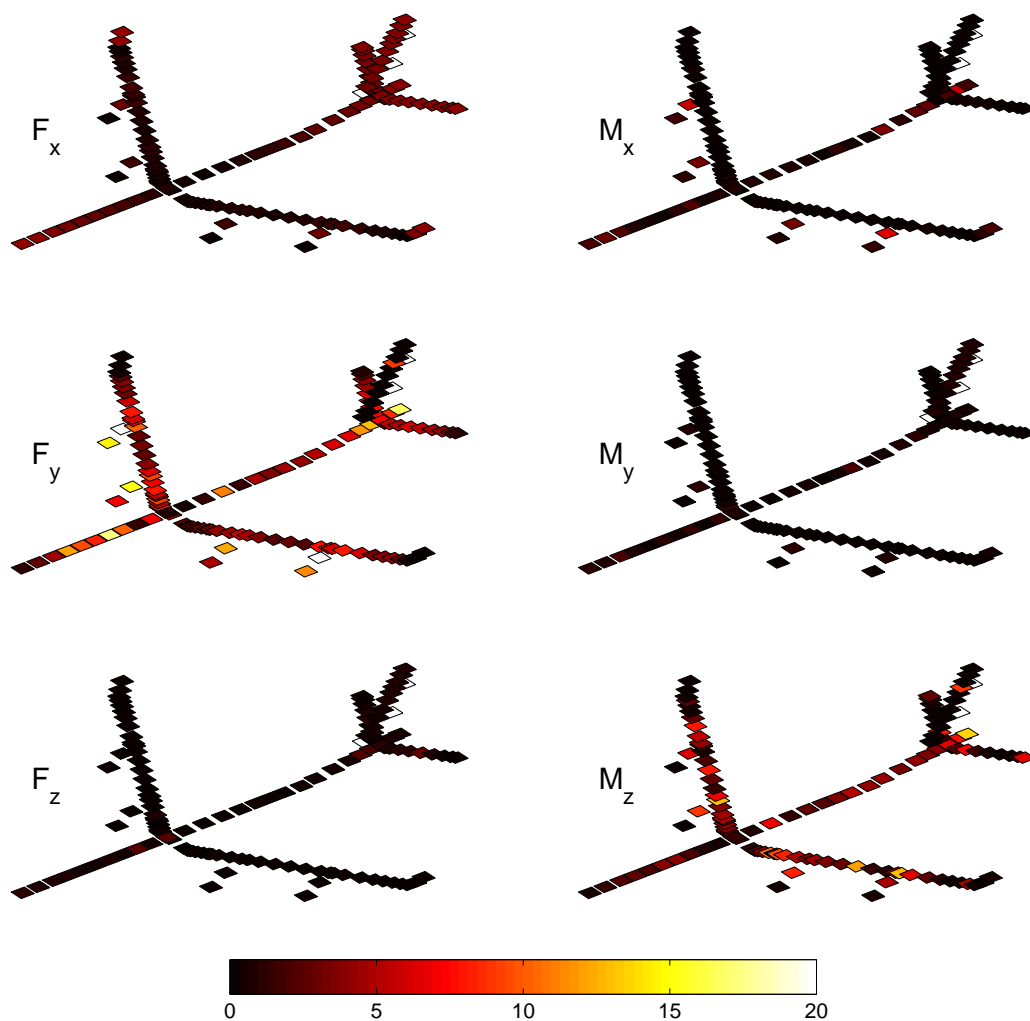


**Figure 5.15:** Relative differences [%] of maximum nodal forces (inertially coupled/uncoupled EOM,FSM) during dynamic simulation

In summary, the chosen test maneuver shows a significant influence of inertial coupling on

local and integrated loads for:

- high angular rate / acceleration conditions,
- highly flexible structures or structural components,
- nodes with large concentrated masses,
- nodes and components where external forces are small.

### 5.3.5 Spin-Off Result

For industrial applications it is common practice to couple a nonlinear flight mechanics model with a linear aeroelastic model. The approaches combine available, agreed on flight mechanic and aeroelastic aircraft models from the respective engineering disciplines. A one directional coupling is given in [56]. This method uses the states of the flight mechanics model as an input to the elastic model. A method with two directional coupling is presented by [71] and [33]. It contains a feedback of incremental dynamic forces from the elastic modes to the flight mechanics model. The latter approach can be cast in the form of the inertially uncoupled EOM. A comparison of two methods, regarding accuracy, implementability, pre-processing and computing effort is presented in [48].

The coupling methods account for the interaction of elastic and rigid body motion. However, the listed references do not account for the inertial coupling effects because of implementation constraints. Due to the traditional use of the approaches it is of practical interest to study the combination of inertially uncoupled EOM with the new form of the force summation method, which includes inertial coupling effects.

The nodal force at the left engine is found to be highly subjected to inertial coupling, it will therefore be used again as a test case. The nodal force at the left grid is shown in Figure 5.16. Nodal forces are obtained from uncoupled and inertially coupled EOM and respective EOL. Additionally the combination of uncoupled EOM with inertially coupled EOL is considered. Interestingly the result is now close to the trajectory of the full inertially coupled formulation.

### Explanation

The inertially coupled force summation method (3.16) may be written in the following form:

$$\mathbf{L}_g^{\text{FSM}} = \mathbf{P}_g(\mathbf{V}_b, \overset{\circ}{\mathbf{V}}_b, \mathbf{\Omega}_b, \overset{\circ}{\mathbf{\Omega}}_b, \boldsymbol{\eta}_E, \overset{\circ}{\boldsymbol{\eta}}_E, \overset{\circ\circ}{\boldsymbol{\eta}}_E) + f(\mathbf{V}_b, \overset{\circ}{\mathbf{V}}_b, \mathbf{\Omega}_b, \overset{\circ}{\mathbf{\Omega}}_b, \boldsymbol{\eta}_E, \overset{\circ}{\boldsymbol{\eta}}_E, \overset{\circ\circ}{\boldsymbol{\eta}}_E) \quad . \quad (5.9)$$

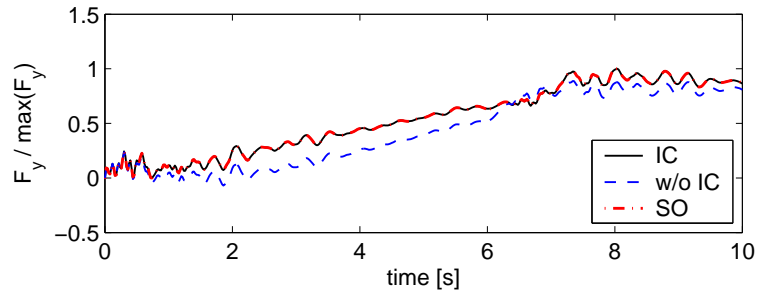


**Figure 5.16:** Nodal lateral force at left engine grid (IC: with inertial coupling, NC: without inertial coupling, SO: uncoupled EOM combined with coupled EOL)

The velocity and acceleration of the mean-axes frame ( $\mathbf{V}_b, \dot{\mathbf{V}}_b$ ) is not directly affected by inertial coupling since the force equation is only driven by the external forces. The angular velocity and acceleration  $\mathbf{\Omega}_b, \dot{\mathbf{\Omega}}_b$  are analyzed in (5.10). The differences between coupled and uncoupled simulation are found to be very small.

The time derivatives of the modal states are shown in Figure 5.17. Especially the second time derivatives yield close results.

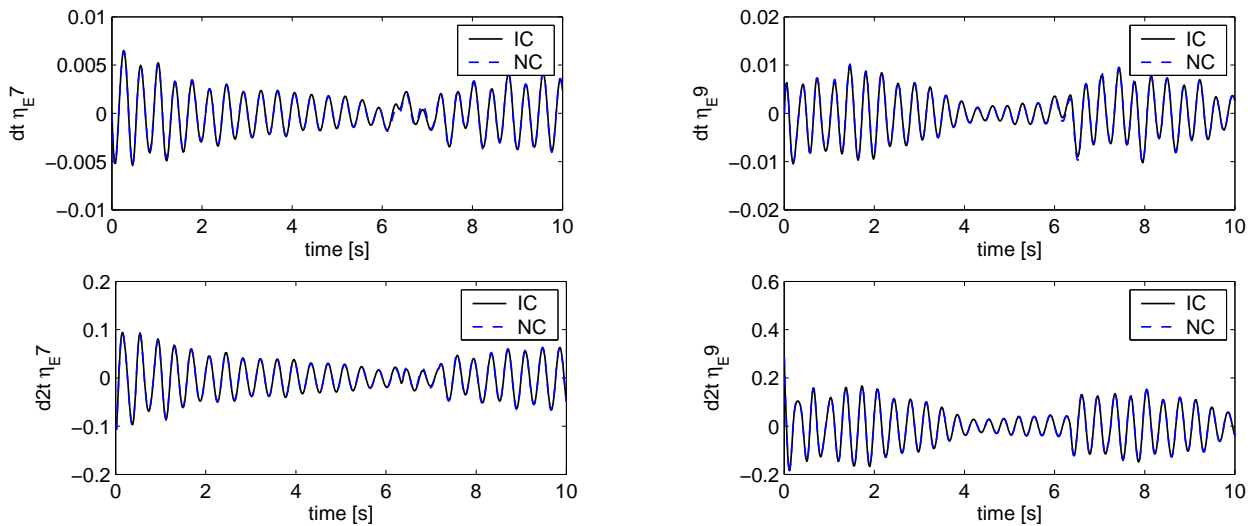


**Figure 5.17:** Time history of inner and outer engine modes. First and Second time derivation (IC: with inertial coupling, NC: without inertial coupling)

A significant difference can be noticed for modal states subjected to inertial coupling, see Figure 5.11. The modal states drive the external forces and the elastic contribution to the centrifugal term, see Table 3.1. The elastic contribution to the centrifugal term is small compared to the rigid contribution. Hence, nodal loads computed with the force summation method (3.16) are also close despite of the affected generalized coordinates.

It can be concluded that simulation results, obtained from an inertially uncoupled formulation may be combined with a force summation method accounting for inertial coupling. This is

possible when:

- inertial coupling does not significantly affect the motion of the mean-axes frame,
- inertial coupling does not significantly affect the external forces,
- rigid body states vary gradually and relatively slowly so that the derivatives of the modal states have nearly identical values.

This is the case for the presented roll maneuver. The inertially coupled EOL can be used for computation of enhanced nodal loads. However it has to be kept in mind that this is only possible if the above assumptions hold. Generally, for consistent modal results and loads based on the same assumptions, both EOM and EOL have to account for inertial coupling effects.

## 5.4 Summary

A practical test case, the FAR roll maneuver is studied. The influence of inertial coupling on local and integrated loads is found to be relevant for flight conditions with high angular rates or high angular accelerations. Especially structural components with large concentrated masses and large offsets are influenced by inertial coupling terms.

The described set of equations EOM and EOL include important physical effects without requiring a different modelling strategy. This may be used to increase the precision of the dynamic simulation and loads recovery while adding minimum computational effort compared to uncoupled formulations.

As a spin-off result it is shown that the new form of the force summation method can be used to account for inertial coupling effects even if the simulation is performed with inertially uncoupled EOM. If the additional assumptions listed in Section 5.3.5 hold, the load computation based on data from uncoupled simulation can be enhanced. This may be used as a simple check of existing data for the relevance of inertial coupling effects.

## 6 Summary and Conclusions

The objective of this thesis is to provide a consistent set of equations of motion (EOM) and equations for loads computation (EOL) for free-flying flexible transport aircraft. The precision of the EOM and EOL is improved by accounting for inertial coupling terms and an enhancement of the aerodynamic database loads by unsteady dynamic load increments induced by deformation of the airframe. The formulation is developed in such a way that industrial FE-data and aerodynamic models used in flight loads calculation can be directly incorporated. No additional data as currently used is required.

The equations of motion for an elastic aircraft are derived using Lagrange's equations in terms of quasi-coordinates. The state equations for a flexible aircraft are nonlinear, where the nonlinearity arise from the large rigid body motion and from inertial coupling terms. As common in present flight loads analysis a system consisting of discrete masses and respective inertia tensors is assumed. Thus available data from FE-models used in loads and aeroelastics can be incorporated directly. The underlying assumptions for the equations development are:

- The aircraft is described as a collection of lumped mass elements, with an associated mass and inertia tensor.
- Linear elastic theory applies.
- Local translational and rotational elastic deformations with respect to the reference shape are small.
- The elastic deformation may be written as a linear combination of the mode shapes.
- Gravity is constant over the airframe.

The present approach extends available formulations for lumped mass systems by rotational degrees of freedom of masses and mass offsets from grid points. The resulting equations are summarized in Figure 2.7. The EOM is capable of fully representing inertial cross coupling. The inertia tensor for the deformed aircraft and the additional  $h$ -term provide coupling of the moment equation with the elastic equation. The forces from angular accelerations of the body frame, Coriolis forces and the centrifugal loading on the elastic modes provide coupling of the elastic equation with the moment equation.

All coupling terms are cast in generalized matrix form for computational efficiency. The validity of the new form is shown by comparison with the physical form. The coupling matrices can be assembled by pre-processing from available FE-data, namely the physical mass matrix and a set of free vibration mode shapes. The operations during simulation are reduced to multiplication with generalized coordinates.

Nodal elastic forces are computed from the rigid body and elastic states available from the EOM. The conventional force summation method is valid for an aeroelastic system with small rigid body motion. A general form of the equations of loads is derived based on the principle of momentum. The new formulation (summarized in Figure 3.5) is suitable for the computation of loads in combination with inertially coupled equations of motion and nonlinear rigid body motion. All underlying assumptions are the same as for the equation of motion development. The general formulation is validated by the comparison of generalized elastic forces from the EOL with those contained in the EOM.

Aerodynamic models for maneuver loads are nonlinear models usually based on table lookup and application rules. The aerodynamic forces account for quasi-steady deformations. For the simulation of a free flying flexible aircraft these aerodynamic loads have to be extended by unsteady aerodynamic increments induced by deformation of the airframe. The combination of the aerodynamic models leaves the nonlinear quasi-flexible aerodynamics unchanged. This is favorable since the database loads have been adapted to experimental and flight test data.

Existing approaches namely the RM-approach apply to generalized aerodynamic models with generalized aerodynamic forces. The computation of flight loads with accurate EOL requires the aerodynamic loads to be available in distributed form. The present thesis provides an extension of the RM-approach for integrating aerodynamic models with distributed quasi-steady forces.

Two example trim cases are considered, namely a high roll rate and pull up condition. In the former, the changes in the inertia tensor caused by the deformation is small, but local elastic deformations itself are significantly affected by inertial coupling. In the latter, the influence on the inertia tensor is more prominent, while the deformation is only slightly affected by inertial coupling.

Then a practical test case, a 1,67g roll maneuver, is studied. The simulation is performed using an uncoupled formulation and the new inertially coupled formulation. The effects on flight mechanic states are found to be very small. Wing bending modes having primary influence on the aerodynamic forces are almost identical in both formulations, hence total aerodynamic forces are almost unaffected. A closer look at the modal responses reveals a

main influence on the first inner and outer engine mode. Hereby the centrifugal term is the most important coupling effect.

The influence of inertial coupling on local and integrated loads is found to be relevant for high angular rate/acceleration flight conditions. Especially flexibly attached structural components with large concentrated masses are influenced by inertial coupling terms. The inaccuracy resulting from an uncoupled simulation is highest for lateral loads on engine pylon and moments in wing areas close to the engine pylons.

The described set of equations EOM and EOL include important physical effects without requiring a different modelling strategy or additional data. This increases the precision of the dynamic simulation and loads recovery while adding minimum computational effort compared to classic uncoupled formulations.

As a spin-off result it is shown that the new form of the force summation method can be used to estimate inertial coupling effects in combination with inertially uncoupled simulation. This result is of great practical relevance. It provides an easy inspection of available simulation data and loads for inertial coupling effects.

The improvements of this work to flight loads calculation can be summarized as follows:

- Derivation of a consistent equations of motion (EOM)/loads equation (EOL) set including full inertial coupling. The precision of flight loads computation is increased while available model data can be directly incorporated.
- The equations of motion are cast in an efficient form of implementation. The fully generalized form of all coupling terms is ideally suited for rapid time domain simulation and loads loop calculation.
- A new loads equation is derived extending the force summation method towards non-linear rigid body motion and inertial coupling.
- The Residualized Model approach is extended towards distributed quasi-flexible aerodynamic loads. The approach can now be used in combination with force summation loads recovery.
- The effects of inertial coupling for transport aircraft in dynamic maneuver is worked out. The inaccuracy in loads resulting from uncoupled formulation is identified.
- As a spin-off result, an approach for estimating inaccuracies of loads from uncoupled simulation, is presented. This is of important practical relevance since uncoupled formulations are frequently used in industry.

## Recommendations

Future work in this field should consider two main tasks. On the structural level, dynamic stiffening should be included in the formulation in order to enlarge the validity of the formulation beyond the application to transport aircraft. The aerodynamic model is currently based on the integration of available data. Future work should focus on the development of a single aerodynamic model for nonlinear unsteady aerodynamic forces. Hereby a time domain formulation could overcome inaccuracies arising from approximation of forces obtained in frequency domain and account directly for the variation of mach number.



# Kurzfassung

Die vorliegende Arbeit befasst sich mit der mathematischen Modellbildung, Simulation und Lastenrechnung eines frei fliegenden flexiblen Transportflugzeuges. Hierbei wird das Problem der inertialen Kopplung zwischen der nichtlinearen Bewegung des körperfesten Koordinatensystems und der elastischen Deformation relativ zu diesem Referenzsystem berücksichtigt.

Das Gebiet der Lastenrechnung umfasst die Berechnung von Strukturlasten, hervorgerufen durch Flugmanöver und Turbulenz. Das komplette Simulationsmodell zur Lastenrechnung setzt sich aus dem Modell für das flexible Flugzeug sowie weiteren Modellen, wie das Electronic Flight Control System (FCS), Pilotenmodell etc. zusammen. Die aeroservoelastische Simulation wird im Zeitbereich für eine Vielzahl von Arbeitspunkten und Beladungen durchgeführt. Anschließend wird aus den jeweils größten auftretenden Lasten eine Einhüllende gebildet, welche die dimensionierenden Lasten für den Design Prozess liefert.

In der Vergangenheit wurden verschiedene Modelle zur Ermittlung von Manöverlasten und Böenlasten verwendet. Modelle für die Manöverlasten besitzen nichtlineare Bewegungsgleichungen und basieren auf Datenbanken zur Bereitstellung der aerodynamischen Kräfte. Zur Bestimmung von Böenlasten werden lineare Aeroelastikmodelle verwendet; Luftkräfte stammen hierbei aus der Potentialtheorie wie z.B. aus der Doublet Lattice Methode.

Insbesondere große flexible Transportflugzeuge erfordern jedoch Modelle, die sowohl große nichtlineare Bewegungen als auch elastische Verformungen der Struktur berücksichtigen. Hierzu existieren Ansätze, existierende Flugmechanik und Aeroelastikmodell zu koppeln. Eine weitere Möglichkeit neben der Kopplung von Modellen ist die Entwicklung von integrierten Modellen. Im Unterschied zur Modellkopplung wird hierbei ein einziges Modell entwickelt, das sowohl die spezifischen Anforderungen zur Berechnung von Manöverlasten als auch von Böenlasten berücksichtigt.

Wird ein integriertes mathematisches Modell verwendet, so ist es erstrebenswert, dass die Zustände des Modells in Analogie zur Flugmechanik und Aeroelastik gewählt werden. Es ergeben sich dann Bewegungsgleichungen, die sowohl nichtlineare Gleichungen für die Bewegung des Referenzsystems als auch lineare Gleichungen für die Deformation enthalten. Die Gleichungen sind dabei über die externen Kräfte, die ihrerseits von der Bewegung des

Referenzsystems und der Deformation abhängen, gekoppelt. Diese Art der Kopplung wird als externe Kopplung bezeichnet. Bei der Bewegung eines flexiblen Körpers im Raum tritt weiterhin eine direkte Kopplung zwischen der Bewegung des Referenzsystems und der Deformation auf. Dabei handelt es sich um inertielle Kopplung, die wie folgt definiert wird:

**Inertielle Kopplung:** Direkte Kopplung zwischen der Bewegung eines körperfesten Referenzsystems und der Deformation des elastischen Körpers bezüglich dieses Referenzsystems.

Mit zunehmender Größe von Transportflugzeugen und der Verwendung von leichteren und flexibleren Strukturen, verringert sich auch der Abstand der Eigenfrequenzen zwischen Flugmechanik und Strukturodynamik. Dies führt zu einer zunehmenden externen und inertialen Wechselwirkung. Weiterhin werden immer größere Winglets und Triebwerke verwendet. Letzteres vergrößert den Abstand zwischen Triebwerksschwerpunkt und der elastischen Achse der Tragfläche. Beides sind Ursachen für eine weitere Erhöhung der inertialen Wechselwirkungen. Derzeit enthalten Simulationsmodelle diese inertialen Kopplungsterme nicht oder die Formulierungen sind nicht auf die Anforderungen der industriellen Lastenrechnung ausgerichtet.

In der Lastenrechnung für elastische Knotenkräfte ist die Force Summation Methode das bevorzugte Verfahren; sie zeichnet sich durch hohe Genauigkeit und ein schnelles Konvergenzverhalten aus. Die Anwendbarkeit ist jedoch auf ein Aeroelastikmodell mit kleiner Starrkörperbewegung beschränkt. Insbesondere ist die inertielle Kopplung nicht berücksichtigt.

Es ist daher erforderlich, ein einheitliches mathematisches Modell aus Bewegungs- und Lastengleichung zu entwickeln. Die Herleitung stützt sich auf grundlegende physikalische Prinzipien und berücksichtigt dabei die Verwendung von verfügbaren Daten für die Strukturodynamik und die Aerodynamik eines kommerziellen Transportflugzeuges. Die Bereitstellung der Datensätze ist in der Industrie mit einem erheblichen Aufwand verbunden. Eine wichtige Anforderung an das mathematische Modell ist daher, die bestmögliche Integration dieser Daten zu ermöglichen. Die vereinheitlichte Theorie ist in eine aeroservoelastische Simulationsumgebung zu integrieren. Der Einfluss der inertialen Kopplung auf lokale und integrierte Lasten ist zu untersuchen.

Daraus ergeben sich für diese Arbeit die folgenden Ziele:

- Erhöhung der Genauigkeit der Lastenrechnung durch Herleitung und Integration eines konsistenten mathematischen Modells für Bewegungsgleichung und Lastenrechnung. Hierbei muss die Integration von existierenden Daten beachtet werden und die Formulierung auf effiziente Zeitbereichssimulation ausgerichtet sein.
- Analyse der inertialen Wechselwirkungen von flugmechanischen und elastischen Größen

sowie deren Einfluss auf Strukturlasten.

Das Vorgehen zur Lösung dieser Probleme ist im folgenden dargestellt. Im ersten Schritt erfolgt die Herleitung der Bewegungsgleichung und der Lastengleichung. Anschließend wird die Modellierung der äußeren Kräfte beschrieben. Schließlich erfolgt die Integration in eine bestehende Simulationsumgebung und die Bewertung anhand eines relevanten Manövers.

## Herleitung der Bewegungsgleichungen

Zur Herleitung der Bewegungsgleichungen werden die Lagrange Gleichungen für Quasi-Koordinaten verwendet. Die Verwendung von Quasi-Koordinaten ist ein effizienter Weg, Zustände in Analogie zu Flugmechanik und Aeroelastik zu erhalten. Dies erleichtert die spätere Integration in bestehende Simulationsumgebungen und ermöglicht einen direkten Vergleich der neuen Form mit bestehenden Ergebnissen. Diese Form der Lagrange Gleichungen berücksichtigt die Bewegungsgrößen für ein körperfestes Koordinatensystem und generalisierte Koordinaten zur Beschreibung der Deformation.

Kinetische und potentielle Energie, sowie die virtuelle Arbeit der nicht konservativen Kräfte, sind für die Lagrange Gleichungen zu formulieren. Hierbei wird angenommen, dass der flexible Körper aus diskreten Punkten besteht, an denen lokale Massen und Trägheitstensoren angebunden sind. Dies ermöglicht eine direkte Einbindung von Massenmatrizen aus FE-Modellen. Da das FE-Modell der Aeroelastik auf linear elastischer Theorie basiert, ist dies auch für die Herleitung der Bewegungsgleichungen anzuwenden. Die potentielle Energie der Verformung kann dann mit der Steifigkeitsmatrix des FE-Modells beschrieben werden.

Zur Beschreibung der Knotenlage wird ein körperfestes Koordinatensystem eingeführt. Grundsätzlich bieten sich hierzu zwei verschiedene Möglichkeiten:

**Feste Lage bezüglich des unverformten Körpers.** Hierbei wird das Koordinatensystem fest mit einem Punkt im unverformten Körper verbunden.

**Bewegt relativ zum unverformten Körper.** Die Position und Orientierung ist dabei variabel und ist durch eine hinreichende Anzahl von Zwangsbedingungen definiert.

Dabei bietet sich die Verwendung eines sog. "Mean-Axes" Systems an. Es ist durch die Minimierung des translatorischen und rotatorischen Impulses relativ zum körperfesten Koordinatensystem definiert. Mit der translatorischen Bedingung fällt die Lage des Ursprungs mit dem Schwerpunkt des verformten Körpers zusammen. Die rotatorische Bedingung wird durch eine Beschreibung der Deformation durch eine Linearkombination von elastischen Eigenformen aus einer frei-frei Modalanalyse erfüllt. Die Orientierung des Koordinatensystems

ändert sich damit in Abhängigkeit von der Verformung bezüglich der unverformten Geometrie.

Durch das Mean-Axes Koordinatensystems reduzieren sich die inertialen Kopplungsterme gegenüber einem körperfesten Koordinatensystem, welches fest mit einem Punkt des Körpers verbunden ist. Während bei letzterem die Translation und Rotation des Referenzsystems inertial gekoppelt sind, führt das Mean-Axes System lediglich zu einer inertialen Kopplung zwischen der Rotation des körperfesten Systems und der Deformation. Das Mean-Axes System liefert weiterhin die kleinsten Deformationen – ein wichtiger Aspekt bei der Annahme linear elastischer Theorie.

Die Anwendung der Lagrange Gleichungen für Quasi-Koordinaten führt zu einem Satz von drei Gleichungen. Je eine Gleichung repräsentiert Translation und Rotation des körperfesten Koordinatensystems und eine Gleichung steht für die generalisierten elastischen Verformungen. Diese Form der Bewegungsgleichungen erweitert die bestehenden Formulierungen für diskrete Systeme um rotatorische Freiheitsgrade der Knotenpunkte und um eine vollständig generalisierte Form der inertialen Kopplungsterme. Diese bestehen aus zeitlich konstanten Matrizen. Im Zusammenhang mit den generalisierten Koordinaten werden dann die zusätzlichen Kräfte der inertialen Kopplung gebildet. Die Gleichung für die Rotation berücksichtigt die Variation des Trägheitstensors aufgrund der Verformungen. Die neue Form der erweiterten generalisierten Kopplungsterme ist durch einen numerischen Vergleich mit der physikalischen Formulierung validiert.

Alle Matrizen für die inertialen Kopplungsterme können vor der Simulation für unterschiedliche Beladungsfälle bereitgestellt werden. Dies ermöglicht die Einbindung in bestehende Datenstrukturen, die auf eine Vielzahl von Beladungsfällen ausgerichtet sind. Konsequente Elimination aller Summationen über Knotenpunkte ist eine Verbesserung gegenüber bestehenden Formulierungen. Dies ist eine wichtige Eigenschaft für eine effektive Zeitbereichssimulation.

Den Bewegungsgleichungen liegen die folgenden Annahmen zugrunde:

1. Der elastische Körper wird mit konzentrierten Massen und Trägheitstensoren modelliert.
2. Linear elastische Theorie wird angenommen.
3. Lokale translationale and rotatorische Deformationen bezüglich der unverformten Geometrie sind klein.
4. Die elastische Deformation wird als Linearkombination der elastischen Eigenformen ausgedrückt.

5. Gravitation ist über der Struktur konstant.

## Herleitung der Lastengleichungen

Aus der Simulation der generalisierten Bewegungsgleichungen sind die Trajektorien der Zustände bekannt. Auf Grundlage dieser Daten sind nun die lokalen Lasten zu ermitteln. Die Lastengleichungen werden daher auf Basis des Impulssatzes hergeleitet. Analog zur Herleitung der Bewegungsgleichung wird nun auch der Impuls eines Masselements durch einen Anteil aus der Bewegung des körperfesten Koordinatensystems und einen Anteil aus der Deformation beschrieben. Nach dem Differenzieren des Impulses nach der Zeit wird die Gleichung nach den gesuchten elastischen Knotenkräften aufgelöst.

Die entwickelten Gleichungen stellen eine Erweiterung der bekannten "Force Summation" Methode um nichtlineare Starrkörperbewegung und inertielle Kopplungsterme dar. Die Konsistenz der neuen Formulierung mit den Bewegungsgleichungen wird durch den Vergleich modaler elastischer Kräfte gezeigt.

Weiterhin wird gezeigt, wie sich eine Formulierung für inertial entkoppelte Bewegungsgleichungen und die linearen Gleichungen der Aeroelastik aus der allgemeinen Form ableiten lassen.

## Modellierung der externen Kräfte

Für die rechte Seite der Bewegungsgleichung sind Gesamtkräfte, Gesamtmomente und generalisierte Kräfte bereitzustellen. Zur Berechnung der Strukturlasten mit einer Force Summation Methode ist jedoch die Modellierung von verteilten externen Kräften erforderlich. Die Gesamtkräfte, Gesamtmomente und generalisierten Kräfte werden aus den verteilten Kräften durch Generalisieren mit translatorischen, rotatorischen und elastischen Eigenformen abgeleitet. Die nichtkonservativen Kräfte setzen sich aus aerodynamischen Kräften und Triebwerksschubkräften zusammen.

Die Triebwerksschubkräfte können allgemein als lokale äußere Kräfte betrachtet werden. Sie sind an den Strukturknoten in das Modell einzuleiten; eine Richtungsänderung durch die elastische Verformung der Struktur wird dabei berücksichtigt. Weitere lokale äußere Kräfte können in gleicher Weise modelliert werden.

Bei der Modellierung der aerodynamischen Kräfte müssen mehrere Faktoren berücksichtigt werden. Durch die große Starrkörperbewegung des Flugzeuges werden Luftkräfte an der Struktur hervorgerufen, die ihrerseits nichtlinear vom Flugzustand abhängen. Anderer-

seits induziert die elastische Verformung der Struktur instationäre Luftkräfte, die wiederum auf die Struktur rückwirken. Ein einheitliches Aerodynamikmodell, das diese Anforderungen berücksichtigt, ist in der industriellen Praxis nicht verfügbar. Daher sind bestehende Aerodynamikmodelle, die zur Berechnung von Manöver- und Böenlasten verfügbar sind, in einem geeigneten Modell zu kombinieren.

In der Manöversimulation werden Aerodynamikmodelle basierend auf Beiwerten und Derivativa verwendet, die mittels Datenbanken bereitgestellt werden. Diese stammen aus CFD-Rechnungen, Experimenten und in einem späteren Entwicklungsstadium aus Flugversuchsdaten. Da die elastische Verformung der Struktur einen wesentlichen Einfluss auf die Verteilung der aerodynamischen Kräfte hat, erfolgt eine Korrektur der Beiwerte in Abhängigkeit von der quasiflexiblen Deformation. Diese so genannten Flex-Faktoren sind im Wesentlichen vom Staudruck und dem Lastvielfachen abhängig. Die Bereitstellung und Validierung der quasi-statischen und quasi-flexiblen Luftkräfte und der entsprechenden Datenbanken ist mit einem erheblichen Aufwand verbunden.

Die Bereitstellung instationärer Luftkräfte ist ein Teilgebiet der Aeroelastik. Dabei sind die auf die Struktur wirkenden Auftriebskräfte von entscheidender Bedeutung. Widerstandskräfte in Strömungsrichtung werden in der Aeroelastik meist vernachlässigt. Die Strömung wird daher als reibungsfrei modelliert. Werden weiterhin kleine Störungen angenommen, kann für das Strömungsfeld eine Störpotenzialgleichung abgeleitet werden. In der industriellen Praxis ist die Doublet-Lattice-Methode das am häufigsten angewendete Verfahren zur Bereitstellung instationärer Luftkräfte. Es bietet einen guten Kompromiss zwischen Rechenaufwand und Genauigkeit. Zur Simulation werden die im Frequenzbereich vorliegenden instationären Luftkräfte approximiert und anschließend in den Zeitbereich transformiert.

Beide Aerodynamikmodelle berücksichtigen damit die Deformation der Struktur. Diese Überlappung ist bei der Kombination der Modelle zu berücksichtigen. Hierzu bietet sich die "Residualized-Model" Methode an. Die validierten quasi-flexiblen Luftkräfte bleiben dabei unverändert, während der quasi-flexible Anteil in den instationären Luftkräften kontinuierlich von diesen abgezogen wird. Die bestehende RM-Methode ermöglicht eine Integration von Gesamtkräften und generalisierten Luftkräften. Für die Lastenrechnung ist eine Erweiterung des Verfahrens notwendig. Die neue Methode ermöglicht die Kombination der verteilten aerodynamischen Kräfte aus den Teilmodellen.

## Simulation

Die initial gekoppelten Bewegungsgleichungen und die Lastengleichung, sowie das erweiterte Aerodynamikmodell werden in die Simulationsumgebung VarLoads<sup>1</sup> integriert. Als Referenzmodell wird die bestehende inertial entkoppelte Bewegungs- und Lastengleichung herangezogen. Mit diesem Modell werden sowohl Trimm-Rechnungen als auch dynamische Simulationen durchgeführt. Dabei werden ein Trimmzustand mit hoher Rollrate und ein Abfangmanöver betrachtet. Für das dynamische Manöver wird das FAR-Rollmanöver verwendet. Dieses enthält sowohl eine hohe Rollrate als auch eine hohe Rollbeschleunigung; beides begünstigt eine inertielle Kopplung.

Der Einfluss auf Bewegungsgrößen, generalisierte Koordinaten und Lasten wird untersucht. Die Ergebnisse zeigen, dass bei einem elastischen Transportflugzeug insbesondere eine hohe Rollrate die elastische Verformung beeinflusst. Dabei ist der Zentrifugalterm maßgeblich für die inertielle Kopplung. An Triebwerken und Pylon mit großen lokalen Massen und großem Abstand zur Rollachse ergeben sich die größten Beeinflussungen. Laterale lokale Kräfte können in diesem Bereich einen erheblichen Anteil an Zentrifugalkräften enthalten.

Für praktische Anwendungen wird untersucht, ob der Einfluss inertialer Kopplung mit Hilfe der neu entwickelten Lastengleichung auch bei vorliegenden Simulationsdaten aus inertial entkoppelter Rechnung ermittelt werden. Am Beispiel der lateralen Triebwerkslasten wird gezeigt, dass mit der erweiterten Force Summation Methode bestehende Ergebnisse verbessert werden und der Fehler bei einer entkoppelten Rechnung abgeschätzt werden kann, ohne eine neue Simulation erforderlich zu machen.

## Zusammenfassung der neuen Beiträge

Die neuen Beiträge dieser Arbeit sind im folgenden zusammengefasst:

- Herleitung eines konsistenten mathematischen Modells für die Simulation und Lastenrechnung eines flexiblen Flugzeuges. Erhöhung der Genauigkeit von Simulation und Lastenrechnung, wobei alle bisher verwendeten Modelldaten integriert werden können.
- Bereitstellung einer Formulierung zur effizienten Implementierung. Die vollständig generalisierte Darstellung der inertialen Kopplungsterme ermöglicht effektive Berechnungen im Zeitbereich.
- Entwicklung einer neuen Lastengleichung für nichtlineare Starrkörperzustände, elastische Zustände und inertielle Kopplung.

---

<sup>1</sup>Variable Loads Environment [24]

- Erweiterung des RM-Ansatzes um verteilte quasi-flexible Luftkräfte. Der Ansatz kann damit auch für eine Lastenrechnung auf Basis der Force Summation Methode verwendet werden.
- Analyse und Bewertung des Einflusses der inertialen Kopplung bei großen flexiblen Transportflugzeugen für zulassungsrelevante Manöver.
- Bereitstellung einer Methodik zur Abschätzung des Einflusses von inertialen Kopplungseffekten auf Basis von Daten aus konventioneller entkoppelter Rechnung.

Für zukünftige Arbeiten auf diesem Gebiet ergeben sich mehrere wichtige Aufgaben. Zum einen ist die Erweiterung der bestehenden Formulierung um geometrische Steifigkeiten bei Anwendungen, die über den Einsatzbereich von Transportflugzeugen hinausgehen, sinnvoll. Zum anderen sollte das Problem der Approximation der instationären Luftkräfte durch eine direkte Formulierung im Zeitbereich gelöst werden. Dadurch können einerseits Ungenauigkeiten durch die Approximation vermieden werden, andererseits kann die Variation der Machzahl ohne Interpolation der aerodynamischen Einflussmatrizen berücksichtigt werden.



# A Mathematical Notes

## A.1 Vectors and Matrices

### Matrix Operations

In the following matrix and vector operations used for the equation development (Chapter 2) are reviewed.

The vector cross product can be written as matrix operation:

$$\mathbf{a} \times \mathbf{b} = \text{sk}(\mathbf{a})\mathbf{b} \quad \mathbf{a}, \mathbf{b} \in \mathbb{R}^3 \quad (\text{A.1})$$

with the skew symmetric matrix

$$\text{sk}(\mathbf{a}) = \begin{bmatrix} 0 & -a_3 & a_2 \\ a_3 & 0 & -a_1 \\ -a_2 & a_1 & 0 \end{bmatrix} . \quad (\text{A.2})$$

Some useful operations are:

$$\begin{aligned} \mathbf{a} \times \mathbf{b} &= -\mathbf{b} \times \mathbf{a} \quad , \\ \text{sk}(\mathbf{a})^T &= -\text{sk}(\mathbf{a}) \quad , \\ \text{sk}(\mathbf{a})\text{sk}(\mathbf{b}) &= \mathbf{b}\mathbf{a}^T - \mathbf{b}^T\mathbf{a}\mathbf{I} \quad , \\ \text{sk}(\mathbf{a})\text{sk}(\mathbf{b})^2\mathbf{a} &= -\text{sk}(\mathbf{b})\text{sk}(\mathbf{a})^2\mathbf{b} \quad . \end{aligned}$$

### Vector Differentiation

A vector differentiation operator is defined as

$$\frac{\partial}{\partial \mathbf{x}} = \begin{bmatrix} \frac{\partial}{\partial x_1} \\ \frac{\partial}{\partial x_2} \\ \frac{\partial}{\partial x_3} \end{bmatrix} \quad \mathbf{x} \in \mathbb{R}^3 \quad . \quad (\text{A.3})$$

Special functions for vector differentiation are:

$$\begin{aligned} \frac{\partial(\mathbf{a}^T \mathbf{x})}{\partial \mathbf{x}} &= \mathbf{a} \quad , \quad \frac{\partial(\mathbf{A} \mathbf{x})}{\partial \mathbf{x}^T} = \mathbf{A} \quad , \quad \frac{\partial(\mathbf{x}^T \mathbf{A})}{\partial \mathbf{x}} = \mathbf{A} \quad , \\ \frac{\partial(\mathbf{x}^T \mathbf{A} \mathbf{x})}{\partial \mathbf{x}} &= (\mathbf{A} + \mathbf{A}^T) \mathbf{x} \quad , \quad \frac{\partial(\mathbf{x}^T \mathbf{A} \mathbf{x})}{\partial \mathbf{x}^T} = \mathbf{x}^T (\mathbf{A} + \mathbf{A}^T) \quad . \end{aligned}$$

## Matrix and Vector Notation

A matrix/vector can be expressed as a sum of matrices/vectors for each element by

$$\langle (\dots)_{jk} \rangle = \sum_{j=1}^3 \sum_{k=1}^3 (\dots)_{jk} \mathbf{e}_j \mathbf{e}_k^T \quad , \quad (\text{A.4a})$$

$$\langle (\dots)_j \rangle = \sum_{j=1}^3 (\dots)_j \mathbf{e}_j \quad , \quad (\text{A.4b})$$

$$\text{with } \mathbf{e}_1 = \begin{bmatrix} 1 \\ 0 \\ 0 \end{bmatrix}, \mathbf{e}_2 = \begin{bmatrix} 0 \\ 1 \\ 0 \end{bmatrix}, \mathbf{e}_3 = \begin{bmatrix} 0 \\ 0 \\ 1 \end{bmatrix} \quad . \quad (\text{A.4c})$$

## Miscellaneous Transformations

A useful transformations that is used in Chapter 3 for the generalization of a half generalized mass matrix with rigid body modes is

$$\begin{aligned} \Phi_{gR,i}^T \mathbf{M}_{gR,i} &= \begin{bmatrix} \mathbf{I} & \mathbf{0} \\ \text{sk}(\mathbf{r}_i) & \mathbf{I} \end{bmatrix} \begin{bmatrix} m_i \mathbf{I} & -m_i \text{sk}(\mathbf{r}_i + \mathbf{s}_i) \\ m_i \text{sk}(\mathbf{s}_i) & \mathbf{J}_{g,i} - m_i \text{sk}(\mathbf{s}_i) \text{sk}(\mathbf{r}_i) \end{bmatrix} \\ &= \begin{bmatrix} m_i \mathbf{I} & -m_i \text{sk}(\bar{\mathbf{r}}_i) \\ m_i \text{sk}(\bar{\mathbf{r}}_i) & \mathbf{J}_i - m_i \text{sk}(\bar{\mathbf{r}}_i)^2 \end{bmatrix} \end{aligned}$$

with the transformation

$$\mathbf{J}_{g,i} + m_i (\text{sk}(\mathbf{r}_i) \text{sk}(\mathbf{r}_i + \mathbf{s}_i) + \text{sk}(\mathbf{s}_i) \text{sk}(\mathbf{r}_i)) = \mathbf{J}_i + m_i \text{sk}(\bar{\mathbf{r}}_i)^2 \quad .$$

Note that  $\mathbf{J} = \sum_i \mathbf{J}_i - m_i \text{sk}(\bar{\mathbf{r}}_i)^2$  is the total inertia tensor in the undeformed condition.

## A.2 Floating Reference Frames

The last three terms in the energy expression (2.26) represent a coupling between the motion of the reference frame and the elastic deformation. The complexity of these terms depends on the choice of the body reference frame. The so-called practical mean-axes constraints significantly reduce the coupling between the overall motion of the reference frame and the elastic deformation (Waszak [66], Milne [42], Shabana [58]). A general description of floating reference frames is given by Canavin [12].

For this reason the practical mean-axes constraints are chosen to locate the body reference frame. The definition of a reference frame requires six constraints. In the case of mean-axes, three constraints are obtained by selecting the frame in a way that the relative momentum w.r.t this frame equals zero. Another three constraints are provided by requesting the relative angular momentum to equal zero.

### Translational Constraints

The first three constraints are formulated by selecting a frame to which the relative translational momentum (momentum with respect to the origin of the reference frame) equals zero. The relative momentum is given by:

$$\mathbf{H}_{\text{rel},t} = \frac{d}{dt} \sum_i (\bar{\mathbf{r}}_i + \bar{\mathbf{d}}_i) m_i = \mathbf{0} \quad (\text{A.5})$$

since  $\overset{\circ}{\mathbf{r}}_i = \mathbf{0}$  the momentum (A.5) simplifies to

$$\mathbf{H}_{\text{rel}} = \sum_i \overset{\circ}{\mathbf{d}}_i m_i = \mathbf{0} \quad . \quad (\text{A.6})$$

This implies that the origin has to be fixed w.r.t the momentary center of gravity, hence

$$\sum_i (\bar{\mathbf{r}}_i + \bar{\mathbf{d}}_i) m_i = \text{const} \quad . \quad (\text{A.7})$$

By locating the reference frame in the center of gravity of the undeformed configuration  $\sum_i \bar{\mathbf{r}}_i m_i = \mathbf{0}$  the above equation simplifies to

$$\sum_i \bar{\mathbf{d}}_i m_i = \mathbf{0} \quad , \quad (\text{A.8})$$

which can be expanded to

$$\sum_i (\mathbf{d}_i + \boldsymbol{\varphi}_i \times \mathbf{s}_i) m_i = \mathbf{0} \quad . \quad (\text{A.9})$$

Thus by choosing the origin of the body reference frame in the center of gravity of the deformed body the relative momentum is minimal.

## Rotational Constraints

Three more constraints are obtained by minimizing the relative angular momentum. The relative angular momentum is given by

$$\mathbf{H}_{\text{rel},r} = \sum_i ((\bar{\mathbf{r}}_i + \bar{\mathbf{d}}_i) \times \frac{d'}{dt}(\bar{\mathbf{r}}_i + \bar{\mathbf{d}}_i))m_i + \mathbf{J}_i \dot{\boldsymbol{\varphi}}_i = \mathbf{0} \quad . \quad (\text{A.10})$$

This expression is nonlinear in the deformation and difficult to realize in practice. Therefore a linearized form of (A.10) is used:

$$\mathbf{H}_{\text{rel},r} = \sum_i (\bar{\mathbf{r}} \times \dot{\bar{\mathbf{d}}})m_i + \mathbf{J}_i \dot{\boldsymbol{\varphi}}_i = \mathbf{0} \quad . \quad (\text{A.11})$$

This constraint is called ‘‘practical mean-axes condition’’ [69]. The terms of (A.11) are now expanded using (2.36),  $\mathbf{J}_{g,i} = \mathbf{J}_i + \text{sk}(\mathbf{s}_i)^T \text{sk}(\mathbf{s}_i)m_i$ , as follows

$$\begin{aligned} \mathbf{H}_{\text{rel},r} &= \sum_i (\bar{\mathbf{r}} \times \dot{\bar{\mathbf{d}}})m_i + \mathbf{J}_i \dot{\boldsymbol{\varphi}}_i \\ &= \sum_i \left[ m_i \mathbf{r}_i \times (\dot{\mathbf{d}}_i + \dot{\boldsymbol{\varphi}}_i \times \mathbf{s}_i) + m_i \mathbf{s}_i \times \dot{\mathbf{d}}_i + (\mathbf{J}_i + \text{sk}(\mathbf{s}_i)^T \text{sk}(\mathbf{s}_i)m_i) \dot{\boldsymbol{\varphi}}_i \right] \\ &= \frac{d'}{dt} \sum_i \left[ m_i \mathbf{r}_i \times (\mathbf{d}_i + \boldsymbol{\varphi}_i \times \mathbf{s}_i) + m_i \mathbf{s}_i \times \mathbf{d}_i + \mathbf{J}_{g,i} \boldsymbol{\varphi}_i \right] \quad . \end{aligned} \quad (\text{A.12})$$

The equations (A.9) and (A.12) are the constraints for the location of the body fixed coordinate frame. It can be shown that these constraints are automatically fulfilled by free vibration mode shapes due to the orthogonality of vibration and rigid body modes with respect to the mass matrix. Hereby the rigid body modes must be expressed w.r.t the center of gravity.

## Orthogonality of Mode Shapes

An linearized rigid body motion of the grid points may be expressed by a linear combination of rigid body mode shapes

$$\begin{bmatrix} \mathbf{d}_{r,i} \\ \boldsymbol{\varphi}_{r,i} \end{bmatrix} = \begin{bmatrix} \boldsymbol{\Phi}_{g_i R_t} \\ \boldsymbol{\Phi}_{g_i R_r} \end{bmatrix} \boldsymbol{\eta}_R = \boldsymbol{\Phi}_{g_i R} \boldsymbol{\eta}_R = \begin{bmatrix} \mathbf{d}_0 + \boldsymbol{\varphi}_0 \times \mathbf{r}_i \\ \boldsymbol{\varphi}_0 \end{bmatrix} \quad (\text{A.13})$$

where  $\mathbf{d}_0, \boldsymbol{\varphi}_0$  denote rigid body translations and rotations. The elastic motion of a grid point is expressed using the modal approach (2.19) by

$$\begin{bmatrix} \mathbf{d}_i \\ \boldsymbol{\varphi}_i \end{bmatrix} = \begin{bmatrix} \boldsymbol{\Phi}_{g_i E_t} \\ \boldsymbol{\Phi}_{g_i E_r} \end{bmatrix} \boldsymbol{\eta}_E = \boldsymbol{\Phi}_{g_i E} \boldsymbol{\eta}_E \quad . \quad (\text{A.14})$$

The orthogonality of rigid and elastic mode shapes w.r.t the mass matrix requires that

$$\begin{aligned} \Phi_{g_i R}^T \mathbf{M}_{gg,i} \Phi_{g_i E} &= \sum_i \begin{bmatrix} \mathbf{d}_{r,i} \\ \boldsymbol{\varphi}_{r,i} \end{bmatrix}^T \begin{bmatrix} m_i \mathbf{I} & -m_i \text{sk}(\mathbf{s}_i) \\ m_i \text{sk}(\mathbf{s}_i) & \mathbf{J}_{g,i} \end{bmatrix} \begin{bmatrix} \mathbf{d}_i \\ \boldsymbol{\varphi}_i \end{bmatrix} = \mathbf{0} \\ &\iff \mathbf{d}_0^T \sum_i (\mathbf{d}_i + \boldsymbol{\varphi}_i \times \mathbf{s}_i) m_i \\ &\quad + \boldsymbol{\varphi}_0^T \sum_i [m_i \mathbf{r}_i \times (\mathbf{d}_i + \boldsymbol{\varphi}_i \times \mathbf{s}_i) + m_i \mathbf{s}_i \times \mathbf{d}_i + \mathbf{J}_{g,i} \boldsymbol{\varphi}_i] = \mathbf{0} \quad . \quad (\text{A.15}) \end{aligned}$$

Since  $\mathbf{d}_0$  and  $\boldsymbol{\varphi}_0$  are independent the coefficients of  $\mathbf{d}_0$  and  $\boldsymbol{\varphi}_0$  in the preceding equation can be set equal to zero. This leads to the following form:

$$\sum_i (\mathbf{d}_i + \boldsymbol{\varphi}_i \times \mathbf{s}_i) m_i = \mathbf{0} \quad , \quad (\text{A.16})$$

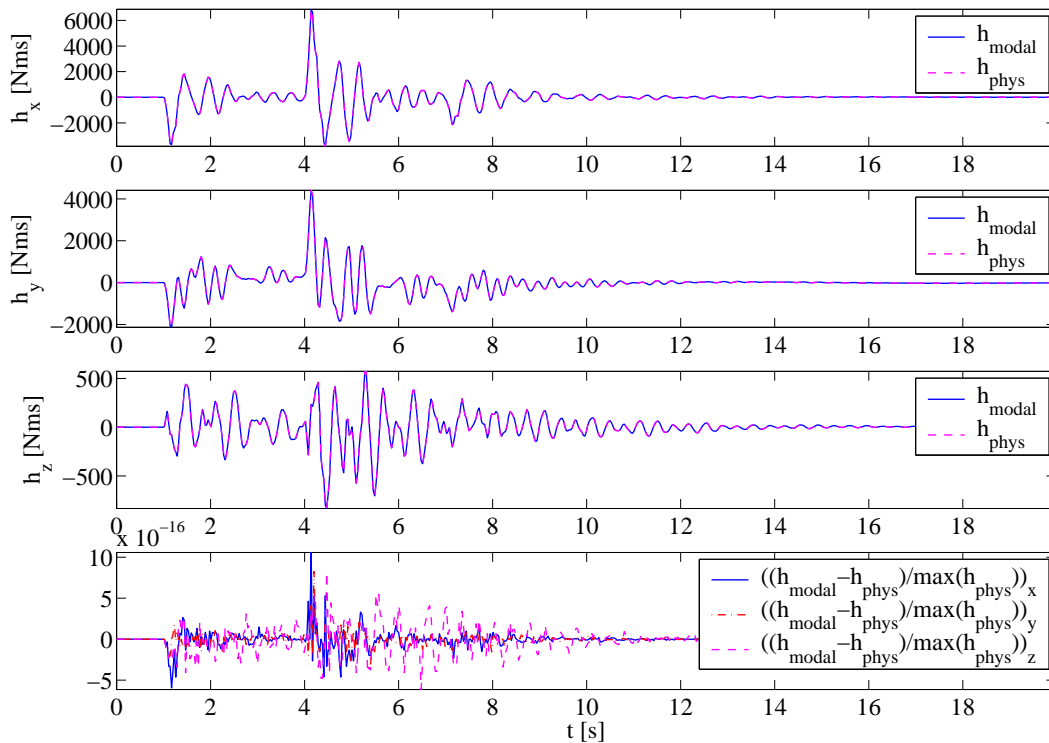
$$\sum_i [m_i \mathbf{r}_i \times (\mathbf{d}_i + \boldsymbol{\varphi}_i \times \mathbf{s}_i) + m_i \mathbf{s}_i \times \mathbf{d}_i + \mathbf{J}_{g,i} \boldsymbol{\varphi}_i] = \mathbf{0} \quad . \quad (\text{A.17})$$

These equations are exactly the practical mean-axes constraints (A.9),(A.12). Hence these constraints are automatically fulfilled by using a set of free-free vibration mode shapes due to their orthogonality with respect to rigid body mode shapes.

## B Numerical Results for the EOM Validation

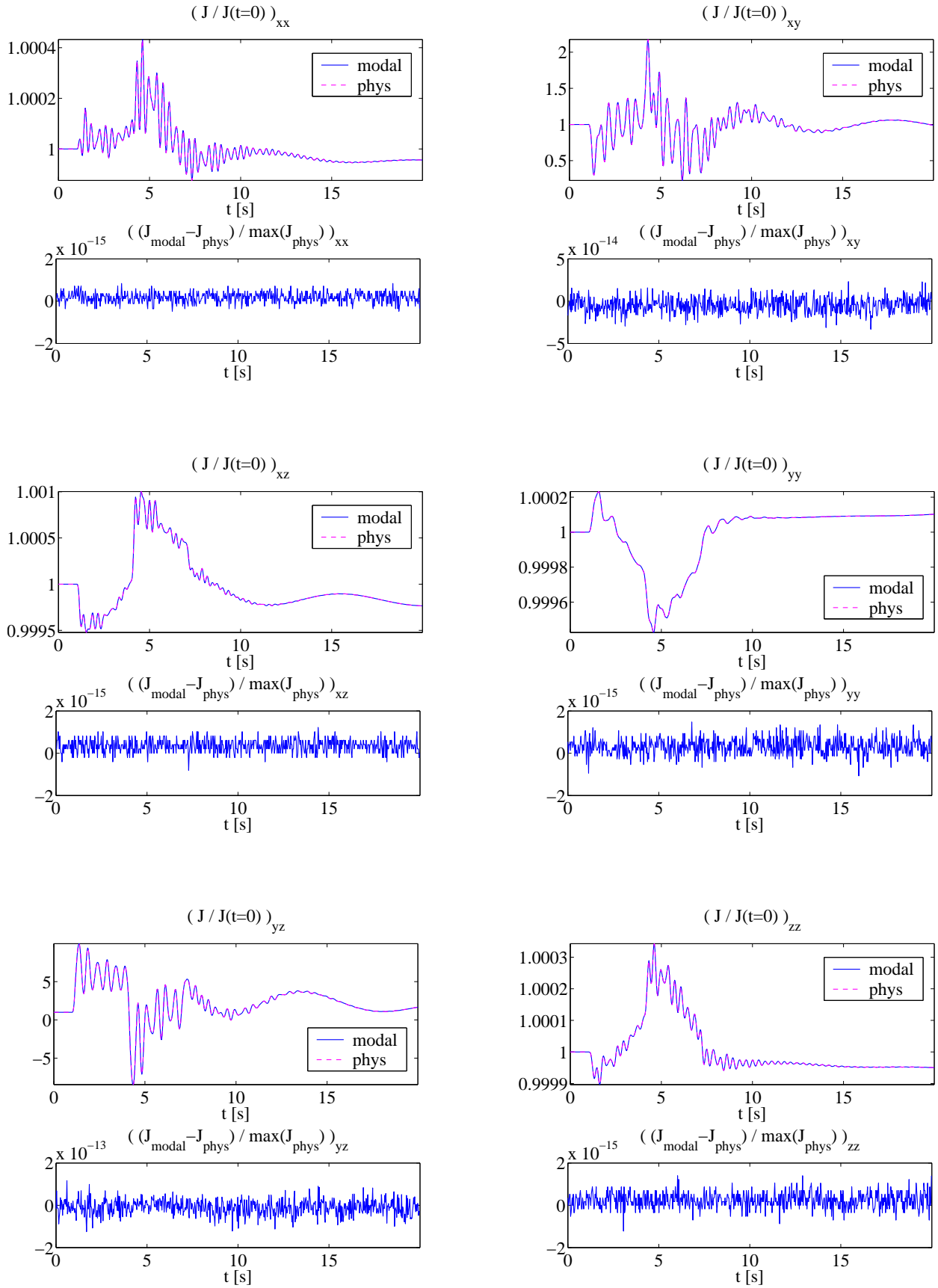
A stair aileron input is used as a test case for the validation of the generalized terms contained in the equations of motion (Chapter 2), since it excites all of the selected elastic mode shapes. Both, physical and modal forms are implemented in a common simulation environment.

Figure B.1 depicts the time response of the  $h$ -term for each component and the difference between the physical and the modal form. The modal form of the  $h$ -term yields the same results as the physical form. Relative differences are of the order of the numerical precision.



**Figure B.1:** Comparison of the physical and the modal implementation of the  $h$ -term

The components of the inertia tensor are given in Fig B.2. Again the differences between the physical and the modal form result from numerical errors.



**Figure B.2:** Comparison of the physical and the modal implementation of the inertia tensor

# C Numerical Data for the Beam Model

Numerical data for the beam model example presented in Section 2.7 is provided.

The element properties for the simple beam model are:

Mass Elements	
$m_1$	1 kg
$m_2$	2 kg
$m_3$	1 kg
$J_1$	$8 \cdot 10^{-4} \text{ kgm}^2$
$J_2$	$2.5 \cdot 10^{-3} \text{ kgm}^2$
$J_3$	$8 \cdot 10^{-4} \text{ kgm}^2$

**Table C.1:** Mass element properties

Beam Elements	
$A$	$1 \cdot 10^{-5} \text{ m}^2$
$E$	$2 \cdot 10^9 \text{ N/m}^2$
$l_0$	1 m
$I$	$1 \cdot 10^{-8} \text{ m}^4$

**Table C.2:** Beam element properties

The displacement vector for the planar example contains the following elements:

$$\mathbf{u}_g = \left[ d_{1y} \ d_{1z} \ \varphi_{1x} \mid d_{2y} \ d_{2z} \ \varphi_{2x} \mid d_{3y} \ d_{3z} \ \varphi_{3x} \right] . \quad (\text{C.1})$$



The system mass matrix of the lumped masses is

$$\mathbf{M}_{gg} = \left[ \begin{array}{ccc|ccc|ccc} m_1 & 0 & 0 & 0 & 0 & 0 & 0 & 0 & 0 \\ & m_1 & 0 & 0 & 0 & 0 & 0 & 0 & 0 \\ & & J_1 & 0 & 0 & 0 & 0 & 0 & 0 \\ \hline & & & m_2 & 0 & 0 & 0 & 0 & 0 \\ & & & & m_2 & 0 & 0 & 0 & 0 \\ & & & & & J_2 & 0 & 0 & 0 \\ \hline & & & & & & m_3 & 0 & 0 \\ & & \text{sym} & & & & & m_3 & 0 \\ & & & & & & & & J_3 \end{array} \right] . \quad (\text{C.2})$$

The stiffness matrix, assembled from Euler-Bernoulli beam elements, is as follows

$$\mathbf{K}_{gg} = \frac{EI}{l_0^3} \left[ \begin{array}{ccc|ccc|ccc} EA l_0^3 & 0 & 0 & -EA l_0^3 & 0 & 0 & 0 & 0 & 0 \\ & 12 & 6l_0 & 0 & -12 & 6l_0 & 0 & 0 & 0 \\ & & 4l_0^2 & 0 & -6l_0 & 2l_0^2 & 0 & 0 & 0 \\ \hline & & & 2 \cdot EA l_0^3 & 0 & 0 & -EA l_0^3 & 0 & 0 \\ & & & & 2 \cdot 12 & 0 & 0 & -12 & 6l_0 \\ & & & & & 2 \cdot 4l_0^2 & 0 & -6l_0 & 2l_0^2 \\ \hline & & & & & & EA l_0^3 & 0 & 0 \\ & & \text{sym} & & & & & 12 & -6l_0 \\ & & & & & & & & 4l_0^2 \end{array} \right] . \quad (\text{C.3})$$

Using the element properties from Table C.1 and Table C.2 the Matrix of elastic mode shapes becomes

$$\Phi_{gE} = \left[ \begin{array}{cccccc} 0 & 0.71 & 0 & -0.5 & 0 & 0 \\ -0.5 & 0 & 0.01 & 0 & -0.03 & 0.03 \\ 1.5 & 0 & -13.59 & 0 & -24.96 & 20.97 \\ \hline 0 & 0 & 0 & 0.5 & 0 & 0 \\ 0.5 & 0 & 0 & 0 & 0.03 & 0 \\ 0 & 0 & 16.78 & 0 & 0 & 10.85 \\ \hline 0 & -0.71 & 0 & -0.5 & 0 & 0 \\ -0.5 & 0 & -0.01 & 0 & -0.03 & -0.03 \\ -1.5 & 0 & -13.59 & 0 & 24.96 & 20.97 \end{array} \right] . \quad (\text{C.4})$$

## D Numerical Results for the EOL Validation

For validation of the loads equation (Chapter 3, Page 54) the loads are transformed from physical into modal space by pre-multiplication with the elastic mode shapes.

A comparison of the generalized load from the loads equation 3.21 and the elastic forces from the equation of motion 2.113 is shown in figures D.1. Loads computed on the basis of the conventional force summation method 3.17 are also depicted.

The trajectories obtained by the general form of the loads equation (3.16) are identical to those obtained directly from the elastic forces in the equations of motion 2.113. The new loads equation is therefore consistent to the inertially coupled equations of motion.

Note that the conventional loads equation for the decoupled equations of motion is not consistent with the equations of motion with inertial coupling.

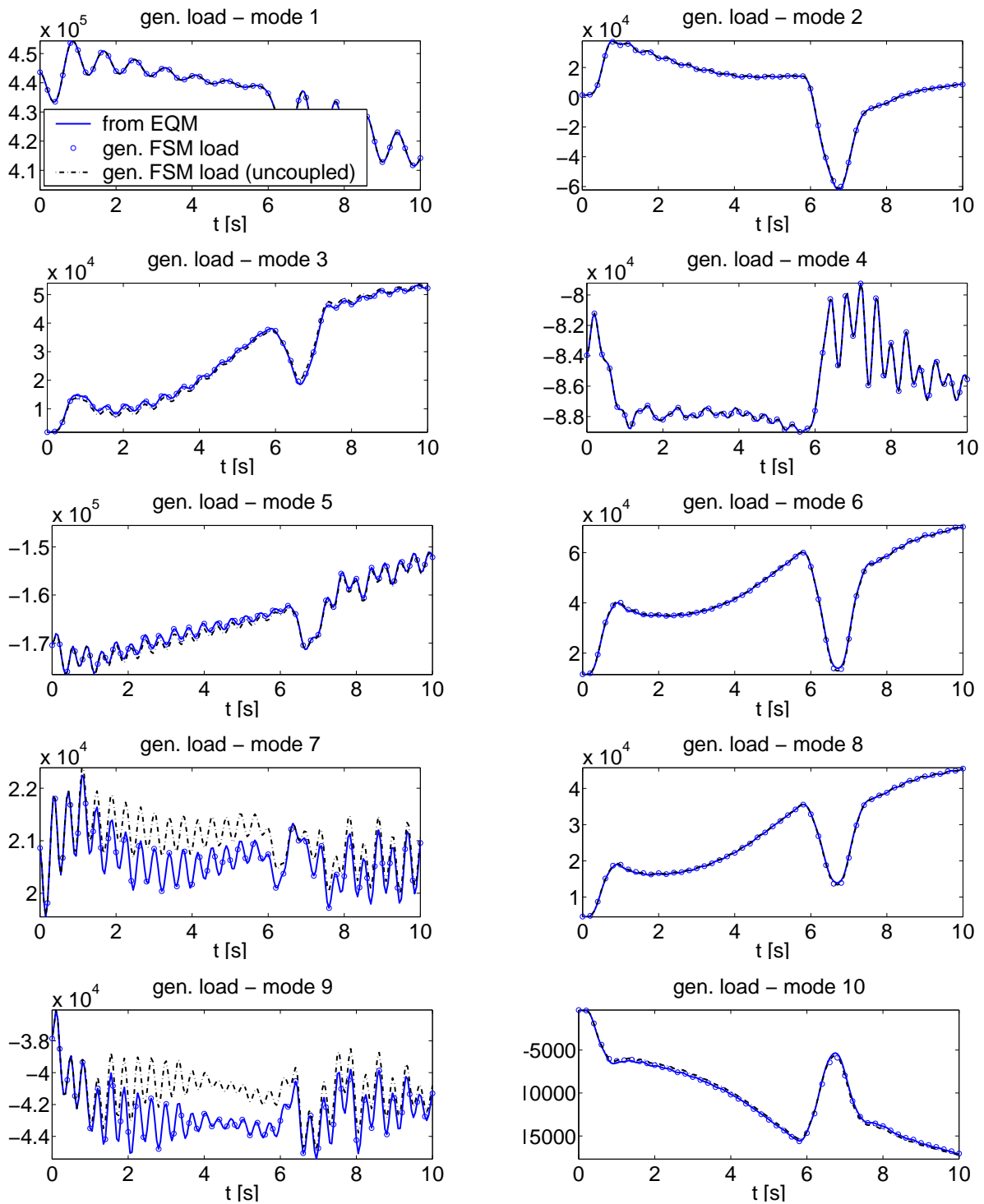


**Figure D.1:** Generalized loads from Equations of Motion and Force Summation Methods

# Bibliography

- [1] Airbus. Donnees Aerodynamiques. Technical Report AS-445-343 Internal Report, Airbus, 1991.
- [2] E. Albano and W.P. Rodden. A Doublet-Lattice Method for Calculating Lift Distributions on Oscillating Surfaces in Subsonic Flows. *Journal of Aircraft*, 7(2):279–285, 1969.
- [3] P. D. Arbuckle and C. S. Buttrill. Simulation Model-Building Procedure for Dynamic Systems Integration. *Journal of Guidance*, 12(6):894–900, 1987.
- [4] A. K. Banerjee and J. M. Dickens. Dynamics of an Arbitrary Flexible Body in Large Rotation and Translation. *Journal of Guidance*, 13(2):221–227, March 1990.
- [5] K.J. Bathe. *Finite Element Procedures*. Prentice Hall, 1996.
- [6] D.F. Bella. DMAP Alters to Add Differential Stiffness and Follower Force Matrices to MSC/NASTRAN Linear Solutions. In *MSC 1995 World Users' Conf. Proc.*, number 33, May 1995.
- [7] K. D. Bilimoria and D. K. Schmidt. Integrated Development of the Equations of Motion for Elastic Hypersonic Vehicles. *Journal of Guidance, Control, and Dynamics*, 18(1):73–81, January-February 1995.
- [8] R. L. Bisplinghoff, H. Ashley, and R. L. Halfman. *Aeroelasticity*. Dover Publications, Inc., 1955.
- [9] M. Blair. A compilation of the mathematics leading to the doublet lattice method. Technical Report WL-TR-95-3022, Air Force Wright Laboratory, 1994.
- [10] R. Brockhaus. *Flugregelung*. Springer-Verlag, 1994.
- [11] C.S. Buttrill, T.A. Zeiler, and P.D. Arbuckle. Nonlinear Simulation of a Flexible Aircraft in Maneuvering Flight. In *AIAA Flight Simulation Technologies Conference*, number AIAA 87-2501. AIAA, 1987.
- [12] J. R. Canavin and P. W. Likins. Floating Reference Frames for Flexible Spacecraft. *Journal of Spacecraft and Rockets*, 14(12):724–732, December 1977.

- [13] R. K. Cavin and A. R. Dusto. Hamilton's Principle: Finite-Element Methods and Flexible Body Dynamics. *AIAA Journal*, 15(12):1684–1690, September 1977.
- [14] R. R. Craig. *Structural Dynamics*. Wiley, 1981.
- [15] F. Engelsen and E. Livne. Mode Acceleration Based Random Gust Stresses in Aeroservoelastic Optimization. *Journal of Aircraft*, 41(2):335–347, 2004.
- [16] B. Etkin. *Dynamics of Flight*. John Wiley & Sons, INC, 1996.
- [17] S.H.J.A. Fransen. An Overview and Comparison of OTM Formulations on the basis of the Mode Displacement Method and the Mode Acceleration Method. In *Worldwide Aerospace Conference & Technology Showcase*, 2001.
- [18] M. Geradin and A. Cardona. *Flexible Multibody Dynamics*. John Wiley & Sons, LTD, 2001.
- [19] K.K. Gupta, M.J. Brenner, and L.S. Voelker. Development of an Integrated Aeroservoelastic Analysis Program and Correlation With Test Data. Technical Report 3120, NASA, 1991.
- [20] R. Guyan. Reduction of Stiffness and Mass Matrices. *AIAA Journal*, 3(2):380–387, 1965.
- [21] M. Hanel. *Robust Integrated Flight and Aeroelastic Control System Design for a Large Transport Aircraft*. PhD thesis, Universität Stuttgart, 2001.
- [22] W. Hauger, W. Schnell, and D. Gross. *Technische Mechanik 3*. Springer-Verlag, 1989.
- [23] F. M. Hoblit. *Gust Loads on Aircraft- Concepts and Applications*. AIAA Education Series. AIAA, 1988.
- [24] J. Hofstee, T. Kier, C. Cerulli, and G. Looye. A Variable, Fully Flexible Dynamic Response Tool for Special Investigations (VARLOADS). In *International Forum on Aeroelasticity and Structural Dynamics*. IFASD, 2003.
- [25] T. P. Kalman, W. P. Rodden, and J. P. Giesing. Application of the Doublet-Lattice Method to Nonplanar Configurations in Subsonic Flow. *Journal of Aircraft*, 8(6):406–413, 1971.
- [26] T. R. Kane, R. R. Ryan, and A. K. Banerjee. Dynamics of a Cantilever Beam Attached to a Moving Base. *Journal of Guidance*, 10(2):139–151, March-April 1987.
- [27] M. Karpel. Reduced-Order Models for Integrated Aeroservoelastic Optimization. *Journal of Aircraft*, 36(1):146–155, 1999.
- [28] M. Karpel and E. Presente. Structural Dynamic Loads in Response to Impulsive Exc-

- tation. In *International Forum on Aeroelasticity and Structural Dynamics*, pages 1059–1075, May 1993.
- [29] M. Karpel and E. Strul. Minimum-State unsteady aerodynamic approximations with flexible constraints. *Journal of Aircraft*, 33(6):1190–1196, 1996.
- [30] M. W. Kehoe. Aircraft Ground Vibration Testing at the NASA Dryden Flight Research Facility. Technical Report 104275, NASA Dryden Flight Research Facility, 1994.
- [31] E. Lavretsky. High Speed Civil Transport (HSCT) Flight Simulation and Analysis Software Development. In *36th Aerospace Sciences Meeting and Exhibit, January 12-15, 1998 / Reno, NV*, number A98-16094. AIAA, January 1998.
- [32] T. L. Lomax. *Structural Loads Analysis for Commercial Aircraft: Theory and Practice*. AIAA Education Series. AIAA, 1995.
- [33] G. Looye. Integration of Rigid and Aeroelastic Aircraft Models using the Residualised Model Method. In *International Forum on Aeroelasticity and Structural Dynamics*, number IF-046. IFASD, 2005.
- [34] G. Looye, S. Hecker, T. Kier, and C. Reschke. Multi-Disciplinary Aircraft Model Development Using Object-Oriented Modelling Techniques. In *Deutscher Luft- und Raumfahrtkongress*. DGLR, 2005.
- [35] T. Mauermann. Residual Unsteady Aerodynamic Model for Maneuvering Aircraft. In *International Forum on Aeroelasticity and Structural Dynamics*, number IF-081, 2005.
- [36] D. McLean. *Automatic Flight Control Systems*. Prentice Hall, 1990.
- [37] L. Meirovitch. *Methods of Analytical Dynamics*. McGraw-Hill Book Company, 1970.
- [38] L. Meirovitch. Hybrid State Equations of Motion for flexible Bodies in Terms of Quasi-Coordinates. *Journal of Guidance*, 14(5):1008–1013, 1988.
- [39] L. Meirovitch and I. Tuzcu. Integrated Approach to the Dynamics and Control of Maneuvering Flexible Aircraft. Technical Report NASA/CR-2003-211748, NASA, June 2003.
- [40] L. Meirovitch and I. Tuzcu. Time Simulation of the Response of Maneuvering Flexible Aircraft. *Journal of Guidance, Control and Dynamics*, 27(5):814–828, September-October 2004.
- [41] R. D. Milne. Dynamics of the Deformable Aeroplane. Technical Report R&M 3345, Her Majesty’s Stationary Office, London, England, 1964.
- [42] R. D. Milne. Some Remarks on the Dynamics of Deformable Bodies. *AIAA Journal*,

- 6(3):556–558, March 1968.
- [43] J. J. Olsen. Unified Flight Mechanics and Aeroelasticity for Accelerating, Maneuvering, Flexible Aircraft. In *RTO AVD Specialists Meeting on Structural Aspects of Flexible Aircraft Control, Ottawa 18-20 October 1999*, number RTO MP-36, October 1999.
- [44] M. Petyt. *Introduction to finite element vibration analysis*. Cambridge University Press, 1990.
- [45] A. S. Pototzky. New and Existing Techniques for Dynamic Loads Analysis of Flexible Airplanes. *Journal of Aircraft*, 23(4):340–347, 1985.
- [46] M. J. Reijerkerk. Flexible Aircraft Modelling with Structural and Aerodynamic Non-Linearities. Master’s thesis, Delft University of Technology, 2004.
- [47] C. Reschke. Berechnung dynamischer Lasten bei elastischen Strukturen. Master’s thesis, Universität Stuttgart, 2003.
- [48] C. Reschke and G. Looye. Comparison of Model Integration Approaches for Flexible Aircraft Flight Dynamics Modelling. In *International Forum on Aeroelasticity and Structural Dynamics*, number IF-154. IFASD, 2005.
- [49] D. J. Rixen. Generalized mode acceleration methods and modal truncation augmentation. In *AIAA/ASME/ASCE/AHS/ASC*, number AIAA-2001-1300. AIAA Structures, Structural Dynamics, and Materials Conference and Exhibit, Apr. 16-19 2001.
- [50] R.E. Robertson and R. Schwertassek. *Dynamics of Multibody Systems*. Springer Verlag, 1988.
- [51] W. P. Rodden and E. H. Johnson. *Aeroelastic Analysis User’s Guide*. MSC.Nastran, 1994.
- [52] W. P. Rodden and J. R. Love. Equations of Motion of a Quasisteady Flight Vehicle Utilizing Restrained Static Aeroelastic Characteristics. *Journal of Aircraft*, 22(9):802–809, September 1985.
- [53] K. L. Roger. Airplane Math Modeling Methods for Active Control Design. In *AGARD Structures and Materials Panel*, number AGARD/CP-228, pages 4–1 – 4–11. AGARD, April 1977.
- [54] W. Schiehlen. Multibody System Dynamics: Roots and Perspectives. *Multibody System Dynamics*, 1(1):149–188, 1997.
- [55] J. Schuler. *Flugregelung und aktive Schwingungsdämpfung für flexible Großraumflugzeuge*. PhD thesis, Universität Stuttgart, 1997.

- [56] J. Schuler and K. König. Integral Control of Large Flexible Aircraft. In *RTO AVD Specialists Meeting on Structural Aspects of Flexible Aircraft Control, Ottawa 18-20 October 1999*, number RTO MP-36. RTO, October 1999.
- [57] R. Schwertassek, O. Wallrapp, and A. A. Shabana. Flexible Multibody Simulation and Choice of Shape Functions. *Nonlinear Dynamics*, 20:361–380, 1999.
- [58] A. A. Shabana. Flexible Multibody Dynamics: Review of Past and Recent Developments. *Multibody System Dynamics*, 1:189 – 222, 1997.
- [59] A. A. Shabana. *Dynamics of Multibody Systems*. Cambridge University Press, 1998.
- [60] T. A. Smith, J. W. Hakanson, S. S. Nair, and R. N. Yurkovich. State-Space Model Generation for Flexible Aircraft. *Journal of Aircraft*, 41(6):1473–1481, November-December 2004.
- [61] M. Spieck. *Ground Dynamics of Flexible Aircraft in Consideration of Aerodynamic Effects*. PhD thesis, Technische Universität München, 2004.
- [62] P. Teufel, M. Hanel, and K. H. Well. Integrated Flight Mechanics and Aeroelastic Aircraft Modeling and Control of a Flexible Aircraft Considering Multidimensional Gust Input. In *RTO AVD Specialists Meeting on Structural Aspects of Flexible Aircraft Control, Ottawa*, number RTO MP-36. RTO, 18-20 October 1999.
- [63] I. Tuzcu. *Dynamics and Control of Flexible Aircraft*. PhD thesis, Virginia Polytechnic Institute and State University, Blacksburg, Virginia, December 2001.
- [64] L. v. Schmidt. *Introduction to Aircraft Flight Dynamics*. AIAA Education Series, 1998.
- [65] M. R. Waszak, C. S. Buttrill, and D. K. Schmidt. Modeling and Model Simplification of Aeroelastic Vehicles: An Overview. Technical Report NASA TM-107691, NASA LARC, 1992.
- [66] M. R. Waszak and D. K. Schmidt. On the Flight Dynamics of Aeroelastic Vehicles. In *AIAA Atmospheric Flight Mechanics Conference*, number AIAA 86-2077, pages 120–133. AIAA, 1986.
- [67] M. R. Waszak and D. K. Schmidt. A Simulation Study of the Flight Dynamics of Elastic Aircraft: Vol. 1 – Experiment, Results and Analysis. Technical Report NASA CR-4102, NASA LARC, 1987.
- [68] M. R. Waszak and D. K. Schmidt. A Simulation Study of the Flight Dynamics of Elastic Aircraft: Vol. 2 – Data. Technical Report NASA CR-4102, NASA LARC, 1987.
- [69] M. R. Waszak and D. K. Schmidt. Flight Dynamics of Aeroelastic Vehicles. *Journal of*



- Aircraft*, 25(6):563–571, 1988.
- [70] B. A. Winther, P.J. Goggin, and J. R. Dykman. Reduced-Order Dynamic Aeroelastic Model Development and Integration with Nonlinear Simulation. *Journal of Aircraft*, 37(5):833–839, 2000.
- [71] B.A. Winther, P.J. Goggin, and J.R. Dykman. Reduced Order Dynamic Aeroelastic Model Development and Integration with Nonlinear Simulation. In *Structural Dynamics and Materials Conference, Los Angeles, April 1998*, pages 1694–1704. AIAA, April 1998.
- [72] H. M. Youssef, A. P. Nayak, and K. G. Gousman. Integrated Total and Flexible Body Dynamics of Fixed Wing Aircraft. In *Structures, Structural Dynamics and Materials Conference*, number AIAA-1988-2364, pages 1230–1236. AIAA, Apr. 18-20 1988.
- [73] T. A. Zeiler and C. S. Buttrill. Dynamic Analysis of an Unrestrained, Rotating Structure through Nonlinear Simulation. In *Structures, Structural Dynamics and Materials Conference*, number AIAA-1988-2232, pages 167–174. AIAA, Apr. 18-20 1988.



# Lebenslauf

## PERSÖNLICHE DATEN

09.09.1976 Christian Reschke  
geboren in Frankfurt am Main

## SCHULBILDUNG

08/1983 - 06/1987 Grundschule in Rosbach  
08/1987 - 07/1996 St. Lioba-Schule Gymnasium Bad Nauheim  
Abschluss: Abitur

## STUDIUM

10/1997 - 01/2003 Universität Stuttgart  
Luft- und Raumfahrttechnik  
Abschluss: Diplom-Ingenieur

## BERUFSTÄTIGKEIT

seit 02/2003 Deutsches Zentrum für Luft- und Raumfahrt  
Wissenschaftlicher Mitarbeiter am Institut für Robotik und  
Mechatronik, Oberpfaffenhofen  
02/2003 - 12/2003 Entsendung zur Airbus Deutschland GmbH, Hamburg  
Abteilung: Loads & Aeroelasticity